TÜRKİYE
FIRAT UNIVERSITY
GRADUATE SCHOOL OF NATURAL AND APPLIED SCIENCES

Exact Solutions for Some Differential Equations Through Different Methods

Karmina Kamal ALI

Ph.D. Thesis

Department of Mathematics

June 2022

TÜRKİYE
FIRAT UNIVERSITY
GRADUATE SCHOOL OF NATURAL AND APPLIED SCIENCES

Department of Mathematics

Ph.D. Thesis

Exact Solutions for Some Differential Equations Through Different Methods

Author

Karmina Kamal ALI

Supervisor

Prof. Dr. Resat YILMAZER

June 2022
Elaziğ

TÜRKİYE
FIRAT UNIVERSITY
GRADUATE SCHOOL OF NATURAL AND APPLIED SCIENCES

Department of Mathematics

Ph.D. Thesis

Title:	Exact Solutions for Some Differential Equations Through Different Methods
Author:	Karmina Kamal ALI
Submission Date:	10.5.2022
Defense Date:	10.6.2022

THESIS APPROVAL

This thesis, which was prepared according to the thesis writing rules of the Graduate School of Natural and Applied Sciences, Fırat University, was evaluated by the committee members who have signed the following signatures and was unanimously approved after the defense exam made open to the academic audience.

		Signature
Supervisor:	Prof. Dr. Resat YILMAZER Firat University, Faculty of Science	Approved
Chair:	Prof. Dr. Hasan BULUT Firat University, Faculty of Science	Approved
Member:	Assoc. Prof. Dr. Asıf YOKUŞ Firat University, Faculty of Science	Approved
Member:	Assoc. Prof. Dr. Hacı Mehmet BAŞKONUŞ Harran University, Faculty of Education	Approved
Member:	Assoc. Prof. Dr. Nuri Murat YAĞMURLU İnönü University, Faculty of Science	Approved

This thesis was approved by the Administrative Board of the Graduate School on .../.../....

Prof. Dr. Kürşat Esat ALYAMAÇ
Director of the Graduate School

DECLARATION

This thesis is dedicated to my father Kamal Ali Othman, my mother Fatma Abdullah Khalifa, my husband Hajar Farhan Ismael, and my daughters Masa Hajar Farhan and Mila Hajar Farhan.

June 2022

Karmina Kamal ALI

PREFACE

My deepest thanks to Allah for giving me the opportunity to compile this thesis in good health condition. My sincere gratitude to my supervisor, Prof. Dr. Resat Yilmazer, for his continuous guidance and moral courage during the long process of completing my thesis, and Prof. Dr. Alireza Khalili Golmankhaneh for being very helpful, supportive and encouraging in the subject of fractal calculus. My special gratitude goes to the jury members for valid comments that help to improve the thesis. Many thanks to my family, my father Kamal Ali Othman, my mother Fatma Abdullah, my brothers (Kami, Karmel and Kamaf) and my sisters (Karina and Kahin) for their unconditional supports. Special thanks to my dear husband Hajar Farhan Ismael for his always support, motivation and encouragement, may Allah continue to raise my daughters Masa Hajar Farhan and Mila Hajar Farhan above their expectations. I would also like to extended my thanks to Mr. Mohammad Hasan Maronisi for his continuous support and help. My deep gratitude also goes to my colleagues, and friends.

Karmina Kamal ALI

Elaziğ, 2022

CONTENTS

Abstract

Exact Solutions for Some Differential Equations Through Different Methods

Karmina Kamal ALI

Ph.D. Thesis

FIRAT UNIVERSITY
Graduate School of Natural and Applied Sciences

Department of Mathematics
June 2022, Page: vi-92

This study looks on finding exact solutions to differential equations in a variety of nonlinear scientific fields. The generalized exponential rational function method is used to study some nonlinear model includes the Gilson-Pickering equation, the strain wave equation in micro-structured solids, and system of equations based on ion sound and Langmuir waves equations. In addition, we modified a new technique named as a modified generalized exponential rational function method. To evaluate the efficiency of the new scheme, we applied the generalized exponential rational function method and the new modified method to the system of equations based on ion sound and Langmuir waves equations, and we chose the same values of the parameters in all families for both methods, as well as we presented the difference between the obtained solutions by two methods in the result and the discussion section. One might easily conclude that the new approach is quite effective and successful in seeking the exact solutions of the nonlinear differential equations. Besides, we study and defined some new basic concepts in fractal calculus. We also, study some fractal differential equation such as the electrical circuits involving fractal time, the fractal battery discharging on fractal time sets, and study the fractal version of both one-term and three-term fractal differential equations. The fractal Laplace transform of the local derivative and the non-local fractal Caputo derivative is applied to investigate the proposed fractal models. Furthermore, the simulation analysis is performed by comparing the underlying fractal derivatives to the classical ones in order to understand the significance of the results. The effects of the fractal parameter and the fractional parameter are also discussed.

Keywords: Exact solutions; Analytical methods; Generalized exponential rational function and its newly modified method; fractal calculus; Local fractal derivative; Non-local fractal Caputo derivative; Local and non-local fractal Laplace transform.

ÖZET

Bazı Diferansiyel Denklemlerin Farklı Yöntemlerle Kesin Çözümleri

Karmina Kamal ALI

Doktora Tezi

FIRAT ÜNİVERSİTESİ
Fen Bilimleri Enstitüsü

Matematik Anabilim Dalı
Haziran 2022, Sayfa: vi-92

Bu çalışmada, çeşitli doğrusal olmayan bilimsel çalışma alanlarındaki diferansiyel denklemlere kesin çözümler bulmak amaçlanmaktadır. Genelleştirilmiş üstel rasyonel fonksiyon yöntemi, Gilson-Pickering denklemini, mikro yapılı katılarda gerinim dalgası denklemini, iyon sesine ve Langmuir dalga denklemlerine dayalı denklem sistemlerini içeren bazı doğrusal olmayan modelleri incelemek için kullanılır. Ek olarak, modifiye edilmiş genelleştirilmiş üstel rasyonel fonksiyon yöntemi olarak adlandırılan yeni bir tekniği modifiye ettik. Yeni şemanın etkinliğini değerlendirmek için, iyon sesi ve Langmuir dalgaları denklemlerine dayalı denklem sistemine genelleştirilmiş üstel rasyonel fonksiyon yöntemini ve yeni modifiye edilmiş yöntemi uyguladık ve her ikisi için de tüm ailelerde aynı parametre değerlerini seçtik. Yöntemlerin yanı sıra iki yöntemle elde edilen çözümler arasındaki farkı sonuç ve tartışma bölümünde sunduk. Yeni yaklaşımın lineer olmayan diferansiyel denklemlerin tam çözümlerini aramada oldukça etkili ve başarılı olduğu sonucuna kolayca varılabilir. Ayrıca, fraktal analizde bazı yeni temel kavramları inceledik ve tanımladık. Ayrıca, fraktal zamanı içeren elektrik devreleri, fraktal zaman kümelerinde boşalan fraktal pil gibi bazı fraktal diferansiyel denklemleri ve hem bir terimli hem de üç terimli fraktal diferansiyel denklemlerin fraktal versiyonu incelendi. Önerilen fraktal modelleri araştırmak için yerel türev ve yerel olmayan fraktal Caputo türevinin fraktal Laplace dönüşümü uygulandı. Bundan başka, sonuçların önemini anlamak için temeldeki fraktal türevleri klasik türevlerle karşılaştırarak simülasyon analizi yapıldı. Fraktal parametrenin ve kesirli parametrenin etkileri de tartışıldı.

Anahtar Kelimeler: Kesin çözümler; Analitik metodlar; Genelleştirilmiş üstel rasyonel fonksiyon ve yeni modifiye edilmiş yöntem; fraktal hesap; Yerel fraktal türev; Yerel olmayan fraktal Caputo türevi; Yerel ve yerel olmayan fraktal Laplace dönüşümü.

List of Figures

Symbols and abbreviations

Symbols

$\mathbf{R}$	: Real number
C^{κ}	: Fractal set
Ψ^{α}	: Mass function
$S^{\alpha}_{C^{\kappa}}(t)$	: The integral stair case function
$\chi C^{\kappa}(\alpha, t)$	: The characteristic function
$D^{\alpha}_{C^{\kappa}} f(t)$	: The local fractal derivative
$\int_{a_1}^{a_2} f(t)\, d^{\alpha}_{C^{\kappa}} t$	: The local fractal integral
${}_{\alpha}\mathbb{J}^{\beta}_{t} f(t)$	: The non-local fractal integral
$\alpha^{C}\mathbb{D}^{\beta}_{t} f(t)$	: The non-local fractal Caputo derivative
$L^{\alpha}_{C^{\kappa}}$	: The fractal Laplace transform
$E^{\alpha}_{C^{\kappa},\gamma}(t)$	: The fractal Mittag-Leffler function of one parameter
$E^{\alpha}_{C^{\kappa},\gamma,\upsilon}(t)$	: The fractal Mittag-Leffler function of two parameters
$W^{\alpha}_{\sigma,\upsilon}(t)$	: The fractal Wright function
${}_{1}\Psi_{1}$	: The generalized Wright function

Abbreviations

NPDEs	: Nonlinear partial differential equations
NODEs	: Nonlinear ordinary differential equations
3D	: Three dimensional
2D	: Two dimensional
GERFM	: Generalized exponential rational function method
MGERFM	: Modified generalized exponential rational function method
SISLWs	: System based on ion sound and Langmuir waves equations
SW	: Soliton waves
FLT	: Fractal Laplace transform

1. Introduction

Nonlinear partial differential equations (NLPDEs) are used to represent a variety of nonlinear physical phenomena in different areas of applied sciences like fluid dynamics, plasma physics, optical fibers, and biology [1]. This prompts the development of a number of analytical ways to dealing with wave or evolution equations.

In a situation whereby the dependent variable u appearing in PDEs associates with a physical quantity (for instance, the magnitude of an electromagnetic wave, the surface height of a water wave), it is pertinent to investigate the oscillation of u. This stimulates the introduction of several approaches to deal with the wave or evolution equations analytically. If the form of these solutions has not changed during oscillation, then, such solutions are regarded as the solitary waves (SW). SW which can remain unchanged in shape during a time of collision are known as solitons [2]. The equilibrium between nonlinearity and dispersion leads to SW and solitons being present.

The history of SW's inception is quite important. Russell discovered in 1834 that a wave bend collapsing at a large velocity traveled as a large heap of water for a long time before spreading into minute ripples. Russell's tests in a massive water tank were rigorous in order to understand this logical phenomena. Furthermore, Stokes, Airy, Rayleigh, and Boussinesq studied SW in an attempt to better understand this important phenomenon [3].

The quest for the exact solutions of nonlinear partial differential equations has long been one of the most important priorities of mathematicians. So, for that purpose, several effective analytical methods have been identified, like the sine-Gordon expansion method [4-6], the Lie symmetry analysis [7], Backland transformation method [8], the Bernoulli sub-equation method [9], the modified auxiliary expansion method [10], the $(m + (G'/G))\,-$expansion method [11,12], Jacobi elliptic function expansion [13,14], the extended sinh-Gordon expansion method, Hirota's simple method [15-20], and so on.

One of the most significant fields of mathematics is partial differential equations which describe a variety of processes in physics and engineering, for example, the third-order Gilson and Pickering equation that have application in plasma physics [6,21,22]. The strain wave equation in micro-structured solids have application is solid physics [23-29]. In solid physics, waves are transmission layers that change energy (or) knowledge from one mark to the other at a finite velocity. Such waves, when traveling, carry energy in the form of pieces, packets, frames, and data-grams that include the source location, the path, and the target address. A complication that occurs throughout wave transport, including path deviation, loss of information, information error, and other problems, must be handled in order to guarantee adequate delivery of information to the terminal. In solids, the different wave forms, including elastic, longitudinal, vibration, shear, shock, sound, and transverse, are responsible for the information conveying processes referred to above. The practical applications of the system of equations for the ion sound and Langmuir (SEISLWEs) [9,30,31] are as follows: the electron temperature of the plasma is determined by calculating the frequency of the standing ion-wave mode [32]. The neutral gas density was predicted by the measurement of the gas damping of different standing ion-wave modes [32]. The waves of Langmuir arise as coherent field structures with peak intensities reaching levels of the collapse of Langmuir [33].

A fractal is a complex geometric figure that, unlike a traditional complicated figure, does not simplify when enlarged. Fractal geometry extends classical geometry by removing the assumption of smoothness to include non-differentiable functions. The word "fractal" was invented in the 1960s by Mandelbrot [34,35]. Fractals have the following properties: complicated structure, the similarity of structures across scale (self-similarity), and fractal dimension, which is describing how much of the next dimension the function takes up by virtue of folding back on itself [36–40]. Scientists have developed various methods to propose fractal analysis, such as harmonic analysis, probabilistic method, fractional space, and time scale methods [41–48]. Fractals have a non-differentiable framework, so ordinary calculations can not be used on them. A. Parvate and A.D. Gangal have introduced the Riemann like method to build a calculus for functions on Cantor sets, such as fractal curves. The proposed method is a generalization of the ordinary calculus, that applies in instances in which the standard calculus is not viable. Another useful feature of the proposed method is the algorithmic method and local [49-51]. Algorithmicity is important in computations with computers, and locality is important because measurements are local in physics [49-51]. Several applications for fractal calculus are addressed in the literature, for example, integrals and derivatives of functions on Cantor tartan spaces were defined and applied to model sub-and super-diffusion on totally disconnected sets [52-55]. The diffraction fringes from the fractal grating Cantor sets have been found in [56]. The analogue of the Euler method and Logistic equation in fractal calculus were investigated in [57], and other related researches in [58,59]. The classical non-local fractional integrals and derivatives have been generalized based on fractal sets [60,61]. A fractal Kronig-Penny model which includes a fractal lattice, a fractal potential energy comb, and a fractal Bloch's theorem on thin Cantor sets was investigated in [62]. The economic models from the viewpoint of local and non-local fractal Caputo derivatives was studied in [63]. The analogues of both local Fourier transform with its related properties and Fourier convolution theorem were proposed with proofs in fractal calculus, also the fractal Dirac delta with its derivative and the fractal Fourier transform of the Dirac delta were defined in [64].

1.1 Aim of the Thesis

The aim of this thesis is to present some new exact solutions to some nonlinear partial differential equations via the generalized exponential rational function method (GERFM) and its modified namely modified generalized exponential rational function method (MGERFM). Various kinds of traveling wave solutions are constructed to the proposed nonlinear partial differential equations. On the other hand, some new results in fractal calculus to some fractal differential equations are obtained by using fractal Laplace transform and non local Laplace transform in the sense of Caputo derivative.

1.2 Outline of Thesis

The organization of this thesis is outlined as follows: Chapter one entails the introduction about nonlinear partial differential equations and their applications, as well as introduction about fractal calculus and their applications. Chapter two of this thesis gives the definitions of some important terms in standard differential equations and some fundamental definitions in fractal calculus. Chapter three presents the descriptions of the used analytic methods in this thesis. Chapter four, we discussed the application of the proposed methods to some certain nonlinear partial differential equations. In chapter five, some necessary theorem and application of fractal Laplace transform to some fractal differential equations are addressed. We present the conclusion of this thesis in chapter six.

2. FUNDAMENTAL DEFINITIONS

2.1 Some Fundamental Definitions of Differential Equation

In this section, some useful fundamental definitions of partial differential equations that are related to the work of this thesis are presented.

Definition 2.1.1 A partial differential equation is a differential equation that has more than one independent variable with one or more dependent variables [65].

Definition 2.1.2 The largest derivative that appears in the equation is called the order of the differential equation [65].

Definition 2.1.3 A partial differential equation is considered to be linear if and only if the following conditions are holds [65]:

- The dependent variable's exponent and each partial derivative included in the equation are both one.
- There are no cross-terms—that is, terms such as uu_x or $u_x u_{xx}$ in which the function or its derivatives occur more than once.

Otherwise, differential equation is said to be nonlinear differential equation.

Definition 2.1.4 A partial differential equations are regarded as homogeneous or in-homogeneous. A partial differential equation of any order is referred as homogeneous if each term of the PDE includes the dependent variable u or one of its derivatives [65].

Examples of homogeneous PDE:

1. $u_t = 4u_{xx}$

2. $u_{xx} + u_{yy} = 0.$

Examples of in-homogeneous PDE:

1. $u_t = u_{xx} + x$

2. $u_{xx} + u_y = u + 4.$

2.2 Some Fundamental Tools of Fractal Calculus

In this subsection, we present some basic tools of the fractal calculus on a thin Cantor set, which is shown in Figure 2.1., and Figure 2.2. Let $p[a_1, a_2]$ be a subdivision of an interval $I = [a_1, a_2]$ which is a collection of points $\{a_1 = t_0, t_1, ..., t_n = a_2\}$, such that $t_i < t_{i+1}$, for more details we referred the reader to see [49-51, 66-70].

Definition 2.2.1 Assume that $F^\kappa \subset \mathbf{R}$ is a thin Cantor set [71] and $p[a_1, a_2]$ is a subdivision.

The mass function is given by [49-51]

$$\Psi^{\alpha}\left(F^{\kappa}, a_1, a_2\right) = \lim_{\varsigma \to 0} \Psi^{\alpha}_{\varsigma}, \tag{2.2.1}$$

where

$$\Psi^{\alpha}_{\varsigma} = \inf_{\{p[a_1,a_2]:|p|\leq\varsigma\}} \sum_{j=0}^{m-1} \Gamma\left(\alpha+1\right)\left(t_{j+1}-t_j\right)^{\alpha} \phi\left(F^{\kappa}, \left[t_{j+1}-t_j\right]\right), \tag{2.2.2}$$

and

$$\phi\left(F^{\kappa}, \left[t_{j+1}-t_j\right]\right) = \begin{cases} 1, & F^{\kappa} \cap \left[t_{j+1}-t_j\right] \neq \emptyset, \\ 0, & \text{otherwise}, \end{cases} \tag{2.2.3}$$

where

$$|p| = \max_{0\leq j\leq m} \left(t_{j+1}-t_j\right).$$

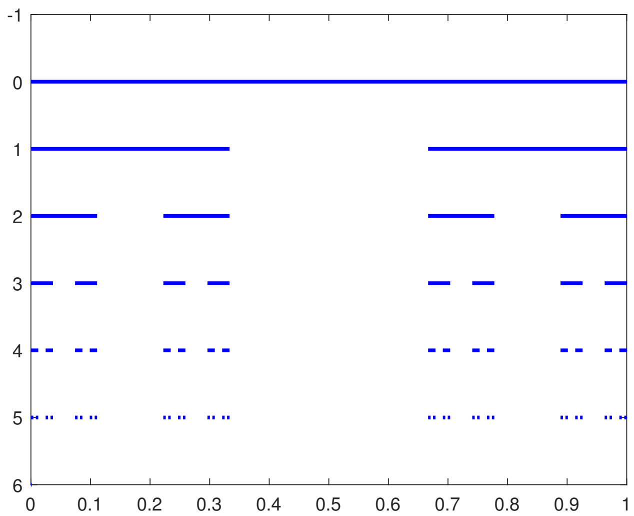

Figure 2.1. The thin Cantor set ($\kappa = 1/3$) by iteration.

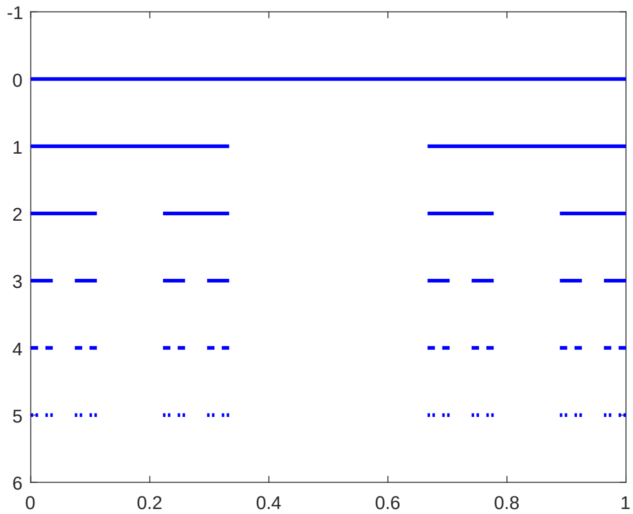

Figure 2.2. The thin Cantor set ($\kappa = 1/5$) by iteration.

Definition 2.2.2 Assume that $c_0 \in \mathbf{R}$. The staircase function of order α is given by [49-51]

$$S^{\alpha}_{F^{\kappa}}\left(t\right)=\begin{cases}\Psi^{\alpha}\left(F^{\kappa},c_0,t\right), & \text{if t} \geq c_0,\\ -\Psi^{\alpha}\left(F^{\kappa},c_0,t\right), & \text{otherwise.}\end{cases} \tag{2.2.4}$$

The graph of the integral staircase function is presented in Figure. 2.3., and Figure 2.4.

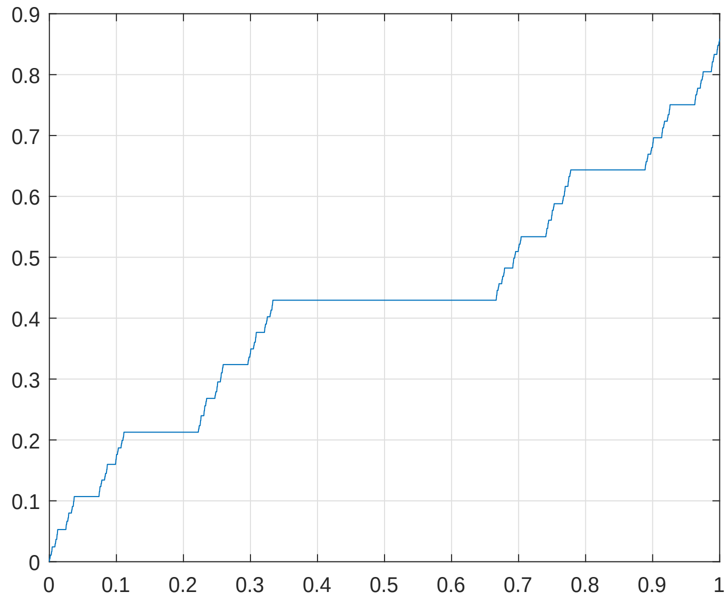

Figure 2.3. The integral staircase function for the thin Cantor set F^{κ} for the case of ($\kappa = 1/3$).

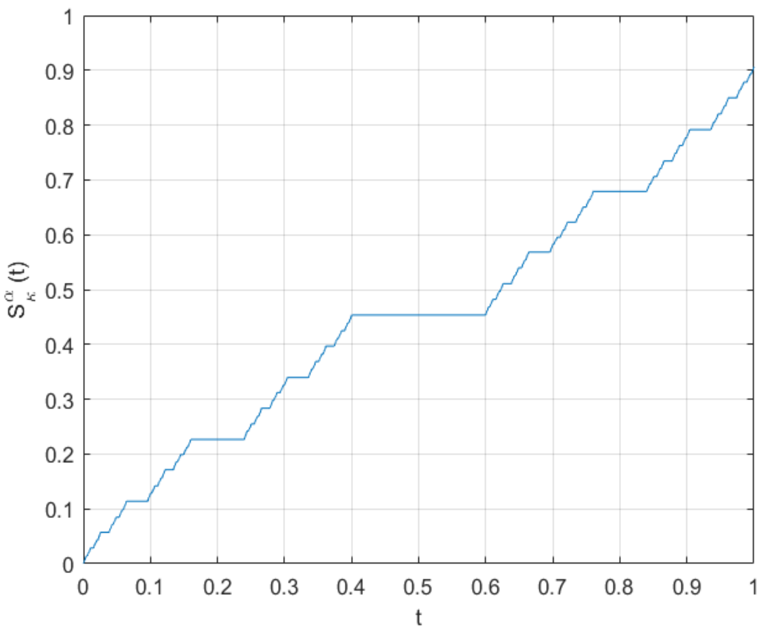

Figure 2.4. The integral staircase function for the thin Cantor set F^{κ} for the case of ($\kappa = 1/5$).

Definition 2.2.3 The $\Psi-$dimension is defines using the mass function as follows [49-51]:

$$\begin{aligned}\dim_{\Psi}\left(F^{\kappa}\cap[a_1,a_2]\right) &= \inf\left\{\alpha : \Psi^{\alpha}\left(F^{\kappa},a_1,a_2\right)=0\right\},\\ &= \text{suf}\left\{\alpha : \Psi^{\alpha}\left(F^{\kappa},a_1,a_2\right)=\infty\right\}.\end{aligned} \tag{2.2.5}$$

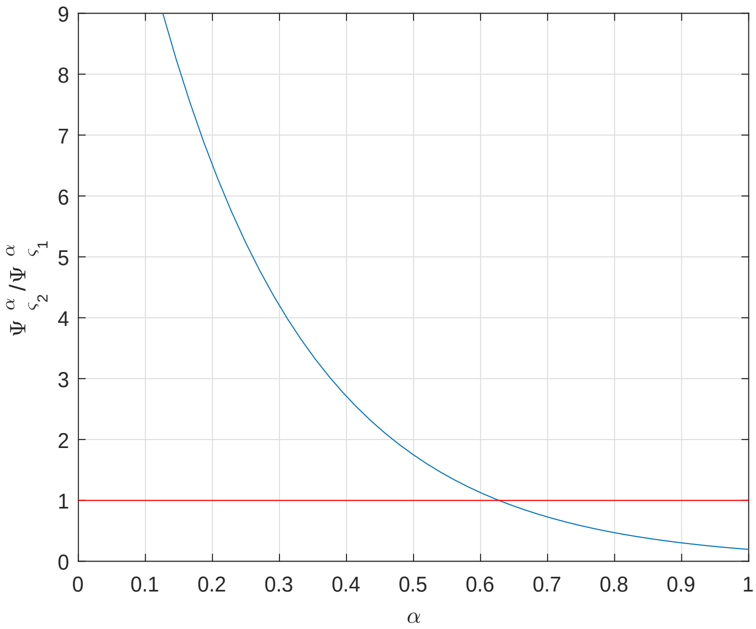

Figure 2.5. $\Psi-$dimension of the thin Cantor set ($\kappa=1/3$).

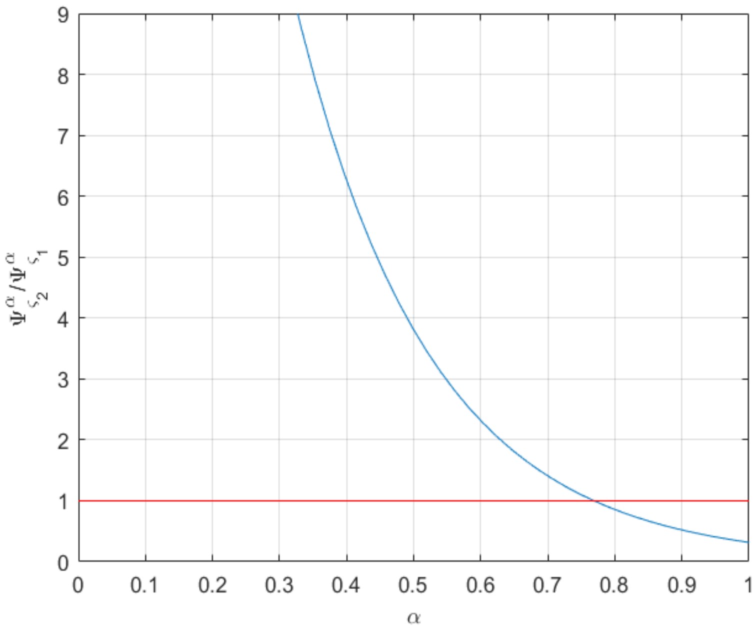

Figure 2.6. $\Psi-$dimension of the thin Cantor set ($\kappa = 1/5$).

Figure 2.5., and Figure 2.6. are the $\Psi-$dimension which is intersection point of the red line with the blue line.

Definition 2.2.4 The characteristic function $\chi_{F^\kappa}(\alpha,t)$ for a given thin Cantor set is defined by [49-51]

$$\chi_{F^\kappa}(\alpha,t)=\begin{cases}\dfrac{1}{\Gamma(\alpha+1)}, & t\in F^\kappa,\\ 0, & \text{otherwise.}\end{cases} \tag{2.2.6}$$

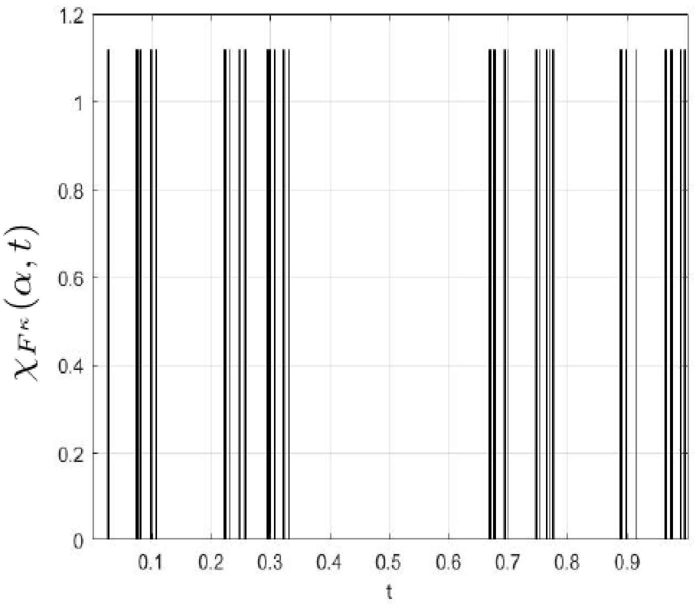

Figure 2.7. Characteristic function for thin Cantor set with ($\kappa = 1/3$).

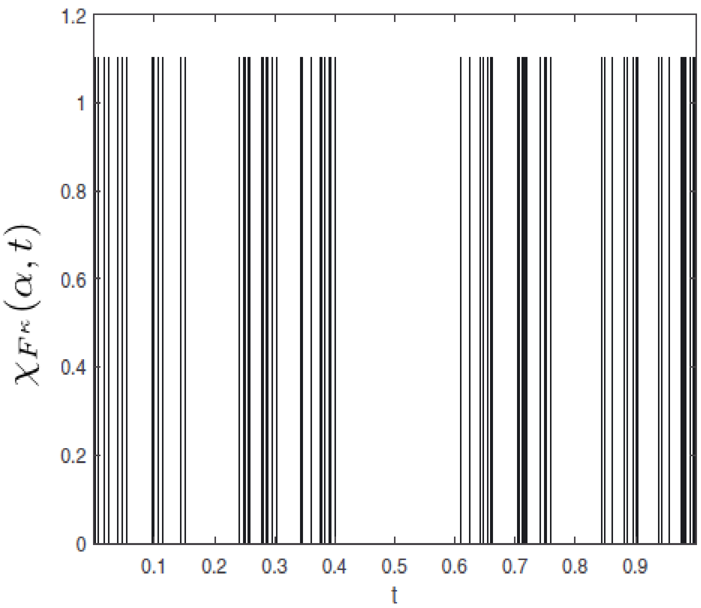

Figure 2.8. Characteristic function for thin Cantor set with ($\kappa = 1/5$).

Figure 2.7., and Figure 2.8. are the characteristic function for thin Cantor set.

Some important formulas:

$$
\begin{aligned}
D^{\alpha}_{F^{\kappa}} c &= 0, \quad c \text{ is constant}, && (2.2.7)\\
D^{\alpha}_{F^{\kappa}} S^{\alpha}_{F^{\kappa}}(t) &= \chi_{F^{\kappa}}(\alpha, t), && (2.2.8)\\
D^{\alpha}_{F^{\kappa}} S^{\alpha}_{F^{\kappa}}(t)^{m} &= m S^{\alpha}_{F^{\kappa}}(t)^{m-1}, && (2.2.9)\\
D^{\alpha}_{F^{\kappa}} \sin(S^{\alpha}_{F^{\kappa}}(t)) &= \chi_{F^{\kappa}}(\alpha, t)\cos(S^{\alpha}_{F^{\kappa}}(t)), && (2.2.10)\\
D^{\alpha}_{F^{\kappa}} \tan(S^{\alpha}_{F^{\kappa}}(t)) &= \chi_{F^{\kappa}}(\alpha, t)\sec^{2}(S^{\alpha}_{F^{\kappa}}(t)), && (2.2.11)\\
D^{\alpha}_{F^{\kappa}} \cos(S^{\alpha}_{F^{\kappa}}(t)) &= -\chi_{F^{\kappa}}(\alpha, t)\sin(S^{\alpha}_{F^{\kappa}}(t)), && (2.2.12)\\
\sin(S^{\alpha}_{F^{\kappa}}(t)) &= S^{\alpha}_{F^{\kappa}}(t) - \frac{S^{\alpha}_{F^{\kappa}}(t)^{3}}{3!} + \frac{S^{\alpha}_{F^{\kappa}}(t)^{5}}{5!} + ... = \sum_{i=1}^{\infty}(-1)^{i-1}\frac{S^{\alpha}_{F^{\kappa}}(t)^{2i-1}}{(2i-1)!}, && (2.2.13)\\
\cos(S^{\alpha}_{F^{\kappa}}(t)) &= 1 - \frac{S^{\alpha}_{F^{\kappa}}(t)^{2}}{2!} + \frac{S^{\alpha}_{F^{\kappa}}(t)^{4}}{4!} + ... = \sum_{i=1}^{\infty}(-1)^{i-1}\frac{S^{\alpha}_{F^{\kappa}}(t)^{2i-2}}{(2i-2)!}, && (2.2.14)\\
e^{S^{\alpha}_{F^{\kappa}}(t)} &= 1 + S^{\alpha}_{F^{\kappa}}(t) + \frac{S^{\alpha}_{F^{\kappa}}(t)^{2}}{2!} + ... = \sum_{i=1}^{\infty}\frac{S^{\alpha}_{\kappa}(t)^{i-1}}{(i-1)!}, && (2.2.15)\\
\ln|1 + S^{\alpha}_{F^{\kappa}}(t)| &= S^{\alpha}_{F^{\kappa}}(t) - \frac{S^{\alpha}_{F^{\kappa}}(t)^{2}}{2} + \frac{S^{\alpha}_{F^{\kappa}}(t)^{3}}{3} - ... = \sum_{i=1}^{\infty}(-1)^{i-1}\frac{S^{\alpha}_{F^{\kappa}}(t)^{i}}{i}. && (2.2.16)
\end{aligned}
$$

2.3 Local Fractal Calculus

In this section, we provided some definitions of the local fractal calculus.

Definition 2.3.1 If F^{κ} is $\alpha-$ perfect set, then the F^{α}-derivative of $f(t)$ at t is defined by [49,50,51]

$$
D^{\alpha}_{F^{\kappa}}(f(t)) = \begin{cases} F^{\kappa} - \lim\limits_{x \to t} \dfrac{f(x) - f(t)}{S^{\alpha}_{F^{\kappa}}(x) - S^{\alpha}_{F^{\kappa}}(t)}, & \text{if } t \in F^{\kappa}, \\ 0, & \text{otherwise}, \end{cases} \tag{2.3.1}
$$

if the limit exist.

Definition 2.3.2 The F^{α}-integral of $f(t)$ on $[a_1, a_2]$ is defined by [49,50,51]

$$
\int_{a_1}^{a_2} f(t)\, d^{\alpha}_{F^{\kappa}} t \approx \sum_{j=1}^{n} f_j(t)\left(S^{\alpha}_{F^{\kappa}}(t_j) - S^{\alpha}_{F^{\kappa}}(t_{j-1})\right). \tag{2.3.2}
$$

2.4 Non-Local Fractal Calculus

In this section, we present some useful concepts of the non-local fractal calculus [60-64, 71-73].

Definition 2.4.1 For a function $f(t)$, $t \in F^{\kappa}$, the fractal left-sided Riemann-Liouville integral is defined by [61]

$$
{}_a\mathbb{J}_t^{\beta} f(t) = \frac{1}{\Gamma_{F^\kappa}^{\alpha}(\beta)} \int_a^t \frac{f(x)}{\left(S_{F^\kappa}^{\alpha}(t) - S_{F^\kappa}^{\alpha}(x)\right)^{\alpha-\beta}} d_{F^\kappa}^{\alpha} x, \tag{2.4.1}
$$

where $t > a$.

Definition 2.4.2 The fractal left-sided Riemann–Liouville derivative is given by [61]

$$
{}_a\mathbb{D}_t^{\beta} f(t) = \frac{1}{\Gamma_{F^\kappa}^{\alpha}(n-\beta)} \left(D_{F^\kappa}^{\alpha}\right)^n \int_a^t \frac{f(x)}{\left(S_{F^\kappa}^{\alpha}(t) - S_{F^\kappa}^{\alpha}(x)\right)^{-n\alpha+\beta+\alpha}} d_{F^\kappa}^{\alpha} x, \tag{2.4.2}
$$

where $n\alpha - \alpha \leq \beta < n\alpha,\ n \in \mathbf{N}$.

Definition 2.4.3 [61] The fractal left-sided Caputo derivative is given by

$$
{}_a^C\mathbb{D}_t^{\beta} f(t) = \frac{1}{\Gamma_{F^\kappa}^{\alpha}(n-\beta)} \int_a^t \frac{\left(D_{F^\kappa}^{\alpha}\right)^n f(x)}{\left(S_{F^\kappa}^{\alpha}(t) - S_{F^\kappa}^{\alpha}(x)\right)^{-n\alpha+\beta+\alpha}} d_{F^\kappa}^{\alpha} x, \tag{2.4.3}
$$

where $n\alpha - \alpha < \beta \leq n\alpha,\ n \in \mathbf{N}$.

2.5 The Local Fractal Laplace Transform and Mittag-Leffler Functions

In this section, we provide definitions of the local fractal Laplace transform and fractal Mittag-Leffler functions to apply them in solving fractal differential equations.

Definition 2.5.1 The **fractal Laplace transform** (FLT) of a function $f(t), t \in$ thin Cantor sets is presented by [60-61, 71-73]

$$
B(w) = L_{F^\kappa}^{\alpha}(f(t)) = \int_0^{\infty} \exp\left(-S_{F^\kappa}^{\alpha}(t)\, S_{F^\kappa}^{\alpha}(w)\right) f(t)\, d_{F^\kappa}^{\alpha} t, \tag{2.5.1}
$$

where $B(w)$ and $L(f) : f(t) \to B(w)$ are called the fractal Laplace transform of $f(t)$. If $\exists\ M > 0$, $\exists\ T > 0$, and $at^{\alpha} < S_{F^\kappa}^{\alpha}(t) < bt^{\alpha},\ a,\ b \in \mathbf{R}$

$$
e^{-\varepsilon S_{F^\kappa}^{\alpha}(t)} |f(t)| < e^{-\varepsilon t^{\alpha}} |f(t)| \leq M \qquad \forall\ t > T, \tag{2.5.2}
$$

then the fractal integral Eq. (2.5.1) exists.

Table 2.1. Fractal Laplace Transform Formulas

$f(t)$	$L^{\alpha}_{F^{\kappa}}\left(f(t)\right)$
a	$\frac{a}{S^{\alpha}_{F^{\kappa}}(w)}$ $a>0$
$e^{aS^{\alpha}_{F^{\kappa}}(t)}$	$\frac{1}{S^{\alpha}_{F^{\kappa}}(w)-a}$
$D^{\alpha}_{F^{\kappa},t}f\left(t\right)$	$S^{\alpha}_{F^{\kappa}}\left(w\right)B\left(w\right)-f\left(0\right)$
$(D^{\alpha}_{F^{\kappa},t})^{2}f\left(t\right)$	$S^{\alpha}_{F^{\kappa}}\left(w\right)^{2}B\left(w\right)-S^{\alpha}_{F^{\kappa}}\left(w\right)f(0)-D^{\alpha}_{F^{\kappa},t}f\left(t\right)\|_{t=0}$
$\int_0^t f(t')d^{\alpha}_{F^{\kappa}}t'$	$\frac{B(\omega)}{S^{\alpha}_{F^{\kappa}}(w)}$
$e^{aS^{\alpha}_{F^{\kappa}}(t)}f(t)$	$B(\omega-a)$
$\left(S^{\alpha}_{F^{\kappa}}\left(t\right)^{n}f(t)\right.$	$(-1)^{n}(D^{\alpha}_{F^{\kappa},\omega})^{n}B(\omega)$
$u^{\alpha}_{F^{\kappa}}(t-c)$	$\frac{1}{S^{\alpha}_{F^{\kappa}}(w)}e^{-cS^{\alpha}_{F^{\kappa}}(w)}$
$u^{\alpha}_{F^{\kappa}}(t-c)f(t-c)$	$e^{-cS^{\alpha}_{F^{\kappa}}(w)}B(\omega)$

Definition 2.5.2 The fractal **Laplace transform of the local fractal derivative** is defined by [60,61,71-73]

$$L^{\alpha}_{F^{\kappa}}\left((D^{\alpha}_{t})^{n}f\left(t\right)\right)=S^{\alpha}_{F^{\kappa}}\left(w\right)^{n}L^{\alpha}_{F^{\kappa}}\left(f\left(t\right)\right)-\sum_{j=0}^{n-1}S^{\alpha}_{F^{\kappa}}\left(w\right)^{n-j-1}(D^{\alpha}_{F^{\kappa},t})^{j}f|_{t=0}. \tag{2.5.3}$$

The **fractal Laplace transform of the fractal left-sided Riemann–Liouville derivative** is defined by [60,61,71-73]

$$L^{\alpha}_{F^{\kappa}}(\Big({}_{0}\mathbb{D}^{\beta}_{t})f\left(t\right)\Big)=S^{\alpha}_{F^{\kappa}}\left(w\right)^{\beta}B(w)-\sum_{j=0}^{n-1}S^{\alpha}_{F^{\kappa}}\left(w\right)^{j}\left[{}_{0}\mathbb{D}^{\beta-j-1}_{F^{\kappa},t}f\left(t\right)\right]_{t=0}. \tag{2.5.4}$$

The fractal Laplace transform of **the fractal Caputo derivative** is defined by [60,61,71-73]

$$L^{\alpha}_{F^{\kappa}}\left({}^{C}_{0}\mathbb{D}^{\beta}_{t}f\left(t\right)\right)=S^{\alpha}_{F^{\kappa}}(w)^{\beta}L^{\alpha}_{F^{\kappa}}\left(f\left(t\right)\right)-\sum_{j=0}^{n-1}S^{\alpha}_{F^{\kappa}}(w)^{\beta-j-1}(D^{\alpha}_{F^{\kappa}})^{j}(f\left(t\right)|_{t=0}. \tag{2.5.5}$$

Definition 2.5.3 The **inverse fractal Laplace transform** is given by [60-61,71-73]

$$f(t)=\left(L^{\alpha}_{F^{\kappa}}\right)^{-1}\left(B\left(w\right)\right). \tag{2.5.6}$$

Example 1. The fractal inverse of the following

$$\frac{S^{\alpha}_{F^{\kappa}}\left(w\right)+3}{(S^{\alpha}_{F^{\kappa}}\left(w\right)-2)(S^{\alpha}_{F^{\kappa}}\left(w\right)+1)},$$

is given by

$$
\begin{aligned}
(L^{\alpha}_{F^{\kappa}})^{-1}\{\frac{S^{\alpha}_{F^{\kappa}}(w)+3}{(S^{\alpha}_{F^{\kappa}}(w)-2)(S^{\alpha}_{F^{\kappa}}(w)+1)}\} &= \frac{5}{3}(L^{\alpha}_{F^{\kappa}})^{-1}\{\frac{1}{S^{\alpha}_{F^{\kappa}}(w)-2}\} \\
&\quad -\frac{2}{3}(L^{\alpha}_{F^{\kappa}})^{-1}\{\frac{1}{S^{\alpha}_{F^{\kappa}}(w)+1}\} \\
&= \frac{5}{3}e^{2S^{\alpha}_{F^{\kappa}}(t)}-\frac{2}{3}e^{-S^{\alpha}_{F^{\kappa}}(t)}.
\end{aligned}
\tag{2.5.7}
$$

Example 2. Consider the fractal differential equation

$$
D^{\alpha}_{F^{\kappa},t}f(t)-5f(t)=e^{5S^{\alpha}_{F^{\kappa}}(t)},\ \ f(0)=0. \tag{2.5.8}
$$

By taking the local fractal Laplace transform to both sides of Eq. (2.5.8), we have

$$
S^{\alpha}_{F^{\kappa}}(w)B(\omega)-5B(\omega)=\frac{1}{S^{\alpha}_{F^{\kappa}}(w)-5}. \tag{2.5.9}
$$

It follows

$$
B(\omega)=\frac{1}{(S^{\alpha}_{F^{\kappa}}(w)-5)^2}. \tag{2.5.10}
$$

Taking the fractal inverse Laplace transform of Eq. (2.5.10), we obtain

$$
f(t)=(L^{\alpha}_{F^{\kappa}})^{-1}\Big\{B(\omega)\Big\}=S^{\alpha}_{F^{\kappa}}(t)e^{5S^{\alpha}_{F^{\kappa}}(t)}, \tag{2.5.11}
$$

which is the solution of Eq. (2.5.8).

Example 3. Consider the fractal system given as follows

$$
\begin{aligned}
&(D^{\alpha}_{F^{\kappa},t})^2y(t)+z(t)+y(t)=0,\\
&(D^{\alpha}_{F^{\kappa},t})z(t)+(D^{\alpha}_{F^{\kappa},t})y(t)=0,
\end{aligned}
\tag{2.5.12}
$$

with the conditions

$$
y(0)=0,\quad D^{\alpha}_{F^{\kappa},t}y(t)|_{t=0}=0,\quad z(0)=1.
$$

Taking the local fractal Laplace transforms of Eq. (2.5.12), gives

$$
\begin{aligned}
&\Big(S^{\alpha}_{F^{\kappa}}(\omega)^2+1\Big)Y(\omega)+Z(\omega)=0,\\
&Z(\omega)+Y(\omega)=\frac{1}{S^{\alpha}_{F^{\kappa}}(\omega)},
\end{aligned}
\tag{2.5.13}
$$

where $Z(\omega)=(L^{\alpha}_{F^{\kappa}})z(t)$ and $Y(\omega)=(L^{\alpha}_{F^{\kappa}})y(t)$. Solving Eqs. (2.5.13), we get

$$
Z(\omega)=\frac{S^{\alpha}_{F^{\kappa}}(\omega)+1}{S^{\alpha}_{F^{\kappa}}(\omega)^2},\ \ Y(\omega)=-\frac{1}{S^{\alpha}_{F^{\kappa}}(\omega)^2}.
$$

Thus, taking the fractal inverse Laplace transform, we conclude that

$$\begin{aligned} y(t) &= -S_{F^{\kappa}}^{\alpha}(t), \\ z(t) &= 1 + S_{F^{\kappa}}^{\alpha}(t). \end{aligned} \tag{2.5.14}$$

Definition 2.5.4 The **fractal Mittag-Lefler function of one parameter** is given by [60,61,71-73]

$$E_{F^{\kappa},\gamma}^{\alpha}(t) = \sum_{j=0}^{\infty} \frac{S_{F^{\kappa}}^{\alpha}(t)^{j}}{\Gamma^{\alpha}(\gamma j + 1)}, \qquad \gamma > 0. \tag{2.5.15}$$

Definition 2.5.5 The **fractal Mittag-Lefler function of two parameters** is given by [73]

$$E_{F^{\kappa},\gamma,\upsilon}^{\alpha}(t) = \sum_{j=0}^{\infty} \frac{S_{F^{\kappa}}^{\alpha}(t)^{j}}{\Gamma^{\alpha}(\gamma j + \upsilon)}, \qquad \gamma > 0,\ \upsilon \in \mathbf{R}. \tag{2.5.16}$$

Definition 2.5.6 The **fractal Laplace transform of the Mittag-Leffler function** is defined by [73]

$$\mathrm{L}_{F^{\kappa}}^{\alpha}\left(S_{F^{\kappa}}^{\alpha}(t)^{\upsilon-1} E_{\gamma,\upsilon}^{\alpha}(\lambda t^{\gamma})\right) = \frac{S_{F^{\kappa}}^{\alpha}(w)^{\gamma-\upsilon}}{S_{F^{\kappa}}^{\alpha}(w)^{\gamma} - \lambda},\ S_{F^{\kappa}}^{\alpha}(w) > 0,\ \left|\lambda S_{F^{\kappa}}^{\alpha}(w)^{-\gamma}\right| < 1. \tag{2.5.17}$$

Definition 2.5.7 The **fractal Wright function** is defined by [73]

$$\mathrm{W}_{\sigma,\upsilon}^{\alpha}(t) = \sum_{j=0}^{\infty} \frac{S_{F^{\kappa}}^{\alpha}(t)^{j}}{j!\,\Gamma^{\alpha}(\sigma j + \upsilon)}, \qquad \gamma > -1,\ \upsilon \in \mathbf{R}. \tag{2.5.18}$$

Eq. (2.5.18) is named the simplest Wright function.

Definition 2.5.8 The **more general Wright function** is given by [73]

$${}_1\Psi_1\left[\begin{array}{c|c} (n+1,1) & \\ & (-\mu)\, S_{F^{\kappa}}^{\alpha}(t)^{\sigma-\upsilon} \\ (\sigma n+1, \sigma-\upsilon) & \end{array}\right] := \sum_{j=0}^{\infty} \frac{\Gamma^{\alpha}(n+j+1)}{\Gamma^{\alpha}(\sigma n + \upsilon + \sigma j)} \frac{S_{F^{\kappa}}^{\alpha}(t)^{j}}{j!}. \tag{2.5.19}$$

Furthermore, **a generalization of three parameters Mittag-Lefler function** is defined as follows:

$$E_{\sigma,\upsilon}^{\alpha,\rho}(t) := \sum_{j=0}^{\infty} \frac{(\rho)_j}{\Gamma^{\alpha}(\sigma j + \upsilon)} \frac{S_{F^{\kappa}}^{\alpha}(t)^{j}}{j!} = \frac{1}{\Gamma^{\alpha}(\rho)}\, {}_1\Psi_1\left[\begin{array}{c|c} (\rho,1) & \\ & S_{F^{\kappa}}^{\alpha}(t) \\ (\upsilon,\sigma) & \end{array}\right], \tag{2.5.20}$$

where $\sigma > 0$, $\upsilon > 0$, σ, υ, $S_{F^{\kappa}}^{\alpha}(t) \in \mathbb{R}$. Using the fact that

$${}_1\Psi_1\left[\begin{array}{c|c} (a,v) & \\ & t \\ (\vartheta,\chi) & \end{array}\right] = \sum_{n=0}^{\infty} \frac{\Gamma^{\alpha}(nv + a)}{\Gamma^{\alpha}(\chi n + \vartheta)\, n!}.$$

Definition 2.5.9 The Laplace transform of the Wright function is defined by [73]

$$L_{F^\kappa}^{\alpha}\left(S_{F^\kappa}^{\alpha}(t)^{\sigma n}{}_1\Psi_1\left[\begin{array}{c|c}(n+1,1) & \\ & (-\mu)\,S_{F^\kappa}^{\alpha}(t)^{\sigma-\upsilon}\\ (\sigma n+1,\sigma-\upsilon) & \end{array}\right]\right)=n!\frac{S_{F^\kappa}^{\alpha}(w)^{(\sigma-\upsilon)-(n\upsilon+1)}}{\left(S_{F^\kappa}^{\alpha}(w)^{\sigma-\upsilon}+\mu\right)^{n+1}}. \tag{2.5.21}$$

Theorem 2.5.1 Fractal convolution theorem. If $\mathrm{L}_{F^\kappa}^{\alpha}(h(t))=H(w)$, and $\mathrm{L}_{F^\kappa}^{\alpha}(k(t))=K(w)$, then [73]

$$\mathrm{L}_{F^\kappa}^{\alpha}(h(t)*k(t))=\mathrm{L}_{F^\kappa}^{\alpha}(h(t))\,\mathrm{L}_{F^\kappa}^{\alpha}(k(t))=H(w)\,K(w)\,. \tag{2.5.22}$$

Or, equivalently,

$$\mathrm{L}_{F^\kappa}^{\alpha,-1}(H(w)\,K(w))=h(t)*k(t)\,, \tag{2.5.23}$$

where $h(t)*k(t)$ is called the **fractal convolution** of $h(t)$ and $k(t)$, which is defined by the integral

$$h(t)*k(t)=\int_0^t h(t-\tau)k(t)\,d_{F^\kappa}^{\alpha}\tau=\int_0^t h(\tau)k(t-\tau)d_{F^\kappa}^{\alpha}\tau, \tag{2.5.24}$$

where $t\in F^\kappa$.

3. Fundamental concepts of each method

This chapter provides the basic concepts of the GERFM and its newly modified version.

3.1 The GERFM

The fundamental steps of the GERFM are addressed in this section as follows [74-79].

Step 1. Consider the NPDE as follows:

$$Q\left(u, u_x, u_t, u_{xx}, \ldots\right) = 0, \tag{3.1.1}$$

using

$$u\left(x, t\right) = U(\zeta), \quad \zeta = \sigma x + \delta y, \tag{3.1.2}$$

in Eq. (3.1.1), we get a nonlinear ordinary differential equation (NODE)

$$W\left(U, U', U'', \ldots\right) = 0. \tag{3.1.3}$$

Step 2. Let we set up the solution of Eq. (3.1.3) as

$$U(\zeta) = A_0 + \sum_{k=1}^{m} A_k \psi(\zeta)^k + \sum_{k=1}^{m} B_K \psi(\zeta)^{-k}, \tag{3.1.4}$$

where

$$\psi\left(\zeta\right) = \frac{r_1 e^{s_1\zeta} + r_2 e^{s_2\zeta}}{r_3 e^{s_3\zeta} + r_4 e^{s_4\zeta}}, \tag{3.1.5}$$

where A_0, A_k, B_k, and r_j, s_j $(1 \leq j \leq 4)$ are constants to be determined, such that the Eq. (3.1.4) verify the NODE Eq. (3.1.3). Note that m can be determine by using the balance principle which is determine between the highest derivative and a nonlinear term.

Step 3. Plugging Eq. (3.1.4) into Eq. (3.1.3), we get a polynomial equation. Setting each coefficient in the polynomial to zero, we achieve a system of algebraic equations.

Step 4. Solving the obtained system given in Step 3 with aid of computational packages, we will find the values of A_0, A_k, and B_k. Eventually, one may simply acquire the exact solutions of Eq. (3.1.3).

3.2 The newly MGERFM

The basic steps of the newly MGERFM are presented in this section as follows:

Step 1. Consider the NPDE as follows:

$$Q\left(u, u_x, u_t, u_{xx}, \ldots\right) = 0, \tag{3.2.1}$$

using

$$u\,(x,t) = U(\zeta), \quad \zeta = \sigma x + \delta y, \tag{3.2.2}$$

in Eq. (3.2.1), then we obtain a NODE as follows

$$W\,(U, U', U'', ...) = 0. \tag{3.2.3}$$

Step 2. Let we set up the solution of Eq. (3.2.3) as

$$U(\zeta) = A_0 + \sum_{k=1}^{m} A_k \psi(\zeta)^k + \sum_{k=1}^{m} B_k \psi(\zeta)^{-k} + \sum_{k=1}^{m} C_k \frac{\psi'(\zeta)^k}{\psi(\zeta)^k}, \tag{3.2.4}$$

where

$$\psi\,(\zeta) = \frac{r_1 e^{s_1 \zeta} + r_2 e^{s_2 \zeta}}{r_3 e^{s_3 \zeta} + r_4 e^{s_4 \zeta}}, \tag{3.2.5}$$

where A_0, A_k, B_k, C_k, and r_j, s_j $(1 \leq j \leq 4)$ are constants to be determined, such that the Eq. (3.2.4) verify the NODE Eq. (3.2.3). Note that m can be determine by using the balance principle.

Step 3. Plugging Eq. (3.2.4) into Eq. (3.2.3) we get a polynomial equation. Setting each coefficient in the polynomial to zero, we achieve a system of algebraic equations.

Step 4. Solving the obtained system given in Step 3 with aid of computational packages, we will find the values of A_0, A_k, and B_k, C_k. Eventually, one may simply acquire exact solutions of Eq. (3.2.3).

4. Mathematical analysis and Application of the methods

In the part of the theses, mathematical analysis of the Gilson-Pickering equation (GPE), the strain wave equation in micro-structured solids, and the system based on the ion sound and Langmuir waves (SISLWs) equations are addressed. In addition, application of the GERF to the GPE, the strain wave equation in micro-structured solids, and the SISEs are analyzed, as well as application of the new modified generalized exponential rational function method to the system based on the ion sound and Langmuir waves (SISLWs) equations are given.

4.1 Gilson-Pickering equation

In this portion, the GERFM is implemented in getting the wave solutions to the third-order nonlinear partial differential equation was introduced in [21] by Gilson and Pickering as

$$u_t - \epsilon u_{xxt} + 2ku_x - uu_{xxx} - \alpha uu_x - \beta u_x u_{xx} = 0, \tag{4.1.1}$$

where $\varepsilon, \alpha, \kappa$ and β are non-zero real numbers. There have been specific instances of Eq. (4.1.1) has been reported in the literature, such as when $\epsilon = 1$, $\alpha = -3$, $\beta = 2$, Eq. (4.1.1) gives the Fuchssteiner-Fokas-Camassa-Holm equation, which is a completely integrable nonlinear partial differential equation which arises at different levels of approximation in shallow water theory [80,81], when $\epsilon = 0$, $\alpha = 1$, $k = 0$, and $\beta = 3$ then Eq. (4.1.1) reduces to the Rosenau-Hyman equation, which arising in the study of the influence of nonlinear dispersion on the structure of patterns in liquid drops [82], when $\epsilon = 1$, $\alpha = -1$, $k = 0.5$, and $\beta = 3$, then Eq. (4.1.1) becomes the Fronberg-Whitham, which was developed to analyze the qualitative characteristics of wave breakage, and admits a wave of the highest height [83-85].

Recently, the Gilson–Pickering equation has been investigated using a variety of methods, such as the (G'/G)-expansion method [86], the Bernoulli sub-equation model [87], the anstaz method [88], and the sine-Gordon expansion method [89]. Consider the following wave transformation

$$u = U(\zeta), \zeta = x - ht, \tag{4.1.2}$$

plugging Eq. (4.1.2) into Eq. (4.1.1), then the following NODE can be obtained:

$$(2k - h) U' + h\epsilon U''' - UU''' - \beta U'U'' - \alpha UU' = 0, \tag{4.1.3}$$

where $\epsilon, \beta, \alpha, h$, and k are non-zero real numbers.

Integrating Eq. (4.1.3) once with respect to ζ, and assuming that the integration constant is zero, we have

$$(2k-h)\,U+(\epsilon h-U)\,U''+\frac{1-\beta}{2}(U')^2-\frac{\alpha}{2}U^2=0. \tag{4.1.4}$$

Applying the balance principle, by taking the nonlinear term U^2, and the highest derivative U'' in Eq. (4.1.4), gives $m=2$, with $m=2$, Eq. (3.1.4) takes the form

$$U(\zeta)=A_0+A_1\psi\left(\zeta\right)+\frac{B_1}{\psi\left(\zeta\right)}+A_2\psi(\zeta)^2+\frac{B_2}{\psi(\zeta)^2}. \tag{4.1.5}$$

Taking Eq. (3.2.5) into account, we have to following family:

Family 1. When $\mathrm{r}_j=\{-2,-1,1,1\}$, $s_j=\{0,1,0,1\}$, then Eq. (3.2.5) reduced to the following form

$$\psi\left(\zeta\right)=\frac{-2-\mathrm{e}^{\zeta}}{1+\mathrm{e}^{\zeta}}. \tag{4.1.6}$$

Case 1. When

$$A_0=\frac{A_1\left(-1+13\alpha\right)}{18\alpha},\ B_1=0,\ A_2=\frac{A_1}{3},\ B_2=0,\ \beta=-2,$$
$$h=\frac{A_1\left(-2+\alpha+\alpha^2\right)}{36\alpha\epsilon},\ k=\frac{A_1\left(-1+\alpha\right)\left(2+\alpha+\alpha\epsilon\right)}{72\alpha\epsilon},$$

we have hyperbolic type solution as shown in Figure 4.1.

$$u_1\left(x,t\right)=\frac{1}{18}A_1\left(1-\frac{1}{\alpha}-\frac{3}{1+\cosh\left[x-\frac{A_1t(-2+\alpha+\alpha^2)}{36\alpha\epsilon}\right]}\right). \tag{4.1.7}$$

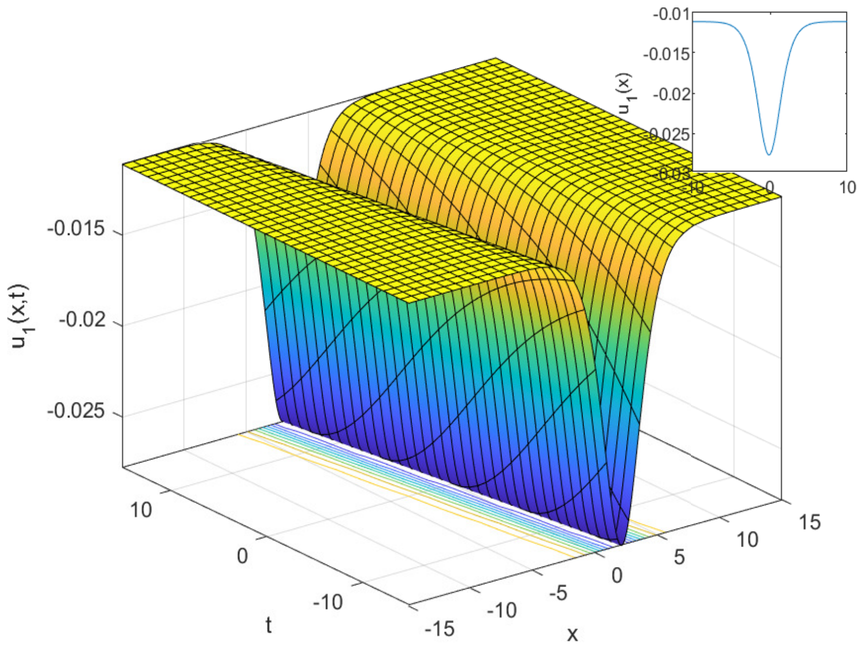

Figure 4.1. 3D profile and 2D graphs of Eq. (4.1.7) using $A_1 = 0.2$, $\alpha = 0.5$ and $\epsilon = 0.1$.

Case 2. When

$$A_0 = -\frac{2\,(h-2k)\,(-1+13\alpha)}{(-1+\alpha)\,\alpha},\; A_1 = 0,\; B_1 = -\frac{72\,(h-2k)}{-1+\alpha},$$
$$A_2 = 0,\; B_2 = -\frac{48\,(h-2k)}{-1+\alpha},\; \epsilon - \frac{(h-2k)\,(2+\alpha)}{h\alpha},\; \beta = -2,$$

we get exponential type solution as seen in Figure 4.2.

$$u_2\,(x,t) = -\frac{2\,(h-2k)\left(4\mathrm{e}^{2ht}\,(-1+\alpha) + \mathrm{e}^{2x}\,(-1+\alpha) - 4\mathrm{e}^{ht+x}\,(1+2\alpha)\right)}{\left(2\mathrm{e}^{ht}+\mathrm{e}^{x}\right)^2(-1+\alpha)\,\alpha}. \tag{4.1.8}$$

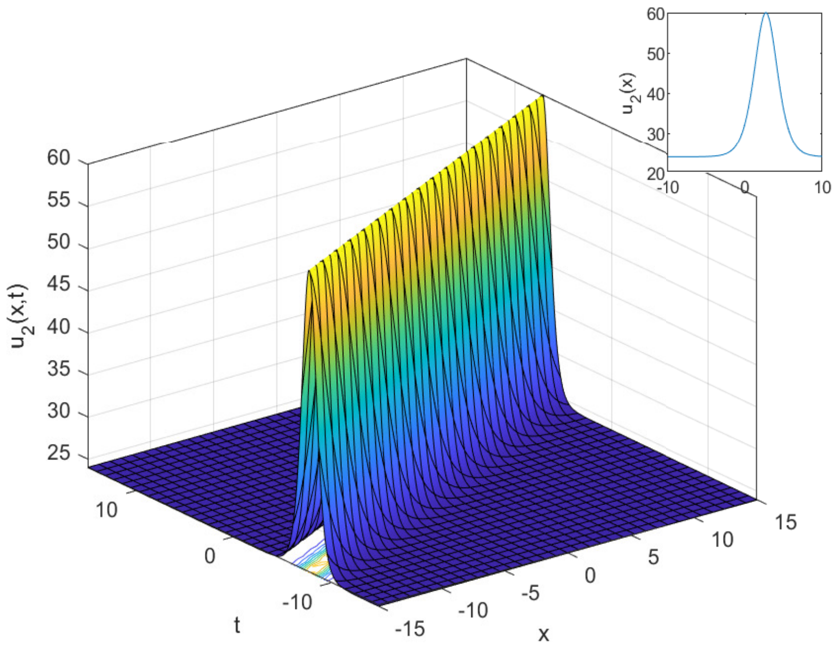

Figure 4.2. 3D profile and 2D graphics of Eq. (4.1.8) using $h = 2$, $\alpha = 0.5$ and $k = 4$.

Family 2. When $\mathrm{r}_j = \{-2-i, 2-i, -1, 1\}, s_j = \{i, -i, i, -i\}$, then Eq. (3.2.5) takes the form

$$\psi(\zeta) = \frac{\cos(\zeta) + 2\sin(\zeta)}{\sin(\zeta)}. \tag{4.1.9}$$

Case 1. When

$$A_0 = \frac{B_1(8-13\alpha)}{60\alpha},\ A_1 = 0,\ A_2 = 0,\ B_2 = -\frac{5B_1}{4},\ \beta = -2,$$
$$h = -\frac{B_1(-8+\alpha)(4+\alpha)}{240\alpha\epsilon},\ k = \frac{B_1(4+\alpha)(8+\alpha(-1+4\epsilon))}{480\alpha\epsilon},$$

we get periodic singular solution as shown in Figure 4.3.

$$u_3(x,t) = \frac{1}{60}B_1\left(\begin{array}{l} -\dfrac{15}{\left(\cos\left(x+\frac{B_1t(-8+\alpha)(4+\alpha)}{240\alpha\epsilon}\right)+2\sin\left(x+\frac{B_1t(-8+\alpha)(4+\alpha)}{240\alpha\epsilon}\right)\right)^2} \\ +2+\dfrac{8}{\alpha} \end{array}\right). \tag{4.1.10}$$

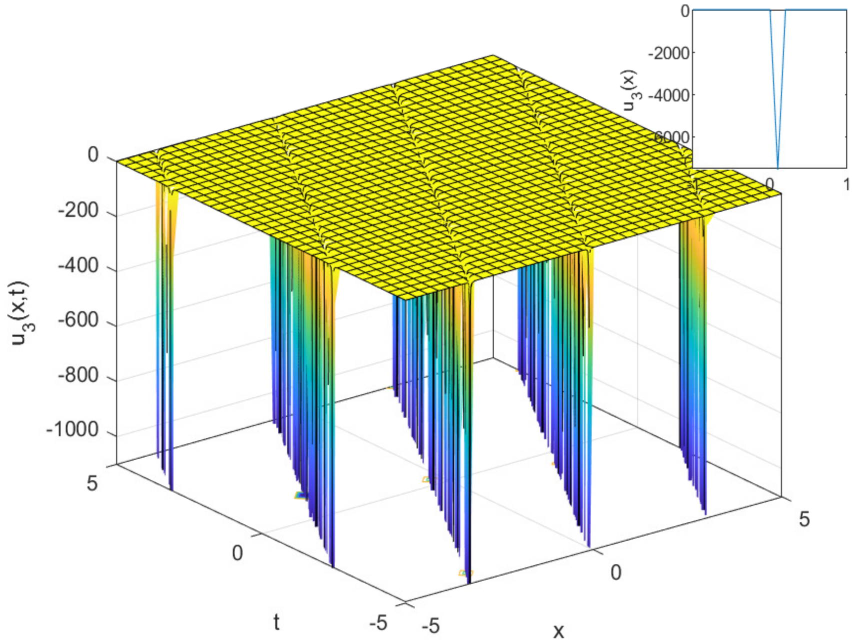

Figure 4.3. 3D profile and 2D graphics of Eq. (4.1.10) using $B_1 = 0.2$, $\alpha = 0.5$ and $\epsilon = 0.1$.

Case 2.

$$A_0 = \frac{A_1 (8 - 13\alpha)}{12\alpha},\ B_1 = 0,\ A_2 = -\frac{A_1}{4},\ B_2 = 0,\ \beta = -2,$$
$$\epsilon - \frac{A_1 (-8 + \alpha)(4 + \alpha)}{48h\alpha},\ k = \frac{1}{24}(12h + A_1 (4 + \alpha)),$$

we get singular solution as seen in Figure 4.4.

$$u_4 (x, t) = -\frac{A_1 \left(-8 + \alpha + 3\alpha \cot (ht - x)^2\right)}{12\alpha}. \tag{4.1.11}$$

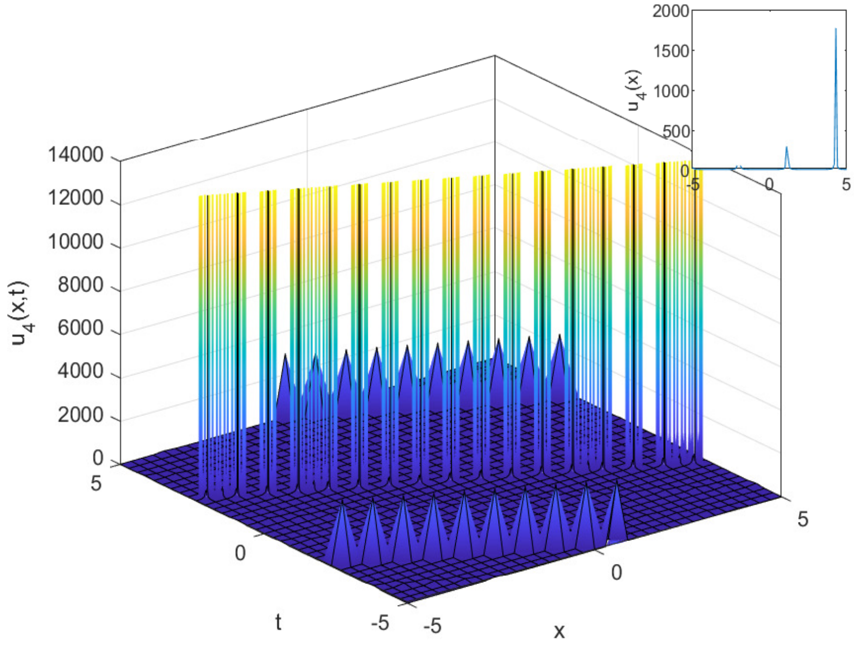

Figure 4.4. 3D profile and 2D graphics of Eq. (4.1.11) using $A_1 = -2$, $\alpha = -0.5$ and $h = -2$.

Family 3. When $r_j = \{2, 0, 1, 1\}, s_j = \{-1, 0, 1, -1\}$, then Eq. (3.2.5) reduced to the following form

$$\psi(\zeta) = \frac{\cosh(\zeta) - \sinh(\zeta)}{\cosh(\zeta)}. \tag{4.1.12}$$

Case 1. When

$$A_0 = -\frac{A_1(-4+\alpha)}{3\alpha}, \; B_1 = 0, \; A_2 = -\frac{A_1}{2}, \; B_2 = 0, \; \beta = -2,$$
$$h = -\frac{A_1(-4+\alpha)(8+\alpha)}{24\alpha\epsilon}, \; k = -\frac{A_1(-4+\alpha)(8+\alpha+4\alpha\epsilon)}{48\alpha\epsilon},$$

we have dark solution as shown in Figure 4.5.

$$u_5(x,t) = \frac{A_1\left(8+\alpha-3\alpha\tanh\left(x+\frac{A_1 t(-4+\alpha)(8+\alpha)}{24\alpha\epsilon}\right)^2\right)}{6\alpha}. \tag{4.1.13}$$

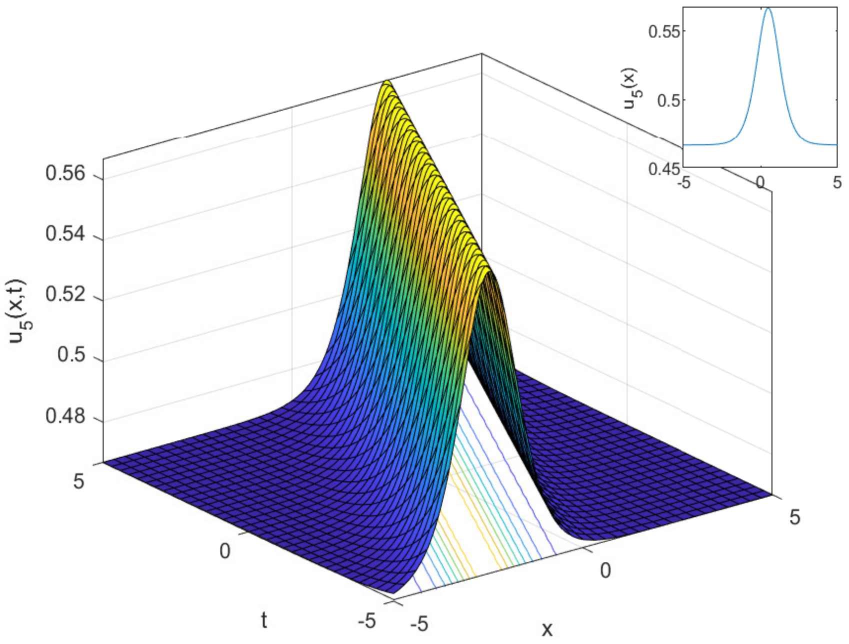

Figure 4.5. 3D profile and 2D graphics of Eq. (4.1.13) using $A_1 = 0.2$, $\alpha = 0.5$ and $\epsilon = 0.1$.

Case 2.

$$
\begin{aligned}
A_0 &= -\frac{h - 2k + \frac{\sqrt{(h-2k)^2}(-4+\alpha)}{\sqrt{(-4+\alpha)^2}}}{\alpha}, B_2 = 0, \beta = -2, \\
\epsilon &= -\frac{4h - 8k + \frac{\sqrt{(h-2k)^2}(-4+\alpha)(4+\alpha)}{\sqrt{(-4+\alpha)^2}}}{4h\alpha}, B_1 = 0, \\
A_1 &= \frac{6\sqrt{(h-2k)^2}}{\sqrt{(-4+\alpha)^2}}, A_2 = -\frac{3\sqrt{(h-2k)^2}}{\sqrt{(-4+\alpha)^2}},
\end{aligned}
$$

we get bright solution solution as shown in Figure 4.6.

$$
\begin{aligned}
u_6(x,t) =& \frac{-\sqrt{(h-2k)^2}\,(-4+\alpha) - (h-2k)\sqrt{(-4+\alpha)^2}}{\sqrt{(-4+\alpha)^2}\alpha} \\
&+ \frac{3\sqrt{(h-2k)^2}\alpha sech(ht-x)^2}{\sqrt{(-4+\alpha)^2}\alpha}.
\end{aligned}
\tag{4.1.14}
$$

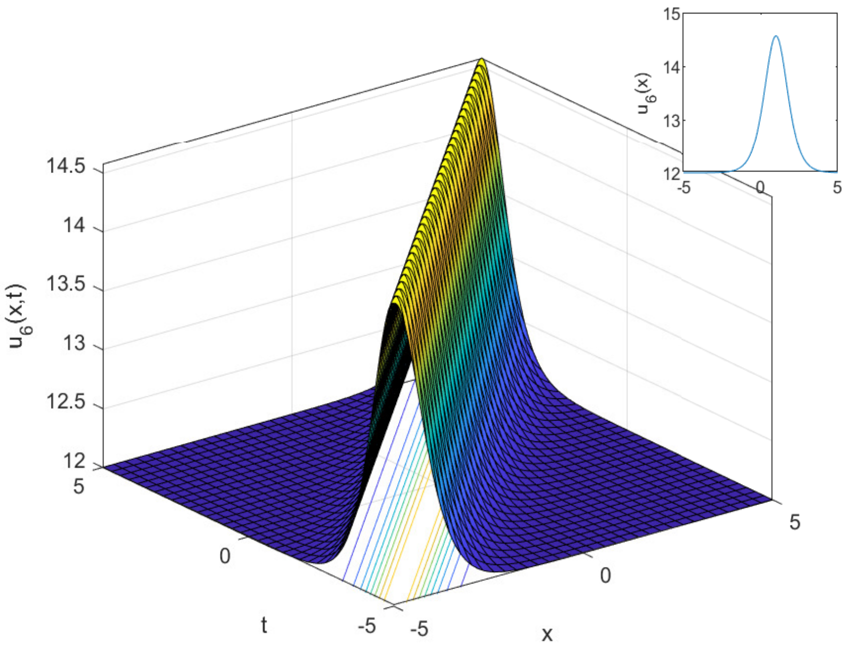

Figure 4.6. 3D profile and 2D graphics of Eq. (4.1.14) using $A_1 = 0.2$, $\alpha = 0.5, h = 1$ and $k = 2$.

Family 4. When $r_j = \{1-i, 1+i, 1, 1\}, s_j = \{i, -i, i, -i\}$, then Eq. (3.2.5) reduced to the following form

$$\psi(\zeta) = \frac{\cos(\zeta) + \sinh(\zeta)}{\cos(\zeta)}. \tag{4.1.15}$$

Case 1. When

$$A_0 = -\frac{B_1(-2+\alpha)}{3\alpha}, A_1 = 0,\ A_2 = 0,\ B_2 = -B_1,\ \ \beta = -2,$$
$$h = -\frac{b1(-8+\alpha)(4+\alpha)}{48\alpha\epsilon}, k = \frac{b1(4+\alpha)(8+\alpha(-1+4\epsilon))}{96\alpha\epsilon},$$

we have periodic singular solution as seen in Figure 4.7.

$$u_7(x,t) = \frac{1}{60}B_1\left(\frac{-15}{\left(\cos\left(x+\frac{B_1 t(-8+\alpha)(4+\alpha)}{240\alpha\epsilon}\right)+2\sin\left(x+\frac{B_1 t(-8+\alpha)(4+\alpha)}{240\alpha\epsilon}\right)\right)^2} + 2 + \frac{8}{\alpha}\right). \tag{4.1.16}$$

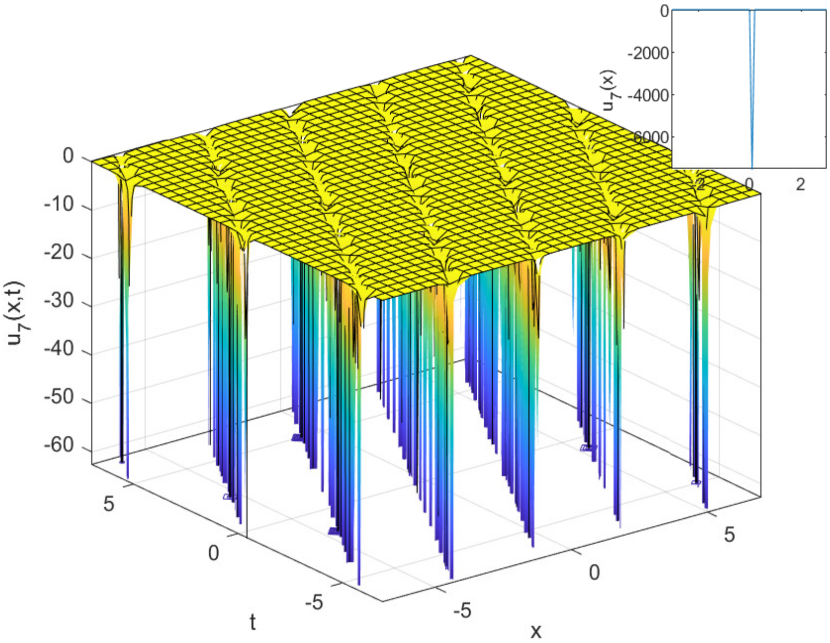

Figure 4.7. 3D profile and 2D graphics of Eq. (4.1.16) using $B_1 = 0.2$, $\alpha = 0.5$ and $\epsilon = 0.1$.

Case 2.

$$A_0 = -\frac{B_1(-2+\alpha)}{3\alpha}, A_1 = 0,\ B_2 = -B_1,\ \beta = -2,\ A_2 = 0,$$
$$h = 2k - \frac{1}{12}B_1(4+\alpha),\ \epsilon = \frac{B_1(-8+\alpha)(4+\alpha)}{4\alpha(-24k+B_1(4+\alpha))},$$

we have periodic singular solution as seen in Figure 4.8.

$$u_8(x,t) = \frac{1}{6}B_1\left(1 + \frac{4}{\alpha} + \frac{3}{-1+\sin\left(4kt - 2x - \frac{1}{6}B_1t(4+\alpha)\right)}\right). \tag{4.1.17}$$

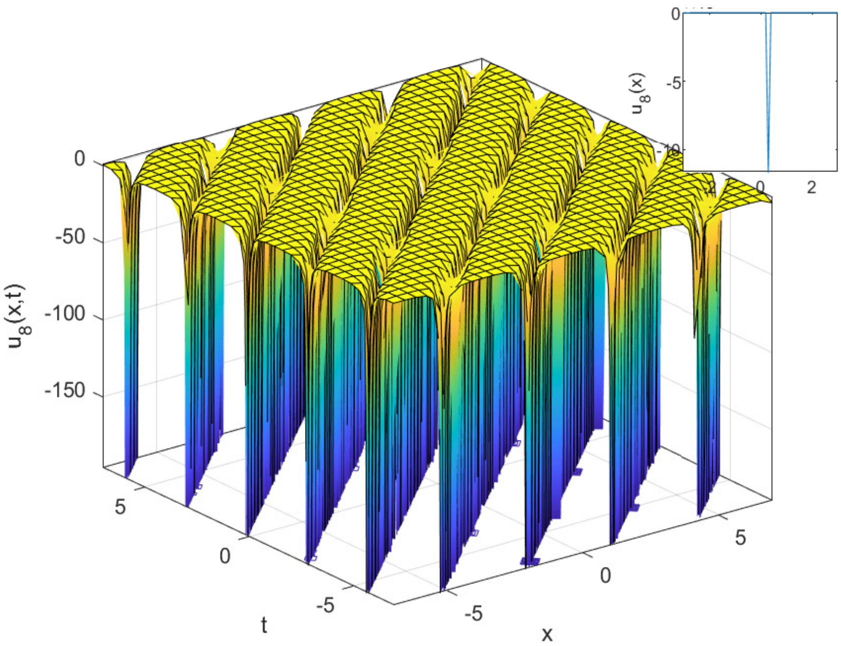

Figure 4.8. 3D profile and 2D graphics of Eq. (4.1.17) using $B_1 = 2$, $\alpha = 1.5, k = 1$ and $A_1 = 2$.

Family 5. When $r_j = \{-1, 3, 1, -1\}, s_j = \{1, -1, 1, -1\}$, then Eq. (3.2.5) reduced to the following form

$$\psi(\zeta) = \frac{\cosh(\zeta) - 2\sinh(\zeta)}{\sinh(\zeta)}. \tag{4.1.18}$$

Case 1. When

$$A_0 = \frac{A_1(-8 + 11\alpha)}{12\alpha}, B_1 = 0, A_2 = \frac{A_1}{4}, B_2 = 0, \beta = -2,$$
$$h = \frac{A_1(-4 + \alpha)(8 + \alpha)}{48\alpha\epsilon}, k = \frac{A_1(-4 + \alpha)(8 + \alpha + 4\alpha\epsilon)}{96\alpha\epsilon},$$

we have a dark soliton solution as shown in Figure 4.9.

$$u_9(x,t) = \frac{A_1\left(8 + \alpha - 3\alpha\tanh\left(x + \frac{A_1 t(-4+\alpha)(8+\alpha)}{24\alpha\epsilon}\right)^2\right)}{6\alpha}. \tag{4.1.19}$$

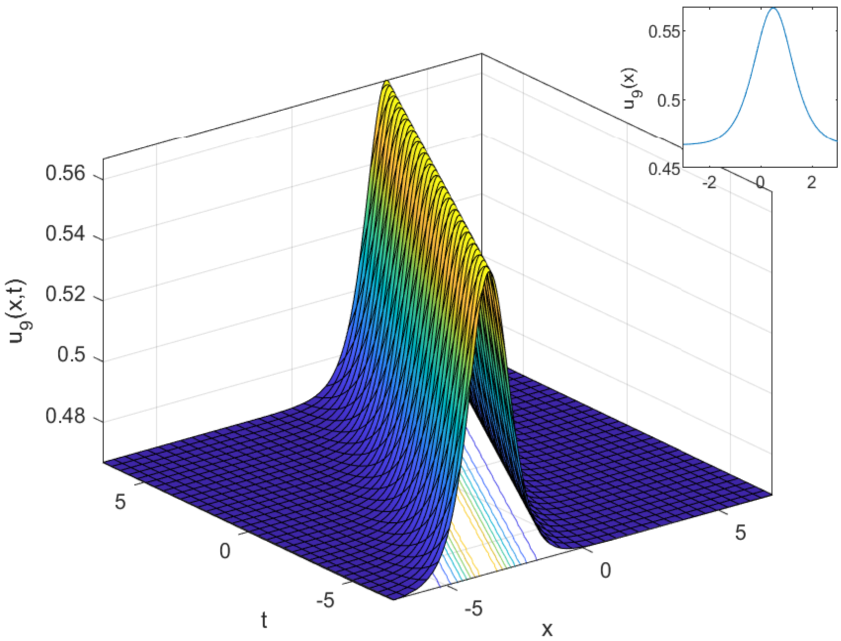

Figure 4.9. 3D profile and 2D graphics of Eq. (4.1.19) using $A_1 = 0.2$, $\alpha = 0.5$ and $\epsilon = 1$.

Case 2.

$$A_0 = \frac{A_1(-8+11\alpha)}{12\alpha}, B_1 = 0, A_2 = \frac{A_1}{4}, B_2 = 0, \beta = -2,$$
$$k = \frac{1}{24}(12h + A_1(-4+\alpha)), \epsilon = \frac{A_1(-4+\alpha)(8+\alpha)}{48h\alpha},$$

we have singular solution as seen in Figure 4.10.

$$u_{10}(x,t) = \frac{A_1\left(-8+2\alpha+3\alpha csch(ht-x)^2\right)}{12\alpha}. \tag{4.1.20}$$

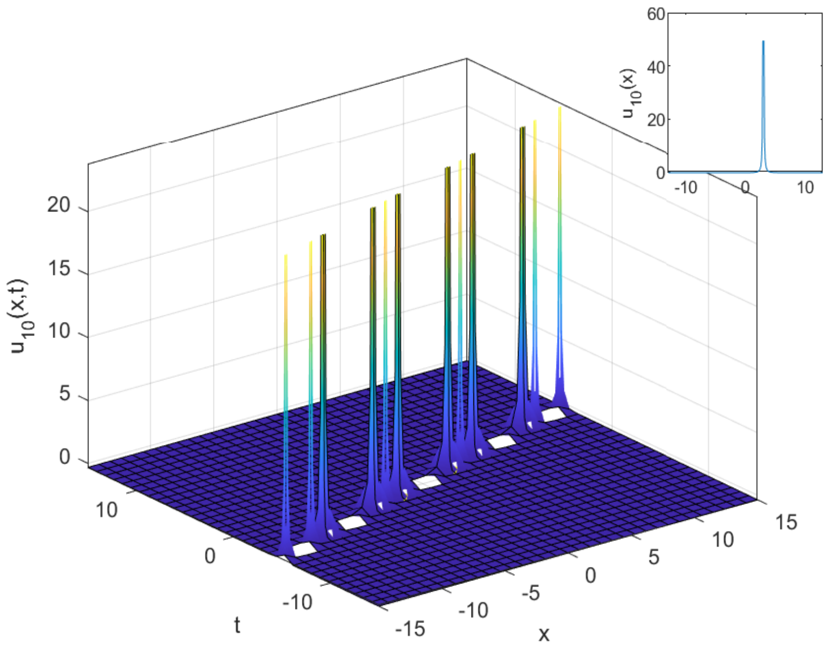

Figure 4.10. 3D profile and 2D graphics of Eq. (4.1.20) using $A_1 = 0.2$, $\alpha 2, h = 3$ and $\alpha = 2$.

Family 6. When $r_j = \{1, 1, -1, 1\}, s_j = \{1, -1, 1, -1\}$, then Eq. (3.2.5) reduced to the following form

$$\psi(\zeta) = \frac{-\cosh(\zeta)}{\sinh(\zeta)}. \tag{4.1.21}$$

Case 1. When

$$h = \frac{a2(-16+\alpha)(32+\alpha)}{12\alpha\epsilon}, k = \frac{a2(-16+\alpha)(32+\alpha+16\alpha\epsilon)}{24\alpha\epsilon},$$
$$A_0 = \frac{2A_2(-64+\alpha)}{3\alpha}, B_1 = 0, B_2 = A_2, \beta = -2,\ A_1 = 0,$$

we have hyperbolic type solution as shown in Figure 4.11.

$$\begin{aligned} u_{11}(x,t) = \frac{2A_2(-64+\alpha)}{3\alpha} &+ A_2 \coth\left(x - \frac{A_2 t(-16+\alpha)(32+\alpha)}{12\alpha\epsilon}\right)^2 \\ &+ A_2 \tanh\left(x - \frac{A_2 t(-16+\alpha)(32+\alpha)}{12\alpha\epsilon}\right)^2. \end{aligned} \tag{4.1.22}$$

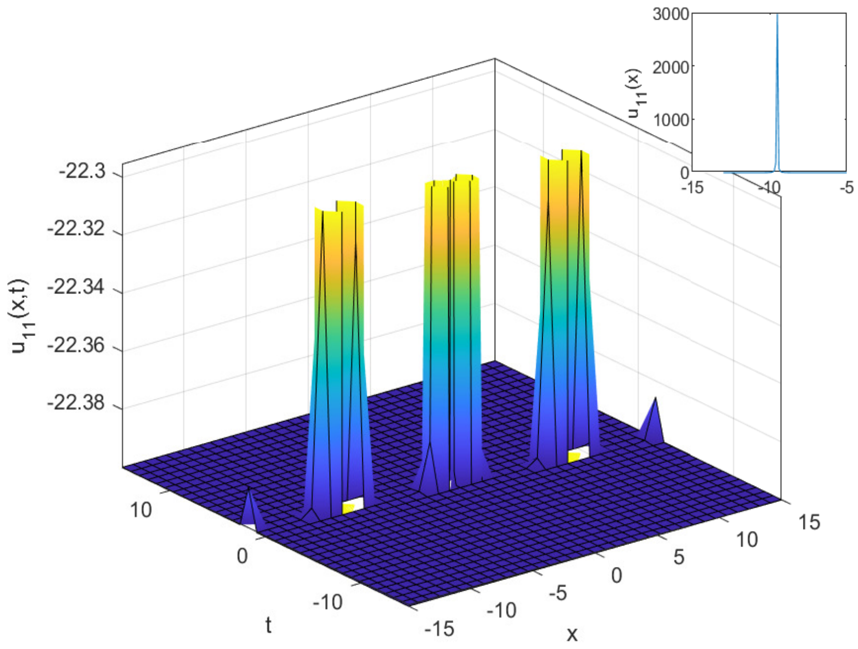

Figure 4.11. 3D profile and 2D graphics of Eq. (4.1.22) using $A_2 = 1.2$, $\alpha = 2$ and $\epsilon = 2.5$.

Case 2.

$$A_0 = \frac{16k\epsilon^2(1+64\epsilon)}{-1+256\epsilon^2}, A_1 = 0, B_1 = 0, A_2 = \frac{24k\epsilon^2}{-1+256\epsilon^2},$$
$$B_2 = \frac{24k\epsilon^2}{-1+256\epsilon^2}, \beta = -2, h = 2k\left(2+\frac{1}{-1+16\epsilon}\right), \alpha = -\frac{1}{\epsilon},$$

we have hyperbolic type solution as shown in Figure 4.12.

$$\begin{aligned} u_{12}(x,t) = {} & \frac{16k\epsilon^2(1+64\epsilon)}{-1+256\epsilon^2} + \frac{24k\epsilon^2 \coth\left(x-2kt\left(2+\frac{1}{-1+16\epsilon}\right)\right)^2}{-1+256\epsilon^2} \\ & + \frac{24k\epsilon^2 \tanh\left(x-2kt\left(2+\frac{1}{-1+16\epsilon}\right)\right)^2}{-1+256\epsilon^2}. \end{aligned} \tag{4.1.23}$$

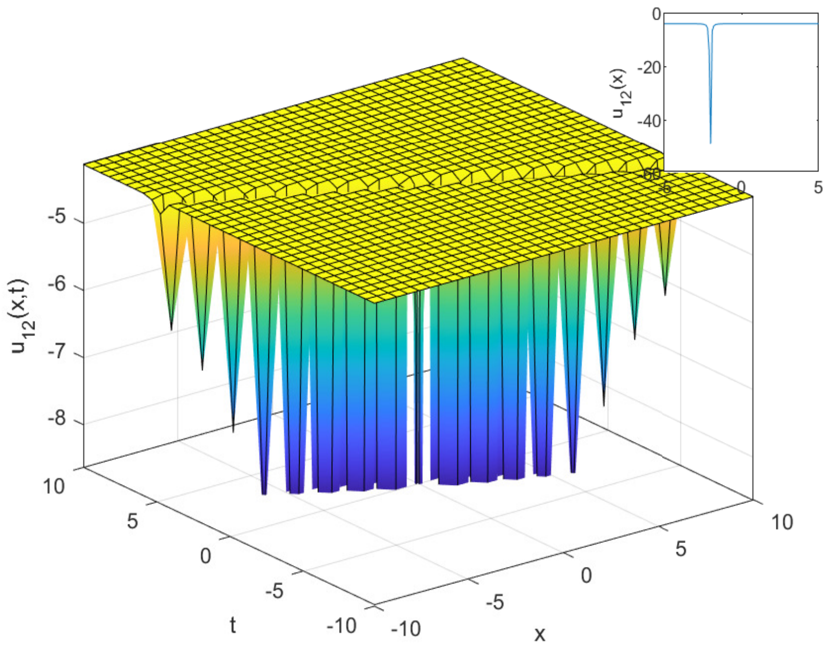

Figure 4.12. 3D profile and 2D graphics of Eq. (4.1.23) using $\epsilon = 2$ and $k = -0.5$.

4.2 The Strain Waves in Micro-Structured Solids

In this portion, we applied the generalized exponential rational function method to the strain waves in micro-structured solids.

The guiding equation for the micro-strain wave in micro-structured solids is defined [23]

$$\begin{aligned} &\phi_{tt} - \phi_{xx} - S\beta_1\left(\phi^2\right)_{xx} - \lambda\beta_2\phi_{xxt} + \delta\beta_3\phi_{xxxx} - \left(\delta\beta_4 - \lambda^2\beta_7\right)_{\phi_{xxtt}} \\ &+ \lambda\delta\left(\beta_5\phi_{xxxxt} + \beta_6\phi_{xxttt}\right) = 0, \end{aligned} \tag{4.2.1}$$

where S stands for an elastic strain, δ represents the ratio between micro-structure size and the length of wave, λ represents the influence of dissipation and $\beta_i \in \mathbb{R} - \{0\}$, for $1 \leq i \leq 7$. The balance among non-linearity and dispersion is said to have occurred when $\delta = O(S)$. Putting λ =0 in Eq. (4.2.1) provides a non-dissipative case that is driven by the following double dispersive equation

$$\phi_{tt} - \phi_{xx} - S\left(\beta_1\left(\phi^2\right)_{xx} - \beta_3\phi_{xxxx} + \beta_4\phi_{xxtt}\right) = 0. \tag{4.2.2}$$

In certain nonlinear strain wave models for adaptable or elastic solids, different methodologies could be used to portray the in uence of macro-dissipation. The synchronized impact of large scale and micro-dissipation on shock wave spread has been investigated in a series of studies by neglecting the micro-structure's inertia and micro-stresses that could be associated with the fine structure [89].

Recently, Eq. (4.2.2) have been investigated by several distinct methods including the new generalized $(G'/G)-$ expansion method [25], the exponential expansion method [26], the Kudryashov and functional variable methods [27], the sine-Gordon expansion method [90], the modified extended mapping technique [91], the modified extended direct algebraic method [92].

Inserting the wave transformation

$$\phi = U(\zeta), \zeta = x - \kappa t, \tag{4.2.3}$$

into Eq. (4.2.2), we get

$$\left(\kappa^2 - 1\right) U'' - S\beta_1 \left(U^2\right)'' + S\left(\beta_3 - \beta_4 \kappa^2\right) U^{(4)} = 0. \tag{4.2.4}$$

Integrating Eq. (4.2.4) twice with respect to ζ, yields

$$S\left(\beta_3 - \beta_4 \kappa^2\right) U'' + \left(\kappa^2 - 1\right) U - S\beta_1 U^2 = 0, \tag{4.2.5}$$

where the integration constants are considered zero.

Using the balance principle between the terms of U'' and U^2 in Eq. (4.2.5), we get $m = 2$, then Eq. (3.1.4) takes the form

$$U(\zeta) = A_0 + A_1 f(\zeta) + \frac{B_1}{f(\zeta)} + A_2 f^2(\zeta) + \frac{B_2}{f^2(\zeta)}. \tag{4.2.6}$$

Taking Eq. (3.2.5) into account, we have to following family:

Family 1. If we set $r_j = \{-2, -1, 1, 1\}, s_j = \{0, 1, 0, 1\}$, then Eq. (3.2.5) turn to the following form

$$\psi(\zeta) = \frac{-2 - e^{\zeta}}{1 + e^{\zeta}}. \tag{4.2.7}$$

Case 1.

$$A_0 = \frac{13\left(-1 + \kappa^2\right)}{S\beta_1}, A_1 = \frac{18\left(-1 + \kappa^2\right)}{S\beta_1}, B_1 = 0, A_2 = \frac{6\left(-1 + \kappa^2\right)}{S\beta_1}, B_2 = 0,$$
$$\beta_3 = \frac{-1 + \left(1 + S\beta_4\right)\kappa^2}{S},$$

we have hyperbolic type solution as shown in Figure 4.13.

$$\phi_1(x,t) = \frac{\left(-1 + \kappa^2\right)\left(-2 + \cosh(x - t\kappa)\right)}{S\beta_1\left(1 + \cosh(x - t\kappa)\right)}. \tag{4.2.8}$$

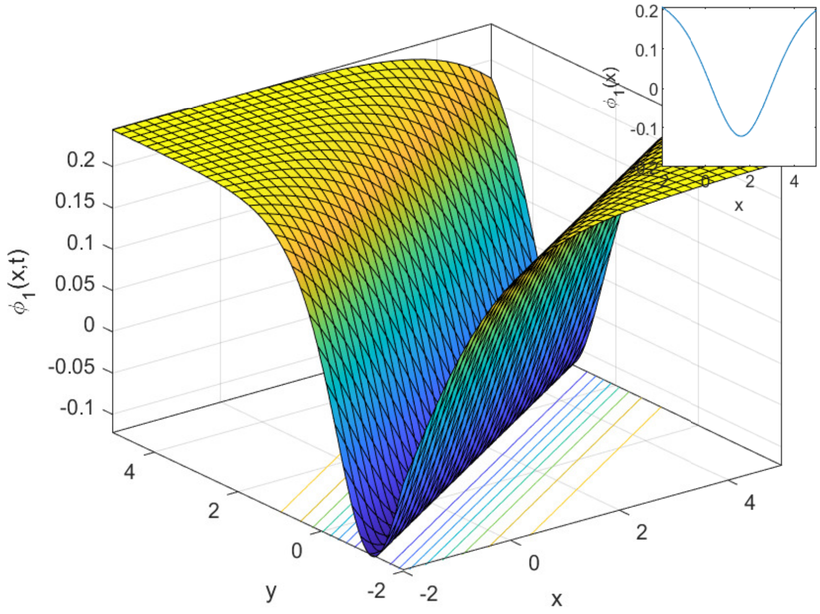

Figure 4.13. Topological type profile of Eq. (4.2.8) using $S = 2.2$, $\beta_1 = 2.9$ and $\kappa = 1.6$.

Case 2.

$$A_0 = \frac{13\left(\beta_3 - \beta_4\right)}{\beta_1 + S\beta_1\beta_4}, A_1 = 0, B_1 = \frac{36\left(\beta_3 - \beta_4\right)}{\beta_1 + S\beta_1\beta_4}, A_2 = 0, B_2 = \frac{24\left(\beta_3 - \beta_4\right)}{\beta_1 + S\beta_1\beta_4},$$
$$\kappa = \frac{\sqrt{1 + S\beta_3}}{\sqrt{1 + S\beta_4}},$$

inserting the above values and Eq. (4.2.7) into Eq. (4.2.5), we have the following exponential solution as presented in Figure 4.14.

$$\phi_2\left(x, t\right) = \frac{\left(\mathrm{e}^{2x} + 4\mathrm{e}^{\frac{2t\sqrt{1+S\beta_3}}{\sqrt{1+S\beta_4}}} - 8\mathrm{e}^{x+\frac{t\sqrt{1+S\beta_3}}{\sqrt{1+S\beta_4}}}\right)\left(\beta_3 - \beta_4\right)}{\left(\mathrm{e}^{x} + 2\mathrm{e}^{\frac{t\sqrt{1+S\beta_3}}{\sqrt{1+S\beta_4}}}\right)^2\left(\beta_1 + S\beta_1\beta_4\right)}. \tag{4.2.9}$$

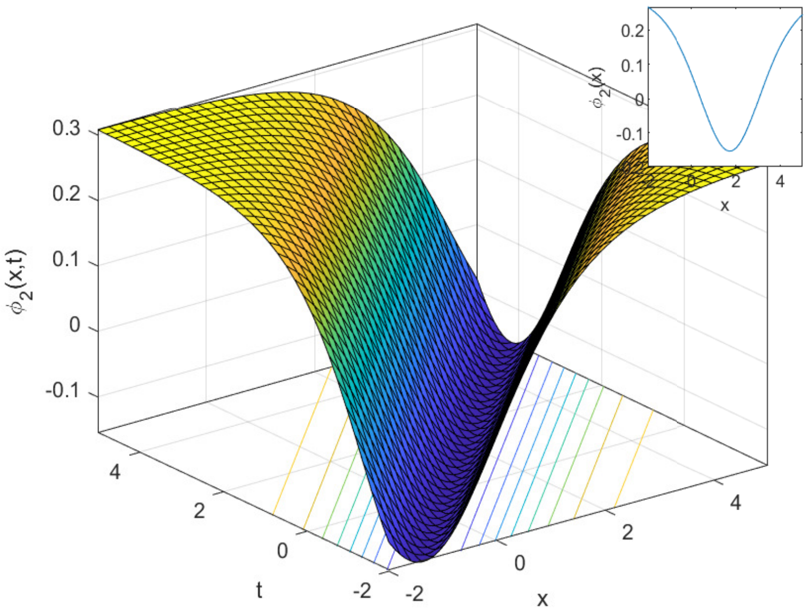

Figure 4.14. Topological type profile of Eq. (4.2.9) using $S = 0.2$, $\beta_1 = 0.9$, $\beta_3 = 0.7$ and $\beta_4 = 0.4$.

Family 2. Let $r_j = \{-2-i, 2-i, -1, 1\}, s_j = \{i, -i, i, -i\}$, then Eq. (3.2.5) takes the following form

$$\psi(\zeta) = \frac{\cos(\zeta) + 2\sin(\zeta)}{\sin(\zeta)}. \tag{4.2.10}$$

Case 1.

$$A_0 = \frac{-1+\kappa^2+14\sqrt{(-1+\kappa^2)^2}}{2S\beta_1}, A_1 = -\frac{6\sqrt{(-1+\kappa^2)^2}}{S\beta_1},$$
$$B_1 = 0, A_2 = \frac{3\sqrt{(-1+\kappa^2)^2}}{2S\beta_1}, B_2 = 0, \beta_3 = \beta_4\kappa^2 + \frac{\sqrt{(-1+\kappa^2)^2}}{4S},$$

substituting the above values and Eq. (4.2.10) into Eq. (4.2.5), we have a periodic singular solution as seen in Figure 4.15.

$$\phi_3(x,t) = \frac{-1+\kappa^2+2\sqrt{(-1+\kappa^2)^2}+3\sqrt{(-1+\kappa^2)^2}\cot(x-t\kappa)^2}{2S\beta_1}. \tag{4.2.11}$$

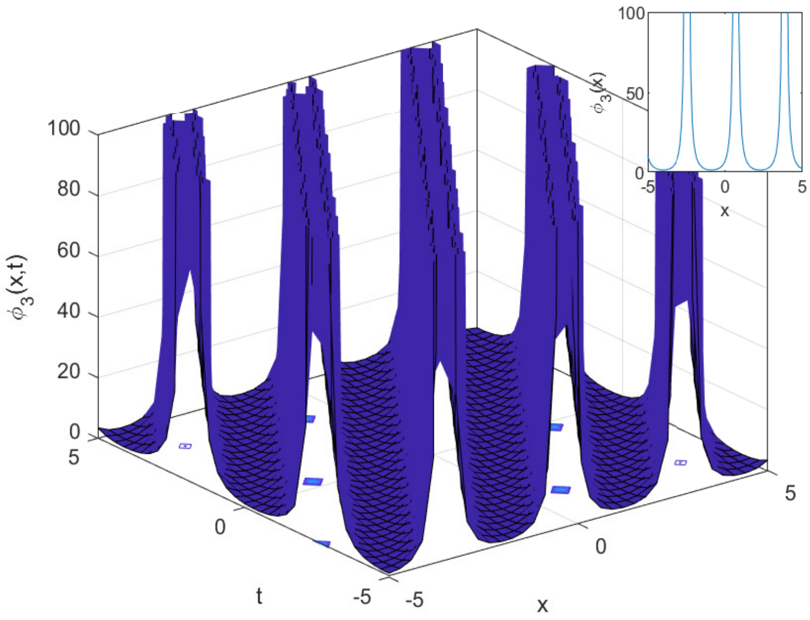

Figure 4.15. Periodic singular type profile of Eq. (4.2.11) using $\beta_1 = 0.5$, $S = 0.4$ and $\kappa = 0.7$.

Case 2

$$A_0 = \frac{26(\beta_3 - \beta_4)}{\beta_1 - 4S\beta_1\beta_4}, A_1 = 0, B_1 = \frac{120(\beta_3 - \beta_4)}{\beta_1(-1 + 4S\beta_4)}, A_2 = 0, B_2 = \frac{150(\beta_3 - \beta_4)}{\beta_1 - 4S\beta_1\beta_4},$$
$$\kappa = \frac{\sqrt{1 - 4S\beta_3}}{\sqrt{1 - 4S\beta_4}},$$

plugging the above values and Eq. (4.2.10) into Eq. (4.2.5), we have a periodic solution as shown Figure 4.16.

$$\phi_4(x,t) = \frac{2(\beta_3 - \beta_4)\left(2 - \frac{15}{\left(\cos\left(x + \frac{t\sqrt{1-4S\beta_3}}{\sqrt{1-4S\beta_4}}\right) + 2\sin\left(x + \frac{t\sqrt{1-4S\beta_3}}{\sqrt{1-4S\beta_4}}\right)\right)^2}\right)}{\beta_1(-1 + 4S\beta_4)}. \tag{4.2.12}$$

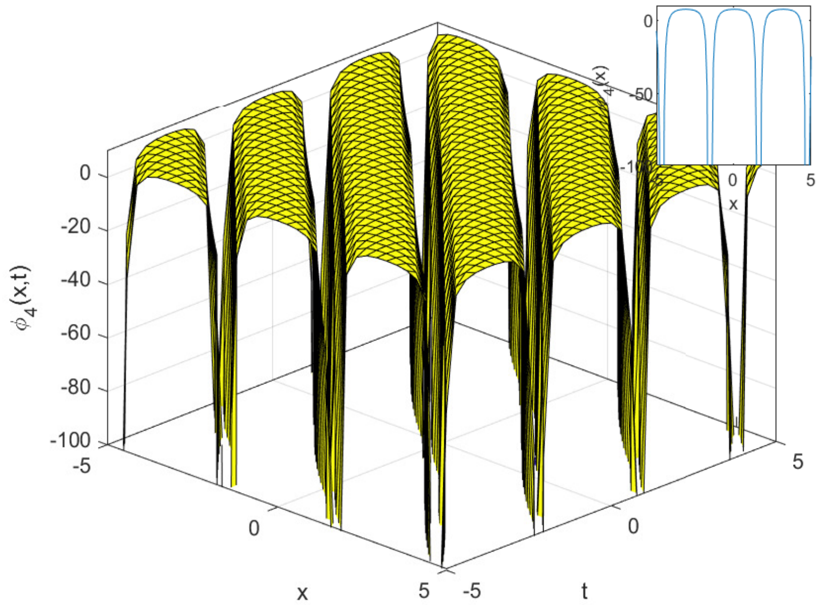

Figure 4.16. Periodic singular type profile of Eq. (4.2.12) using $\beta_3 = 0.5$, $S = 0.1$, $\beta_4 = 0.7$ and $\beta_1 = 0.9$.

Family 3. When $r_j = 2, 0, 1, 1, s_j = -1, 0, 1, -1$, then Eq. (3.2.5) takes the form

$$\psi(\zeta) = \frac{\cosh(\zeta) - \sinh(\zeta)}{\cosh(\zeta)}. \tag{4.2.13}$$

Case 1.

$$A_0 = \frac{4\left(\beta_3 - \beta_4\right)}{\beta_1 + 4S\beta_1\beta_4}, A_1 = \frac{12\left(-\beta_3 + \beta_4\right)}{\beta_1 + 4S\beta_1\beta_4}, B_1 = 0, A_2 = \frac{6\left(\beta_3 - \beta_4\right)}{\beta_1 + 4S\beta_1\beta_4}, B_2 = 0,$$
$$\kappa = \frac{\sqrt{-1 - 4S\beta_3}}{\sqrt{-1 - 4S\beta_4}},$$

inserting the above values and Eq. (4.2.13) into Eq. (4.2.5), we have non-topological type profile as shown in Figure 4.17.

$$\phi_5\left(x, t\right) = \frac{2\left(\beta_3 - \beta_4\right)\left(2 - \frac{15}{\left(\cos\left(x + \frac{t\sqrt{1-4S\beta_3}}{\sqrt{1-4S\beta_4}}\right) + 2\sin\left(x + \frac{t\sqrt{1-4S\beta_3}}{\sqrt{1-4S\beta_4}}\right)\right)^2}\right)}{\beta_1\left(-1 + 4S\beta_4\right)}. \tag{4.2.14}$$

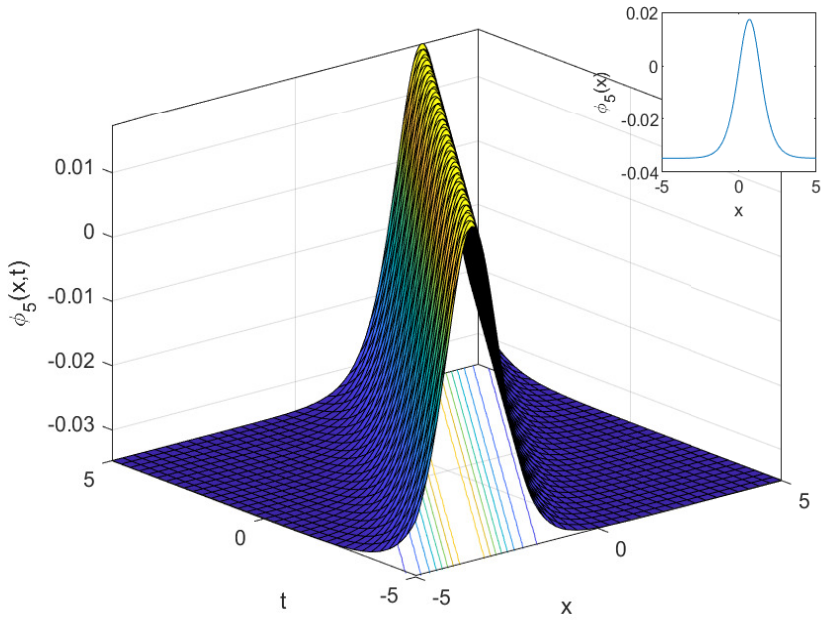

Figure 4.17. Non-topological type profile of Eq. (4.2.14) using $\beta_4 = -2$, $\beta_1 = 5$, $\beta_3 = -1$ and $S = 3$.

Case 2.

$$A_0 = \frac{-1+\kappa^2+\sqrt{(-1+\kappa^2)^2}}{2S\beta_1}, A_1 = -\frac{3\sqrt{(-1+\kappa^2)^2}}{S\beta_1},$$
$$B_1 = 0, A_2 = \frac{3\sqrt{(-1+\kappa^2)^2}}{2S\beta_1}, B_2 = 0, \beta_3 = \beta_4\kappa^2 + \frac{\sqrt{(-1+\kappa^2)^2}}{4S},$$

inserting the above values and Eq. (4.2.13) into Eq. (4.2.5), we have a bright solution as given in Figure 4.18.

$$\phi_6(x,t) = \frac{-1+\kappa^2+\sqrt{(-1+\kappa^2)^2} - 3\sqrt{(-1+\kappa^2)^2}sech(x-t\kappa)^2}{2S\beta_1}. \tag{4.2.15}$$

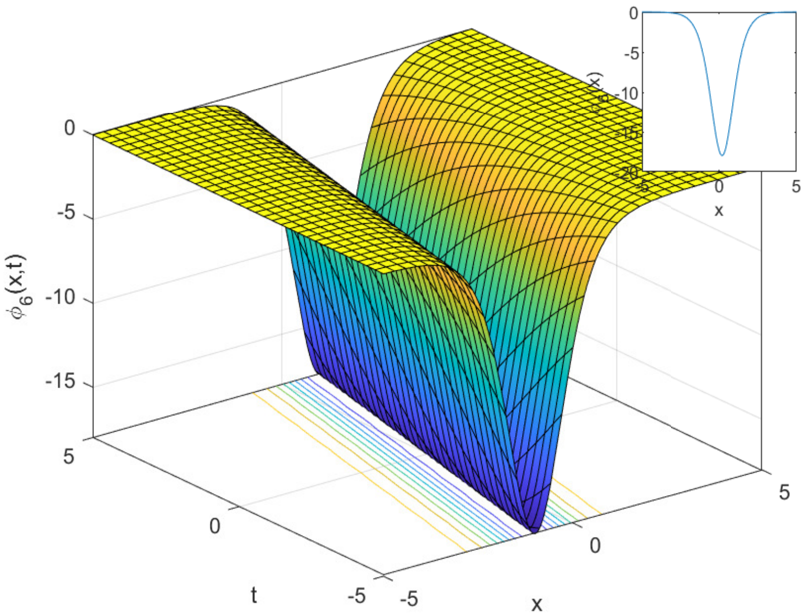

Figure 4.18. Topological type profile of Eq. (4.2.15) using $\beta_1 = 0.2$, $S = 0.4$ and $\kappa = 0.2$.

Family 4. By setting $r_j = \{-1, 1, 1, 1\}, s_j = \{1, -1, 1, -1\}$, then Eq. (3.2.5) turn to the following form

$$\psi(\zeta) = \frac{-\sinh(\zeta)}{\cosh(\zeta)}. \tag{4.2.16}$$

Case 1.

$$A_0 = -\frac{4(\beta_3 - \beta_4)}{3\beta_1}, A_1 = 0, B_1 = 0, A_2 = -\frac{2(\beta_3 - \beta_4)}{\beta_1},$$
$$B_2 = -\frac{2(\beta_3 - \beta_4)}{\beta_1}, S = -\frac{1}{4\beta_4}, \kappa = -\frac{\mathrm{i}\sqrt{-4\beta_3 + \beta_4}}{\sqrt{3}\sqrt{\beta_4}},$$

we have singular solutions as seen in Figure 4.19.

$$\begin{aligned}\phi_7(x,t) = \frac{4(\beta_3 - \beta_4)}{\beta_1} &- \frac{2(\beta_3 - \beta_4)\coth\left(x - \frac{\mathrm{i}t\sqrt{-4\beta_3+\beta_4}}{\sqrt{3}\sqrt{\beta_4}}\right)^2}{\beta_1} \\ &- \frac{2(\beta_3 - \beta_4)\tanh\left(x - \frac{\mathrm{i}t\sqrt{-4\beta_3+\beta_4}}{\sqrt{3}\sqrt{\beta_4}}\right)^2}{\beta_1}.\end{aligned} \tag{4.2.17}$$

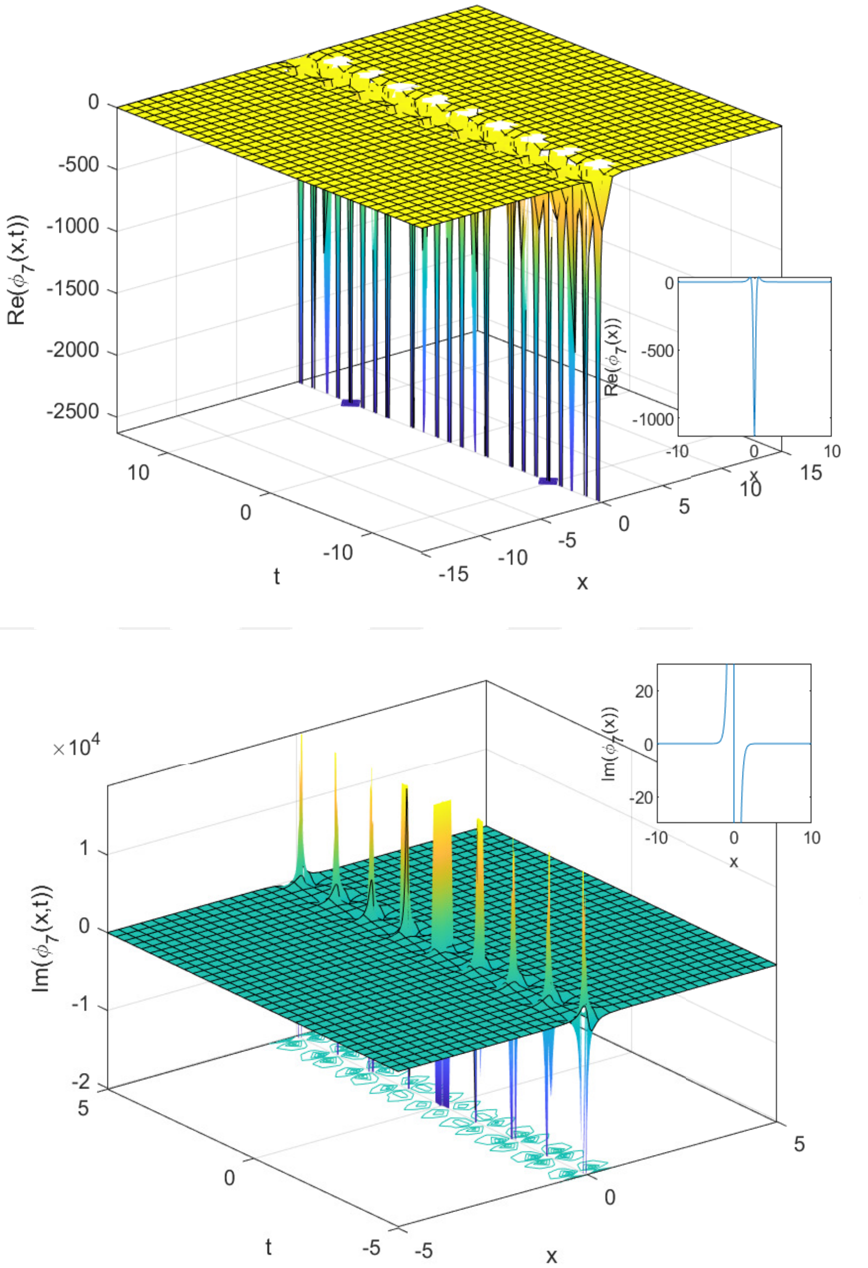

Figure 4.19. Singular type profiles of Eq. (4.2.17) using $\beta_4 = 4$, $\beta_1 = 0.2$ and $\beta_3 = -4$.

Case 2.

$$A_0 = \frac{12\,(\beta_3 - \beta_4)}{\beta_1\,(-1 + 16S\beta_4)}, A_1 = 0, A_2 = \frac{6\,(\beta_3 - \beta_4)}{\beta_1 - 16S\beta_1\beta_4},$$
$$B_2 = \frac{6\,(\beta_3 - \beta_4)}{\beta_1 - 16S\beta_1\beta_4}, B_1 = 0,\ \kappa = -\frac{\sqrt{1 - 16S\beta_3}}{\sqrt{1 - 16S\beta_4}},$$

we have hyperbolic solution as shown in Figure 4.20.

$$\phi_8\left(x,t\right)=\frac{12\left(\beta_3-\beta_4\right)}{\beta_1\left(-1+16S\beta_4\right)}+\frac{6\left(\beta_3-\beta4\right)\coth\left(x+\frac{t\sqrt{1-16S\beta_3}}{\sqrt{1-16S\beta_4}}\right)^2}{\beta_1-16S\beta_1\beta_4}$$
$$+\frac{6\left(\beta_3-\beta_4\right)\tanh\left(x+\frac{t\sqrt{1-16S\beta_3}}{\sqrt{1-16S\beta_4}}\right)^2}{\beta_1-16S\beta_1\beta_4}. \tag{4.2.18}$$

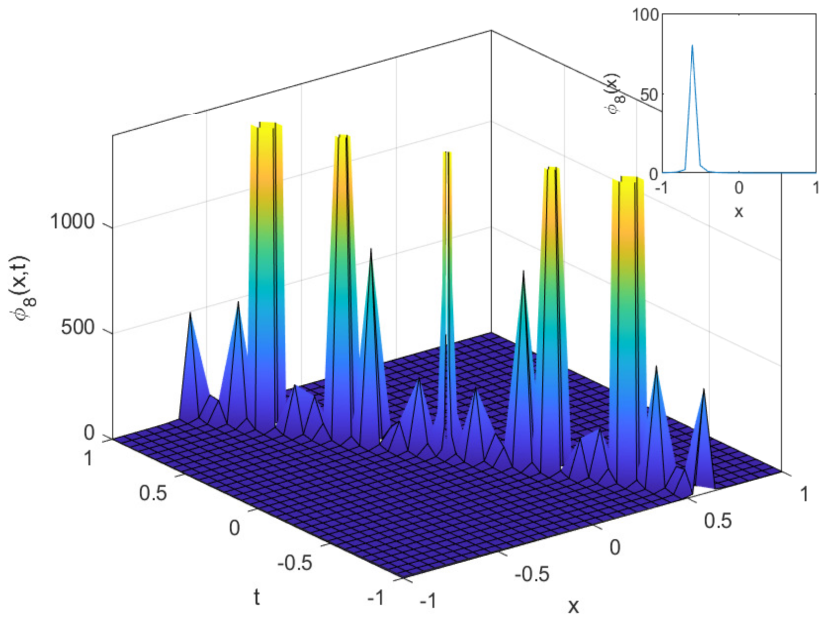

Figure 4.20. Singular type profile of Eq. (4.2.18) using $\beta_4=-3$, $\beta_1=2$, $\beta_3=-1$ and $S=4$.

Family 5. By setting $r_j=\{i,-i,1,1\}\,,s_j=\{i,-i,i,-i\}$, then Eq. (3.2.5) turns to the form

$$\psi(\zeta)=-\frac{\sin(\zeta)}{\cos(\zeta)}. \tag{4.2.19}$$

Case 1.

$$A_0=\frac{-1+\kappa^2}{4S\beta_1},A_1=0,B_1=0,A_2=-\frac{3\left(-1+\kappa^2\right)}{8S\beta_1},$$
$$B_2=-\frac{3\left(-1+\kappa^2\right)}{8S\beta_1},\beta_3=\frac{1+\left(-1+16S\beta_4\right)\kappa^2}{16S},$$

using the above values and Eq. (4.2.19) into Eq. (4.2.5), we have periodic singular solution as illustrated in Figure 4.21.

$$\phi_9(x,t) = \frac{-1+\kappa^2+2\sqrt{(-1+\kappa^2)^2}+3\sqrt{(-1+\kappa^2)^2}\cot(x-t\kappa)^2}{2S\beta_1}. \tag{4.2.20}$$

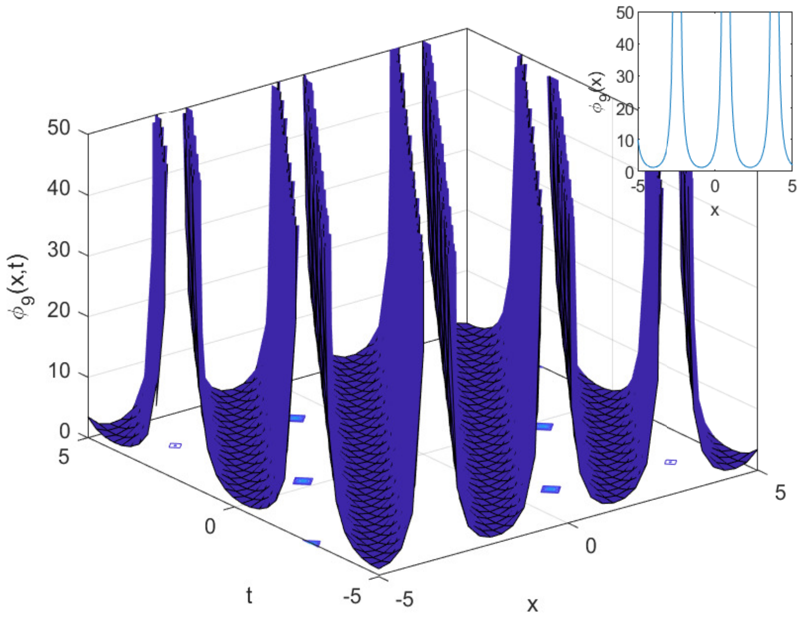

Figure 4.21. Periodic singular type profile of Eq. (4.2.20) using $\beta_1 = 0.5$, $S = 0.4$ and $\kappa = 0.7$.

Case 2.

$$A_0 = \frac{4(\beta_3-\beta_4)}{3\beta_1},\ A_1 = 0,\ B_1 = 0,\ A_2 = -\frac{2(\beta_3-\beta_4)}{\beta_1},$$
$$B_2 = -\frac{2(\beta_3-\beta_4)}{\beta_1},\ S = \frac{1}{4\beta_4},\ \kappa = -\frac{\mathrm{i}\sqrt{-4\beta_3+\beta_4}}{\sqrt{3}\sqrt{\beta_4}},$$

we get periodic singular solution as seen in Figure 4.22.

$$\phi_{10}(x,t) = \frac{4(\beta_3-\beta_4)}{3\beta_1} - \frac{2(\beta_3-\beta_4)\cot\left(x+\frac{\mathrm{i}t\sqrt{-4\beta_3+\beta_4}}{\sqrt{3}\sqrt{\beta_4}}\right)^2}{\beta_1} - \frac{2(\beta 3-\beta 4)\tan\left(x+\frac{\mathrm{i}t\sqrt{-4\beta_3+\beta_4}}{\sqrt{3}\sqrt{\beta_4}}\right)^2}{\beta_1}. \tag{4.2.21}$$

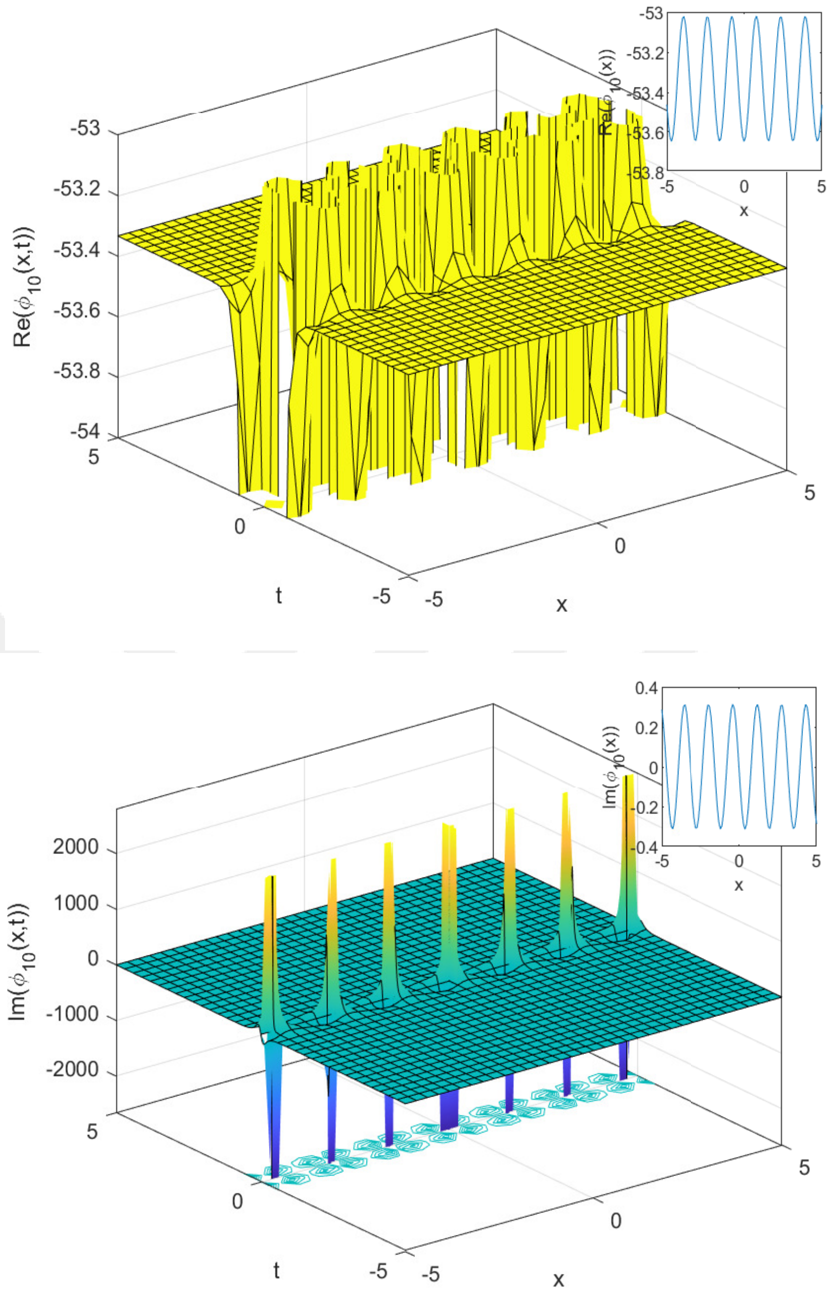

Figure 4.22. Periodic like lump type profiles of Eq. (4.2.21) using $\beta_1 = 0.3$, $\beta_3 = -2$ and $\beta_4 = 1$.

4.3 The System Based on the Ion Sound and Langmuir Waves

In the present portion, mathematical analysis of the SEISLWEs equations are addressed, as well as application of the GERF and the new MGERF methods on the proposed system are discussed.

Consider the system based on the ion sound and Langmuir waves equations by

[9,30,31,93,94]

$$\begin{cases} i\dfrac{\partial E}{\partial t}+\dfrac{1}{2}\dfrac{\partial^2 E}{\partial x^2}-nE=0, \\ \dfrac{\partial^2 n}{\partial t^2}-\dfrac{\partial^2 n}{\partial x^2}-2\dfrac{\partial^2 \left|E\right|^2}{\partial x^2}=0, \end{cases} \tag{4.3.1}$$

it is under the influence of the power-motive force arising from the non-linear force that charged the particle experience in the in-homogeneous electromagnetic oscillating region due to the high-frequency effect, Ee^{iwpt} and n respectively show the normalized electrical field of the Longmuir oscillation and the normalized density perturbation [95]. The structure of the constitution and relationship of the solitons of Langmuir and the heavy chaos have been studied in [96]. Langmuir cave through pumping and wave energy dissipation have been provided in [97]. Simulation of the collapse of the Langmuir waves is performed via the PIC method [98]. The evolution of the isolated cavity of Langmuir is explored, for this aim, the Vlasov equations for electrons and ions are solved by numericaI method for two spatial variables [99]. Numerical simulation have been studied for two-dimensional Langmuir collapse in plasma [100]. Strong Langmuir turbulence in laser plasma have been investigated in [101]. Weak Langmuir turbulence has been considered in [102]. Nonlinear Langmuir waves in multi-ion-component low-temperature plasma have been studied, the Sagdeev potential method has been used to examine the characteristics of solitary waves, and it has also been observed that the properties of soliton in multi-ion-component plasma are distinct from those of soliton in electron-ion plasma [103]. The meaning of the spectra as a symbol of nonlinear collapse of the electron-sound and ion-sound secondary waves of the Langmuir waves has been addressed in [104]. The relationship between Langmuir solitons, coupled solitons and sound waves has been investigated in [105]. The trapping of Langmuir waves in Ion Holes have been studied in [106]. The problem of the nonlinear level of instability of the monochromatic wave of Langmuir have been addressed [107]. The spacial location of Langmuir waves create from an electron ray spread in an inhomogeneous plasma have investigated in [108].

Take the wave transformation as

$$E\left(x,t\right)=e^{i\gamma}U\left(\zeta\right),\ n\left(x,t\right)=V\left(\zeta\right),\gamma=kx+wt \text{ and } \zeta=\alpha x+\beta t, \tag{4.3.2}$$

where k, w, α, and β are none zero scalars, as well as

$$V\left(\zeta\right)=\frac{2}{\beta^2-k^2}U^2\left(\zeta\right). \tag{4.3.3}$$

Using Eq. (4.3.2) and Eq. (4.3.3) into Eq. (4.3.1), one may obtain

$$\rho U''-\bar{\omega}U-4U^3=0, \tag{4.3.4}$$

where $\rho=\alpha^2\left(k^2-1\right), \bar{\omega}=\left(k^2-1\right)\left(2w+k^2\right)$.

4.4 Application of the GERFM

In this subsection, the application of the GERFM to Eq. (4.3.1) is presented. By using the balance principle between U'' and U^3 in Eq. (4.3.4), we get $m = 1$. Using $m = 1$, then Eq. (3.1.4) reduces to the following form

$$U(\zeta) = A_0 + A_1\psi(\zeta) + B_1\psi(\zeta)^{-1}. \tag{4.4.1}$$

Using Eq. (4.4.1) into Eq. (4.3.4), then after some processes the following families of exact solutions of Eq. (4.3.1) can be obtain:

Family 1. Using $r_i = \{-1, -2, 1, 1\}$, $s_i = \{1, 0, 1, 0\}$ in Eq. (3.1.5), one may get

$$\psi(\zeta) = \frac{-\mathrm{e}^{\zeta} - 2}{\mathrm{e}^{\zeta} + 1}. \tag{4.4.2}$$

Taking Eq. (4.4.2), Eq. (4.4.1), and Eq. (4.3.4) into account, the following cases can be obtain:

Case 1. For

$$A_0 = \frac{3B_1}{4},\ A_1 = 0,\ w = \frac{{B_1}^2 - 4k^2 + 4k^4}{8 - 8k^2},\ \alpha = -\frac{\mathrm{i}B_1}{\sqrt{2 - 2k^2}},$$

we get a complex exponential type solutions as given in Figure 4.23., and Figure 4.24.

$$\begin{aligned}
n(x,t) &= \frac{2}{-1 + k^2}\left(\frac{B_1\left(2\mathrm{e}^{\frac{\mathrm{i}B_1kt}{\sqrt{2-2k^2}}} - \mathrm{e}^{\frac{\mathrm{i}B_1x}{\sqrt{2-2k^2}}}\right)}{4\left(2\mathrm{e}^{\frac{\mathrm{i}B_1kt}{\sqrt{2-2k^2}}} + \mathrm{e}^{\frac{\mathrm{i}B_1x}{\sqrt{2-2k^2}}}\right)}\right)^2, \\
E(x,t) &= \mathrm{e}^{\mathrm{i}\left(\frac{\left(B1^2 - 4k^2 + 4k^4\right)t}{8 - 8k^2} + kx\right)}\left(\frac{B_1\left(2\mathrm{e}^{\frac{\mathrm{i}B_1kt}{\sqrt{2-2k^2}}} - \mathrm{e}^{\frac{\mathrm{i}B_1x}{\sqrt{2-2k^2}}}\right)}{4\left(2\mathrm{e}^{\frac{\mathrm{i}B_1kt}{\sqrt{2-2k^2}}} + \mathrm{e}^{\frac{\mathrm{i}B_1x}{\sqrt{2-2k^2}}}\right)}\right).
\end{aligned} \tag{4.4.3}$$

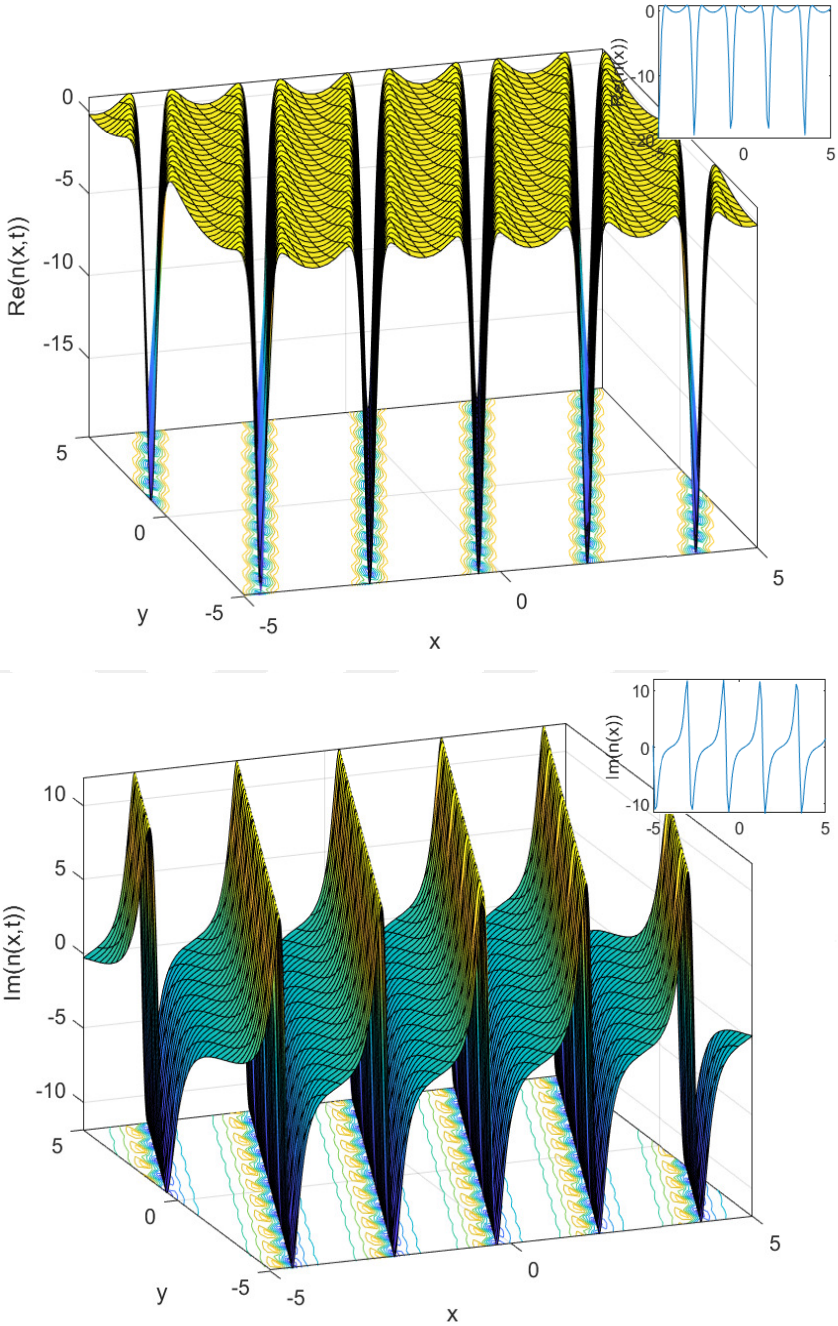

Figure 4.23. 3D surfaces and 2D graphs of $n(x,t)$ in Eq. (4.4.3) using $B_1 = 4$ and $k = 0.3$.

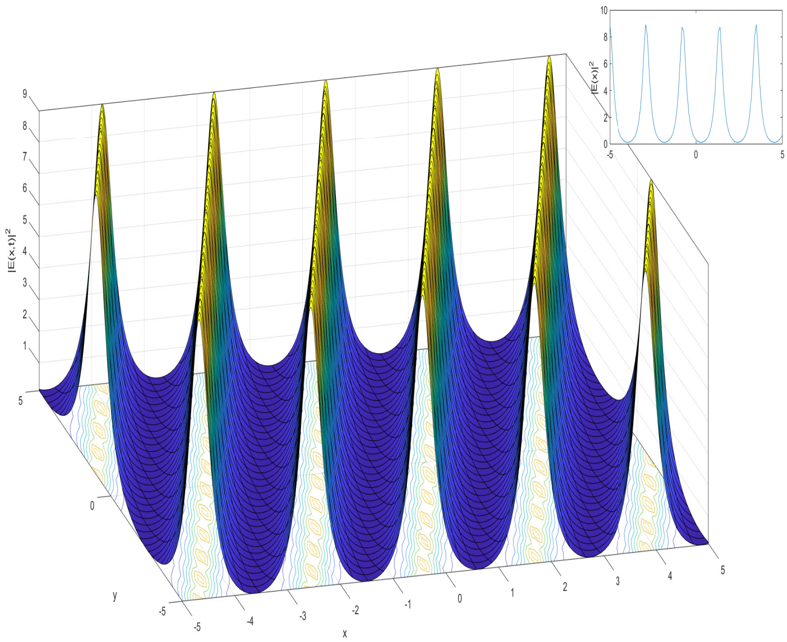

Figure 4.24. 3D surfaces and 2D graphs of $E(x,t)$ in Eq. (4.4.3) using $B_1 = 4$ and $k = 0.3$.

Case 2. For

$$A_0 = \frac{3\sqrt{-1+k^2}\alpha}{2\sqrt{2}},\ A_1 = \frac{\sqrt{-1+k^2}\alpha}{\sqrt{2}},\ B_1 = 0,\ w = \frac{1}{4}\left(-2k^2-\alpha^2\right),$$

we have dark type solutions as shown in Figure 4.25., and Figure 4.26.

$$\begin{aligned} n(x,t) &= \frac{2}{-1+k^2}\left(-\frac{\sqrt{-1+k^2}\alpha\tanh\left(\frac{1}{2}(kt-x)\alpha\right)}{2\sqrt{2}}\right)^2, \\ E(x,t) &= e^{i\left(kx+\frac{1}{4}t\left(-2k^2-\alpha^2\right)\right)}\left(-\frac{\sqrt{-1+k^2}\alpha\tanh\left(\frac{1}{2}(kt-x)\alpha\right)}{2\sqrt{2}}\right). \end{aligned} \tag{4.4.4}$$

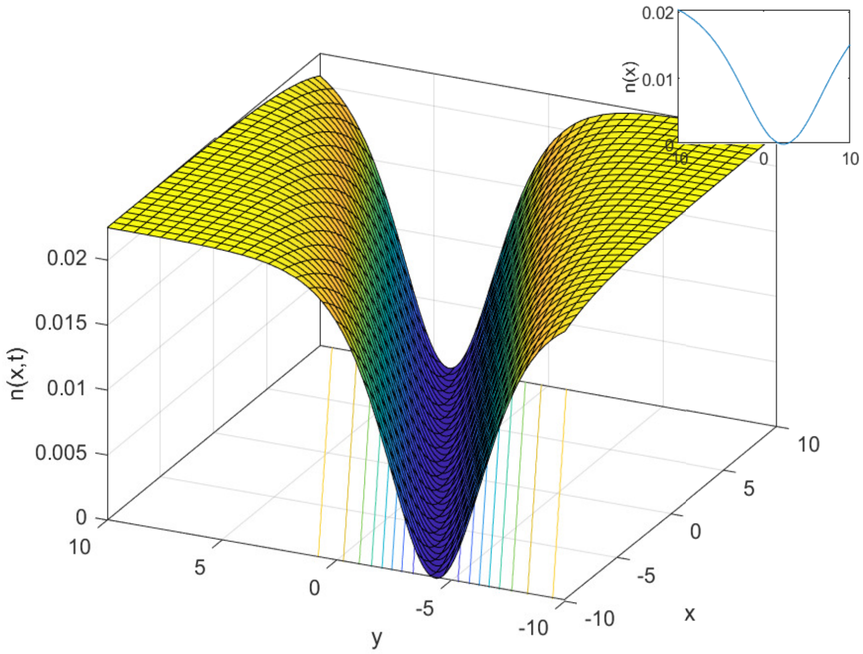

Figure 4.25. 3D surfaces and 2D graphs of $n(x,t)$ in Eq. (4.4.4) using $k = 2.3$ and $\alpha = 0.3$.

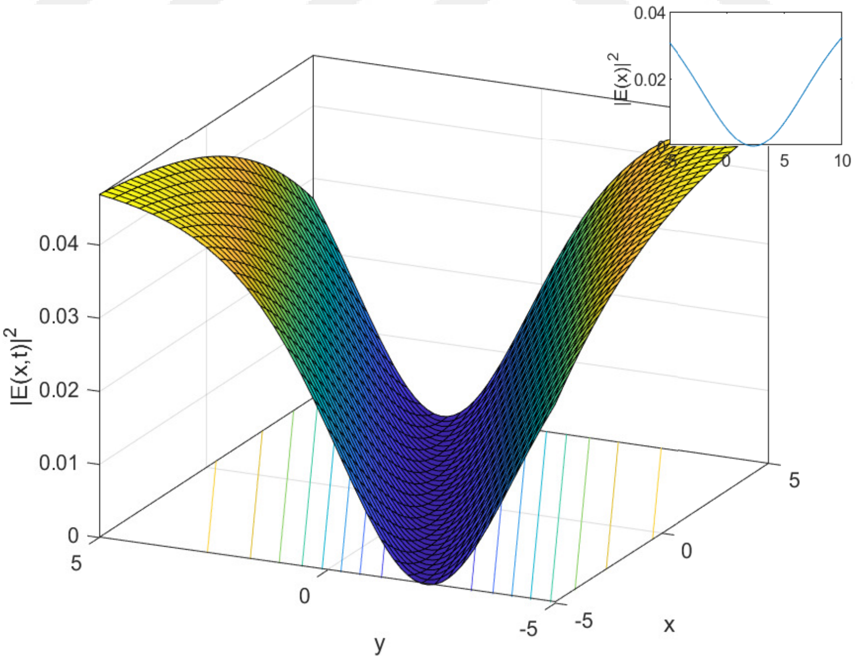

Figure 4.26. 3D surfaces and 2D graphs of $E(x,t)$ in Eq. (4.4.4) using $k = 2.3$ and $\alpha = 0.3$.

Family 2. Using $r_j = \{-2-i, -2+i, 1, 1\}$, $s_j = \{i, -i, i, -i\}$, then Eq. (3.1.5) reduced to the following form

$$\psi(\zeta) = \frac{-2\cos(\zeta) + \sin(\zeta)}{\cos(\zeta)}, \tag{4.4.5}$$

by using Eq. (4.4.5) with Eq. (4.4.1) into Eq. (4.3.4), we have

Case 1. When

$$A_0 = \frac{2bB_1}{5},\ A_1 = 0,\ w = -\frac{k^2}{2} + \frac{2b_1^2}{25(-1+k^2)},\ \alpha = \frac{\sqrt{2}B_1}{5\sqrt{-1+k^2}},$$

we get a singular solutions as seen in Figure 4.27., and Figure 4.28.

$$\begin{aligned} n(x,t) &= \frac{2}{-1+k^2}\left(\frac{2B_1}{5} - \frac{B_1}{2+\tan\left(\frac{\sqrt{2}(kt-x)B_1}{5\sqrt{-1+k^2}}\right)}\right)^2, \\ E(x,t) &= e^{i\left(kx+t\left(-\frac{k^2}{2}+\frac{2B_1^2}{25(-1+k^2)}\right)\right)}\left(\frac{2B_1}{5} - \frac{B_1}{2+\tan\left(\frac{\sqrt{2}(kt-x)B_1}{5\sqrt{-1+k^2}}\right)}\right). \end{aligned} \tag{4.4.6}$$

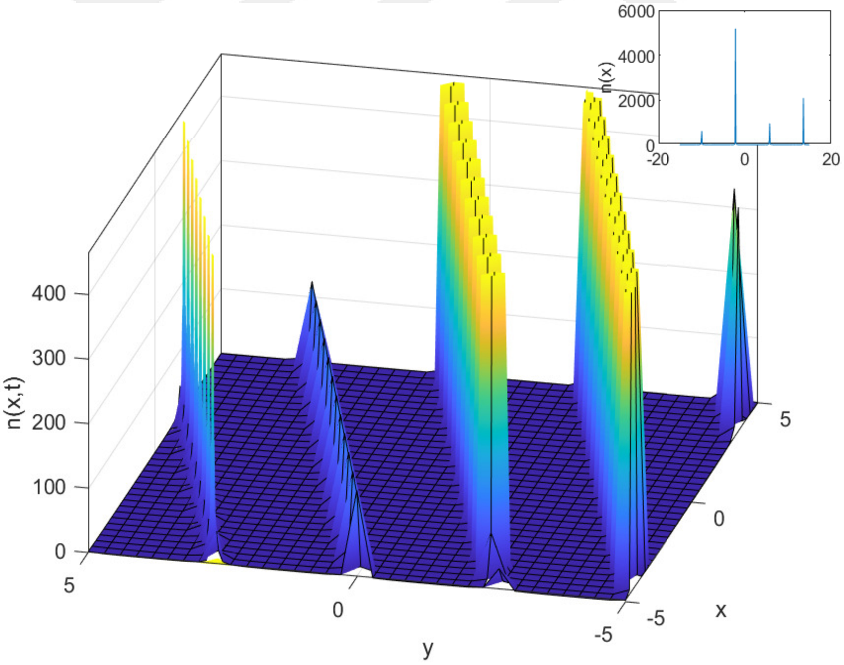

Figure 4.27. 3D surfaces and 2D graphs of $n(x,t)$ in Eq. (4.4.6) using $k=3$ and $B_1=4$.

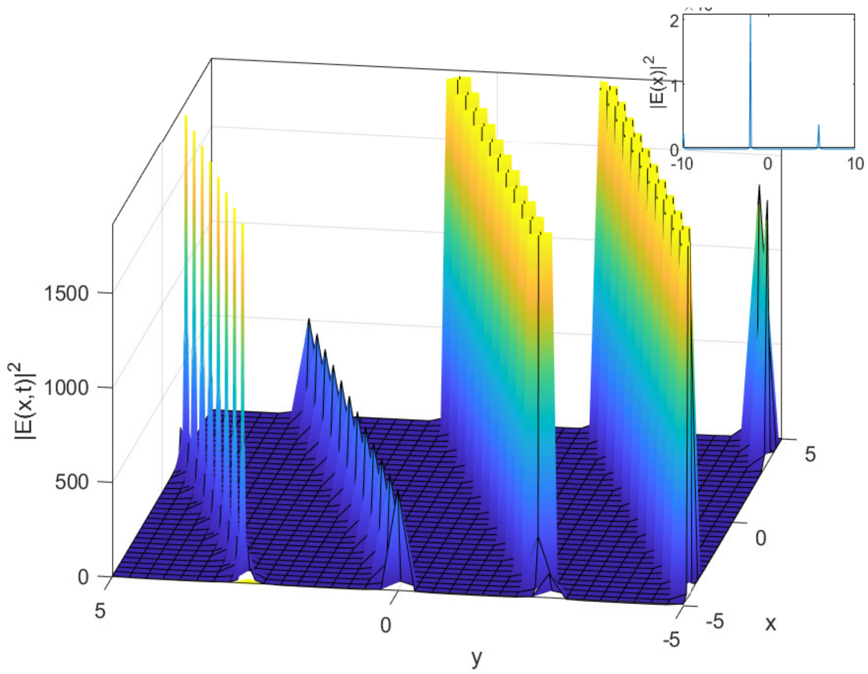

Figure 4.28. 3D surfaces and 2D graphs of $E(x,t)$ in Eq. (4.4.6) using $k=3$ and $B_1=4$.

Case 2. When

$$A_0=\sqrt{-1+k^2}\sqrt{k^2+2w},\ A_1=\frac{1}{2}\sqrt{-1+k^2}\sqrt{k^2+2w},\ B_1=0,$$
$$\alpha=-\sqrt{\frac{k^2}{2}+w},$$

we get periodic singular solution as shown in Figure 4.29., and Figure 4.30.

$$\begin{aligned} n\left(x,t\right)&=\frac{2}{-1+k^2}\left(\frac{1}{2}\sqrt{-1+k^2}\sqrt{k^2+2w}\tan\left(\sqrt{\frac{k^2}{2}+w}\left(kt-x\right)\right)\right)^2,\\ E\left(x,t\right)&=\mathrm{e}^{\mathrm{i}(tw+kx)}\left(\frac{1}{2}\sqrt{-1+k^2}\sqrt{k^2+2w}\tan\left(\sqrt{\frac{k^2}{2}+w}\left(kt-x\right)\right)\right).\end{aligned}\tag{4.4.7}$$

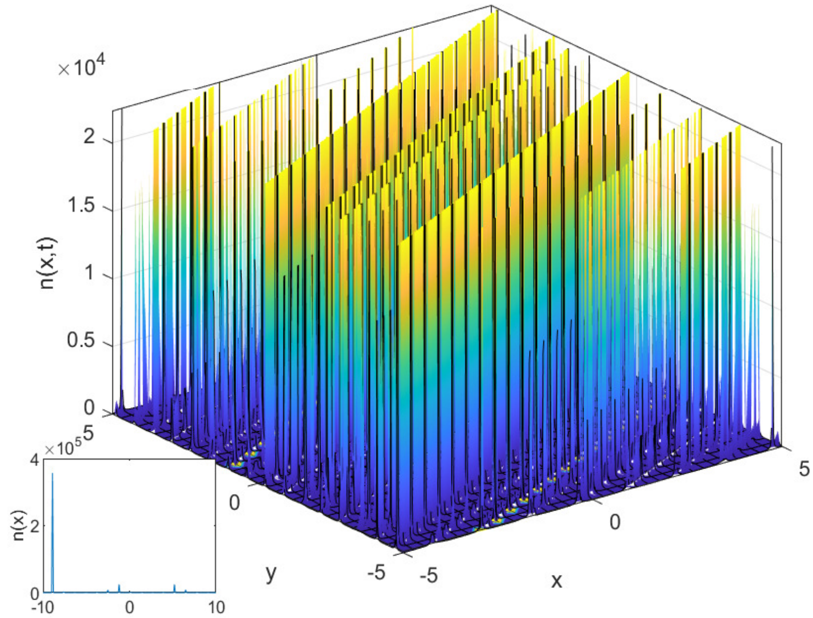

Figure 4.29. 3D surfaces and 2D graphs of $n(x,t)$ in Eq. (4.4.7) using $k = 2$ and $w = 4$.

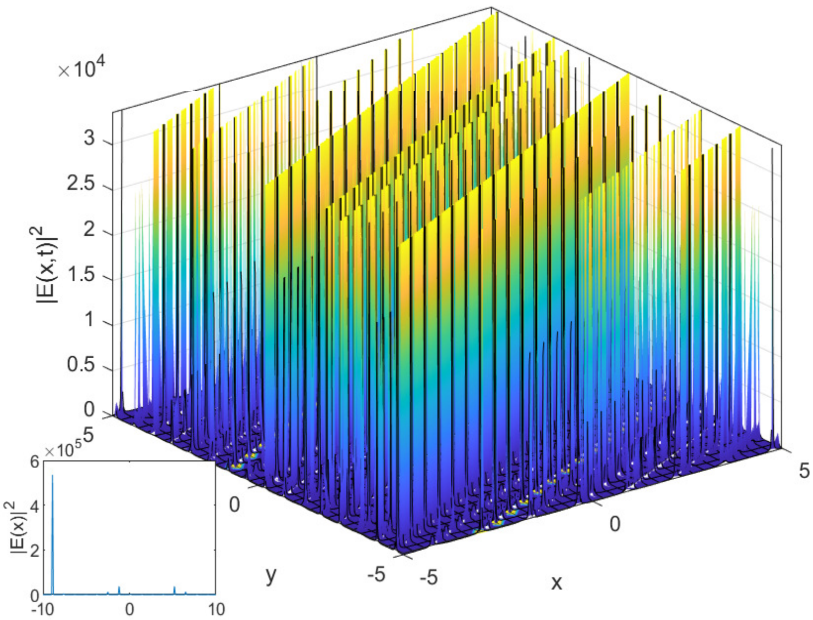

Figure 4.30. 3D surfaces and 2D graphs of $E(x,t)$ in Eq. (4.4.7) using $k = 2$ and $w = 4$.

Family 3. Using $r_j = \{2, 0, 1, 1\}$, $s_j = \{-1, 0, 1, -1\}$ in Eq. (3.2.5), then we have

$$\psi(\zeta) = \frac{\cosh(\zeta) - \sinh(\zeta)}{\cosh(\zeta)}, \tag{4.4.8}$$

by using Eq. (4.4.8) with Eq. (4.4.1) into Eq. (4.3.4), we get

Case 1. When

$$A_0 = \frac{\sqrt{-\alpha^2\left(1+2w+2\alpha^2\right)}}{\sqrt{2}},\ A_1 = -\frac{\sqrt{-\alpha^2\left(1+2w+2\alpha^2\right)}}{\sqrt{2}},\ B_1 = 0,$$
$$k = -\sqrt{2}\sqrt{-w-\alpha^2},$$

we get dark solutions as shwon in Figure 4.31., and 4.32.

$$\begin{aligned} n\left(x,t\right) &= \left(\frac{\sqrt{-\alpha^2\left(1+2w+2\alpha^2\right)}\tanh\left(\alpha\left(x+\sqrt{2}t\sqrt{-w-\alpha^2}\right)\right)}{\sqrt{2}}\right)^2 \times \\ &\quad \frac{2}{-1+2\left(-w-\alpha^2\right)}, \\ E\left(x,t\right) &= \left(\frac{\sqrt{-\alpha^2\left(1+2w+2\alpha^2\right)}\tanh\left(\alpha\left(x+\sqrt{2}t\sqrt{-w-\alpha^2}\right)\right)}{\sqrt{2}}\right) \times \\ &\quad e^{i\left(tw-\sqrt{2}x\sqrt{-w-\alpha^2}\right)}. \end{aligned} \tag{4.4.9}$$

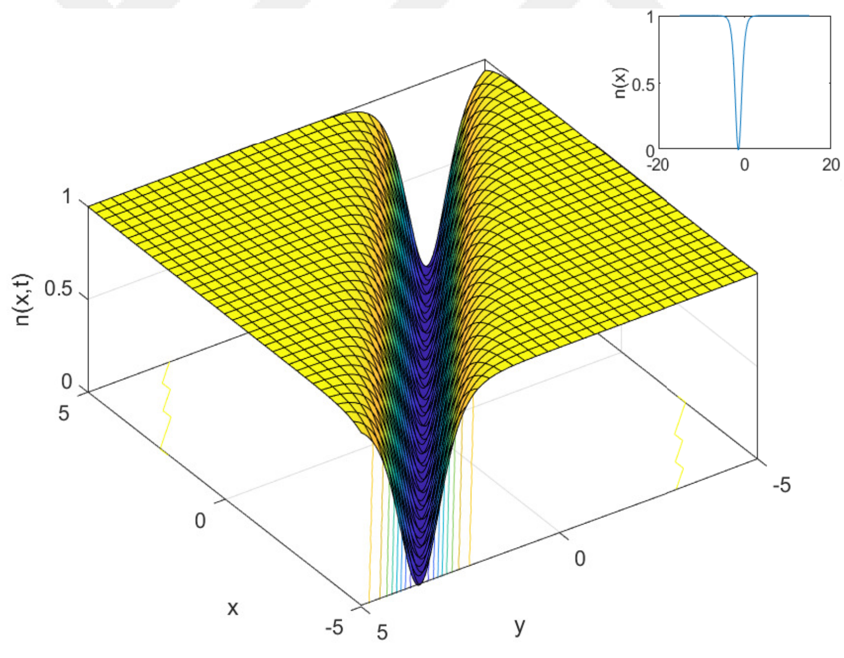

Figure 4.31. 3D surfaces and 2D graphs of $n(x,t)$ of Eq. (4.4.9) using $\alpha = 1$ and $w = -2$.

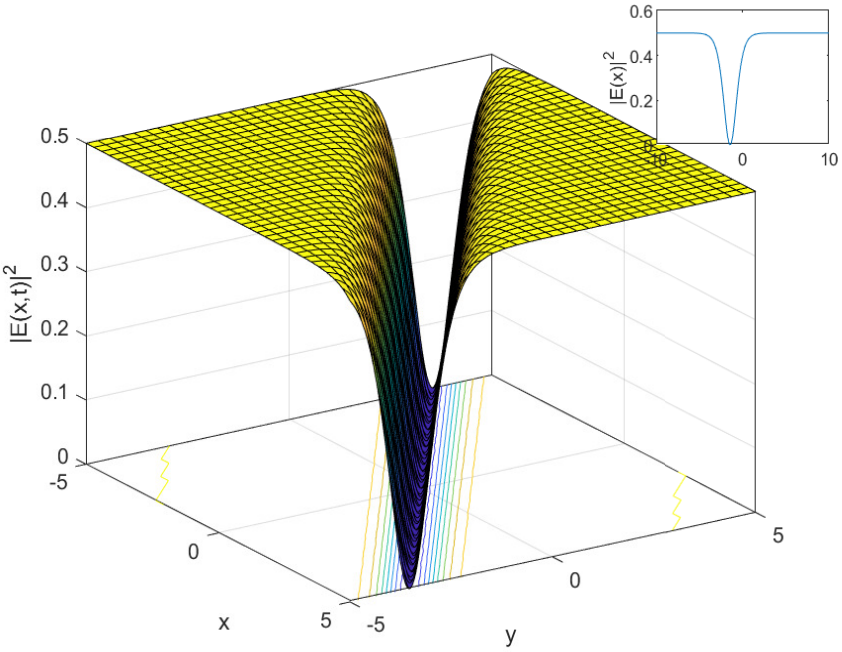

Figure 4.32. 3D surfaces and 2D graphs of $E(x,t)$ of Eq. (4.4.9) using $\alpha = 1$ and $w = -2$.

4.5 Application of the new MGERF method

In this portion, application of the new MGERF to the Eq. (4.3.1) are presented. Using the balance principle between U'' and U^3 in Eq. (4.3.4), we get $m = 1$. Using $m = 1$, Eq. (3.2.4) reduces to the form

$$U(\zeta) = A_0 + A_1\psi(\zeta) + B_1\psi(\zeta)^{-1} + C_1\frac{\psi'(\zeta)}{\psi(\zeta)}. \tag{4.5.1}$$

By using Eq. (4.5.1) into Eq. (4.3.4), then after some processes the families of exact solutions of Eq. (4.3.1) can be produces as follows:

Family 1. Taking Eq. (4.4.2) and Eq. (4.5.1) into account, one may get

Case 1. When

$$A_0 = \frac{3}{4}(2A_1 + A_1), \; C_1 = \frac{B_1}{2}, \; w = -\frac{(-2A_1 + B_1)^2 - 4k^2 + 4k^4}{8(-1 + k^2)},$$
$$\alpha = \frac{\mathrm{i}(2A_1 - B_1)}{\sqrt{2 - 2k^2}},$$

we get dark solution as shown in Figure 4.33., and Figure 4.34.

$$
\begin{aligned}
n\left(x,t\right) &= \frac{2}{-1+k^2}\left(\frac{\sqrt{\left(-1+k^2\right)\alpha^2}\tanh\left(\frac{1}{2}\left(kt-x\right)\alpha\right)}{2\sqrt{2}}\right)^2,\\
E\left(x,t\right) &= \mathrm{e}^{\mathrm{i}\left(kx+\frac{1}{4}\left(-2k^2-\alpha^2\right)t\right)}\left(\frac{\sqrt{\left(-1+k^2\right)\alpha^2}\tanh\left(\frac{1}{2}\left(kt-x\right)\alpha\right)}{2\sqrt{2}}\right).
\end{aligned}
\tag{4.5.2}
$$

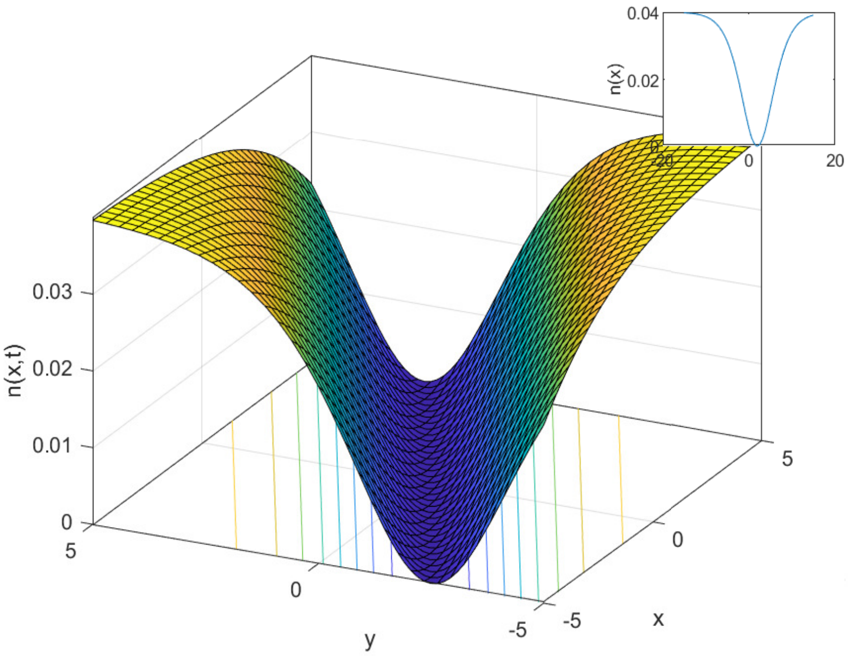

Figure 4.33. 3D surfaces and 2D graphs of $n(x,t)$ of Eq. (4.5.2) using $\alpha = 1$ and $w = -2$.

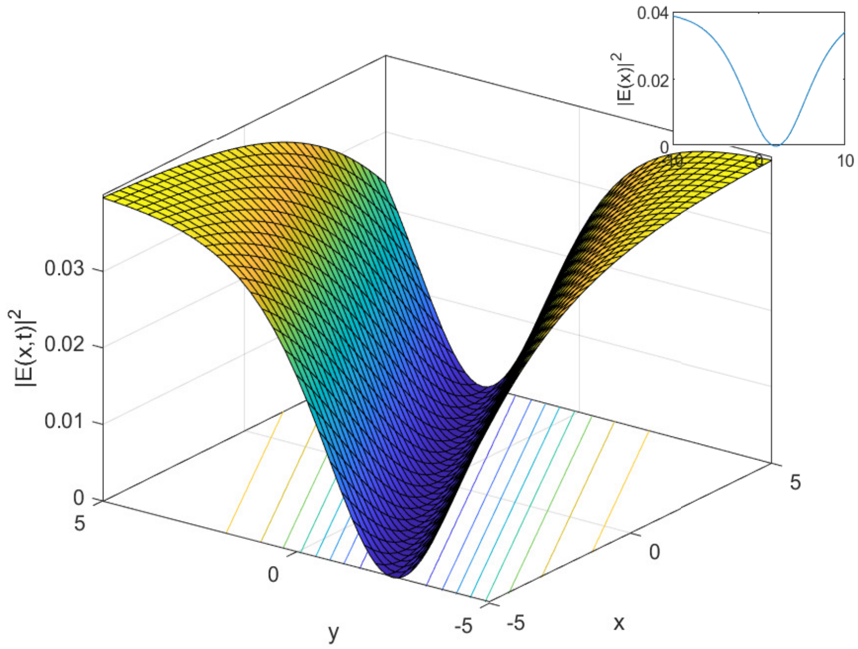

Figure 4.34. 3D surfaces and 2D graphs of $E(x,t)$ of Eq. (4.5.2) using $\alpha = 1$ and $w = -2$.

Case 2. When

$$A_0 = 3A_1 + \frac{3\sqrt{(-1+k^2)\,\alpha^2}}{2\sqrt{2}},\ B_1 = 2A_1 + \sqrt{2}\sqrt{(-1+k^2)\,\alpha^2},$$
$$C_1 = A_1 + \frac{\sqrt{(-1+k^2)\,\alpha^2}}{\sqrt{2}}, w = \frac{1}{4}(-2k^2 - \alpha^2),$$

we get exponential solutions as illustrated in Figure 4.35., and Figure 4.36.

$$\begin{aligned} n\,(x,t) &= \frac{2}{-1+k^2}\left(\frac{\left(\mathrm{e}^{kt\alpha} - \mathrm{e}^{x\alpha}\right)\sqrt{(-1+k^2)\,\alpha^2}}{2\sqrt{2}\,(\mathrm{e}^{kt\alpha} + \mathrm{e}^{x\alpha})}\right)^2, \\ E\,(x,t) &= \mathrm{e}^{\mathrm{i}\left(kx + \frac{1}{4}t\left(-2k^2-\alpha^2\right)\right)}\left(\frac{\left(\mathrm{e}^{kt\alpha} - \mathrm{e}^{x\alpha}\right)\sqrt{(-1+k^2)\,\alpha^2}}{2\sqrt{2}\,(\mathrm{e}^{kt\alpha} + \mathrm{e}^{x\alpha})}\right). \end{aligned} \tag{4.5.3}$$

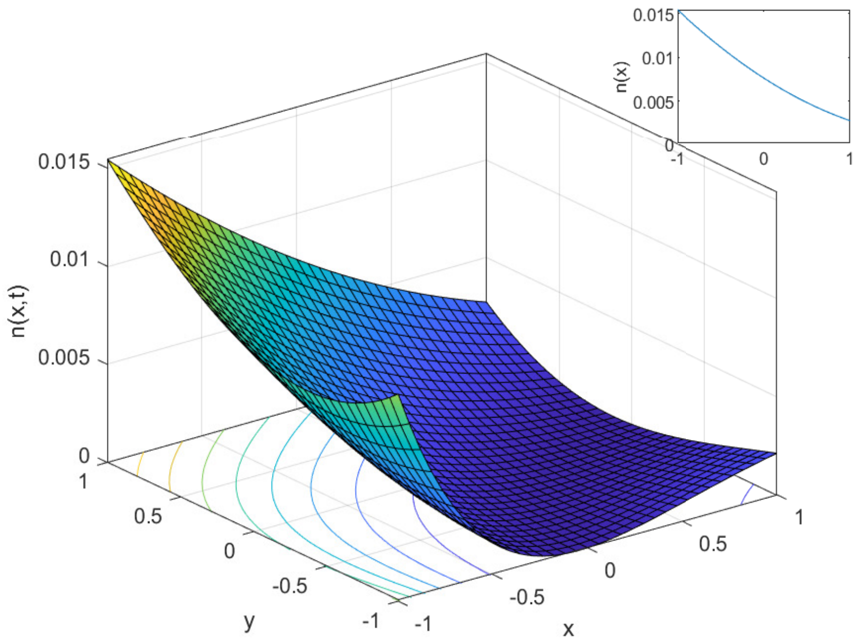

Figure 4.35. 3D surfaces and 2D graphs of $n(x,t)$ of Eq. (4.5.3) using $\alpha = 0.4$ and $k = 2$.

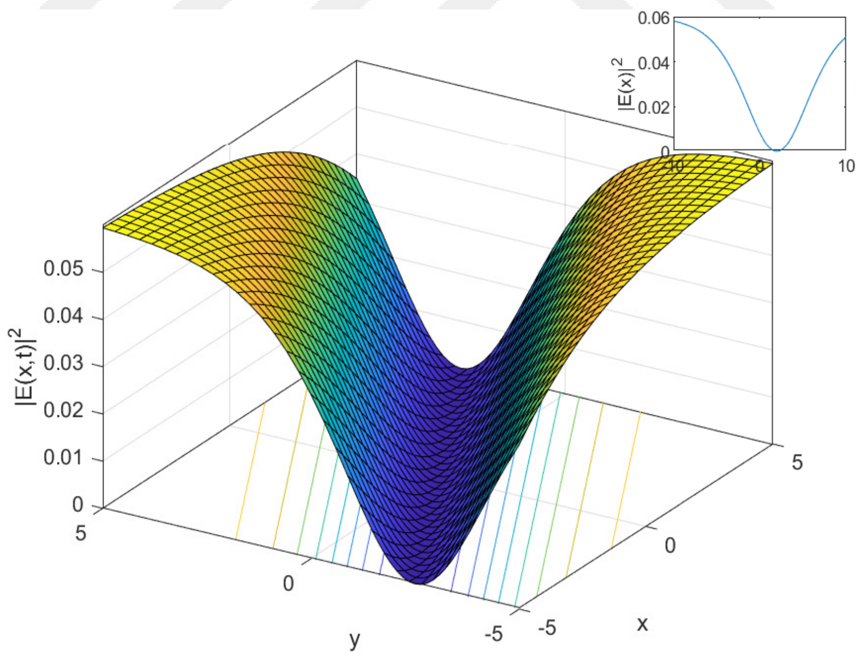

Figure 4.36. 3D surfaces and 2D graphs of $E(x,t)$ of Eq. (4.5.3) using $\alpha = 0.4$ and $k = 2$.

Family 2. Taking Eq. (4.4.7) and Eq. (4.5.1) into account, we get

Case 1. When

$$C_1 = -\frac{B_1}{5},\ w = \frac{-25\,(-1+k)\,k^2\,(1+k) + 4(-5A_1+B_1)^2}{50\,(-1+k^2)},$$
$$\alpha = \frac{\sqrt{2}\,(-5A_1+B_1)}{5\sqrt{-1+k^2}}, A_0 = \frac{2}{5}\,(5A_1+B_1)\,,$$

we get periodic singular solutions as shown in Figure 4.37, and Figure 4.38.

$$\begin{aligned} n\,(x,t) &= \frac{2}{-1+k^2}\left(\frac{1}{5}\,(5A_1-B_1)\tan\left(\frac{\sqrt{2}\,(kt-x)\,(5A_1-B_1)}{5\sqrt{-1+k^2}}\right)\right)^2, \\ E\,(x,t) &= \mathrm{e}^{\mathrm{i}\left(kx+\frac{t\left(-25(-1+k)k^2(1+k)+4(-5A_1+B_1)^2\right)}{50\left(-1+k^2\right)}\right)} \\ &\qquad \left(\frac{1}{5}\,(5A_1-B_1)\tan\left(\frac{\sqrt{2}\,(kt-x)\,(5A_1-B_1)}{5\sqrt{-1+k^2}}\right)\right). \end{aligned} \tag{4.5.4}$$

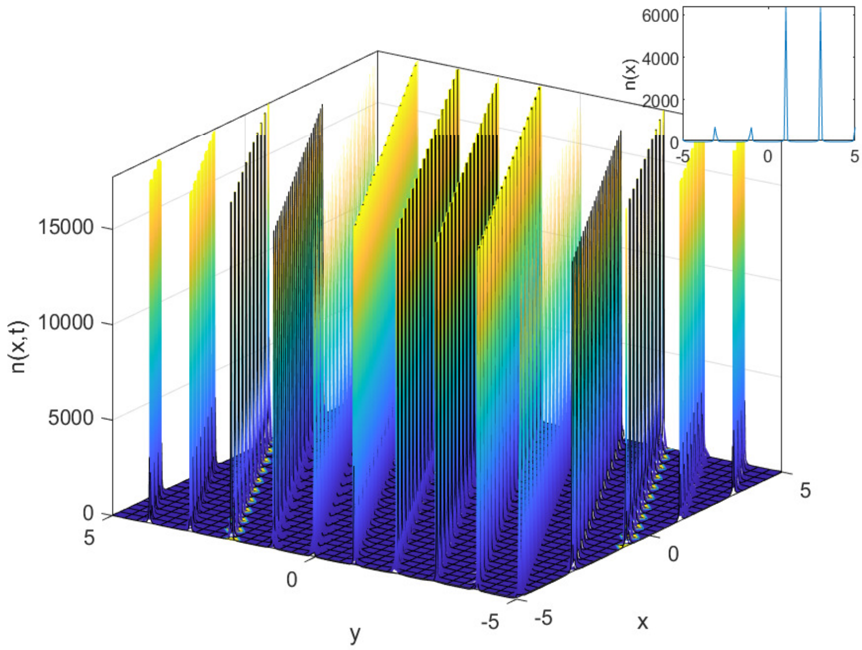

Figure 4.37. 3D surfaces and 2D graphs of $n(x,t)$ of Eq. (4.5.4) using $A_1 = 2, B_1 = 0.5$ and $k = 2$.

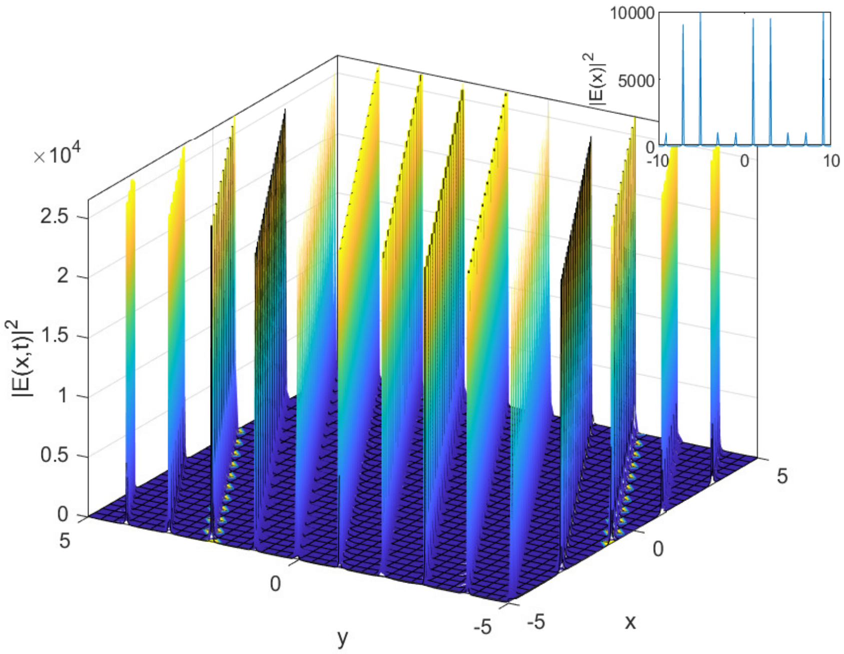

Figure 4.38. 3D surfaces and 2D graphs of $E(x,t)$ of Eq. (4.5.4) using $A_1 = 2, B_1 = 0.5$ and $k = 2$.

Case 2. When

$$A_0 = \sqrt{(-1+k^2)(k^2+2w)} + 4A_1,\ B_1 = \frac{5}{2}\left(\sqrt{(-1+k^2)(k^2+2w)} + 2A_1\right),$$
$$C_1 = -\frac{1}{2}\sqrt{(-1+k^2)(k^2+2w)} - A_1,\ \alpha = \sqrt{\frac{k^2}{2}+w},$$

we have trigonometric type solutions as seen in Figure 4.39., and Figure 4.40.

$$n(x,t) = \frac{2}{-1+k^2}\left(\frac{\sqrt{(-1+k^2)(k^2+2w)}\left(-1+2\tan\left(\sqrt{\frac{k^2}{2}+w}\,(kt-x)\right)\right)}{2\left(2+\tan\left(\sqrt{\frac{k^2}{2}+w}\,(kt-x)\right)\right)}\right)^2,$$
$$E(x,t) = \mathrm{e}^{\mathrm{i}(tw+kx)}\left(\frac{\sqrt{(-1+k^2)(k^2+2w)}\left(-1+2\tan\left(\sqrt{\frac{k^2}{2}+w}\,(kt-x)\right)\right)}{2\left(2+\tan\left(\sqrt{\frac{k^2}{2}+w}\,(kt-x)\right)\right)}\right). \tag{4.5.5}$$

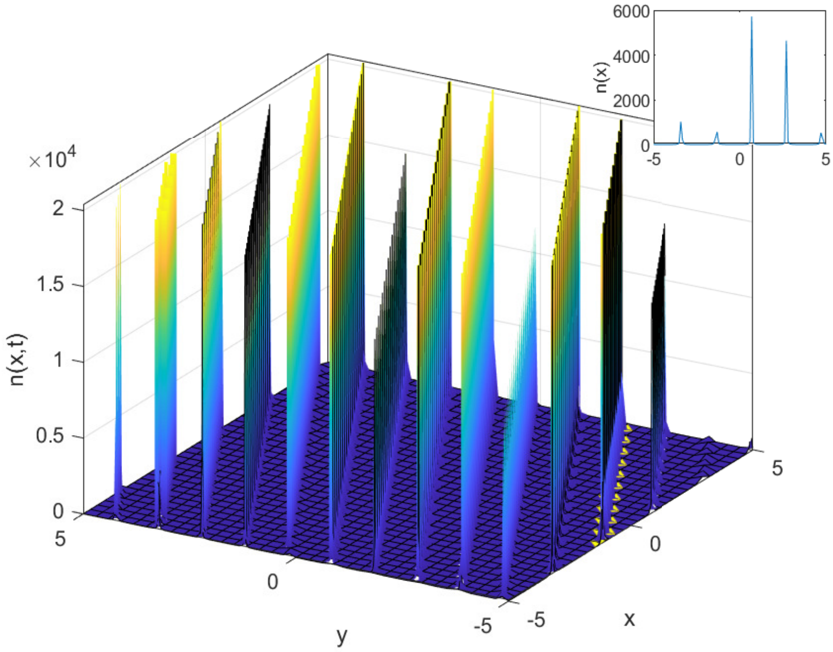

Figure 4.39. 3D surfaces and 2D graphs of $n(x,t)$ in Eq. (4.5.5) using $w = 0.4$ and $k = 2$.

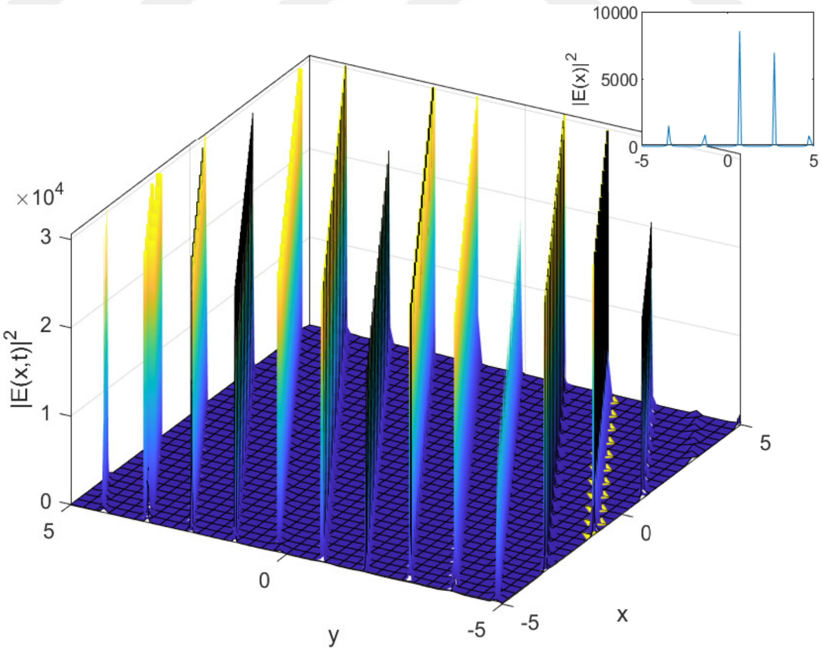

Figure 4.40. 3D surfaces and 2D graphs of $E(x,t)$ in Eq. (4.5.5) using $w = 0.4$ and $k = 2$.

Family 3. Taking Eq. (4.4.12) and Eq. (4.5.1) into account, then the following cases can be obtained:

Case 1. When

$$A_0=\frac{1}{2}\left(\sqrt{-\left(-1+k^2\right)\left(k^2+2w\right)}+4C_1\right), B_1=0,$$
$$A_1=-\frac{1}{2}\sqrt{-\left(-1+k^2\right)\left(k^2+2w\right)}-C_1, \alpha=\sqrt{-\frac{k^2}{2}-w},$$

we have hyperbolic type solutions as shown in Figure 4.41., and Figure 4.42.

$$n\left(x,t\right)=\frac{2}{-1+k^2}\left(\begin{array}{l}-\frac{1}{2}\left(-1+\mathrm{e}^{\sqrt{-\frac{k^2}{2}-w}(kt-x)}\right)\sqrt{-\left(-1+k^2\right)\left(k^2+2w\right)}- \\ \left(-1+\cosh\left(\sqrt{-\frac{k^2}{2}-w}\left(kt-x\right)\right)\right)\times \\ C_1\left(1+\tanh\left(\sqrt{-\frac{k^2}{2}-w}\left(kt-x\right)\right)\right)\end{array}\right)^2,$$

$$E\left(x,t\right)=\mathrm{e}^{\mathrm{i}(tw+kx)}\left(\begin{array}{l}-\frac{1}{2}\left(-1+\mathrm{e}^{\sqrt{-\frac{k^2}{2}-w}(kt-x)}\right)\sqrt{-\left(-1+k^2\right)\left(k^2+2w\right)}- \\ \left(-1+\cosh\left(\sqrt{-\frac{k^2}{2}-w}\left(kt-x\right)\right)\right)\times \\ C_1\left(1+\tanh\left(\sqrt{-\frac{k^2}{2}-w}\left(kt-x\right)\right)\right)\end{array}\right). \tag{4.5.6}$$

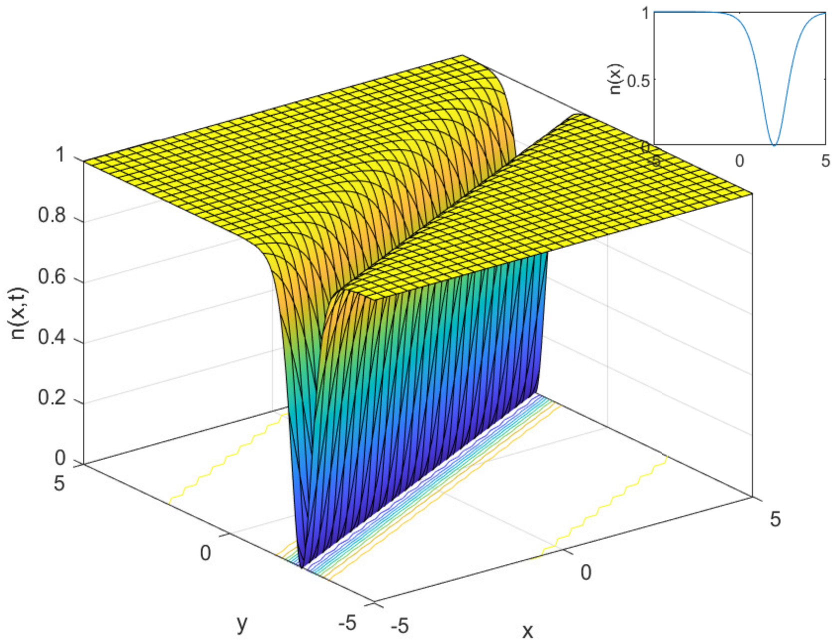

Figure 4.41. 3D surfaces and 2D graphs of $n(x,t)$ in Eq. (4.5.6) using $w = 0.4$ and $k = 2$.

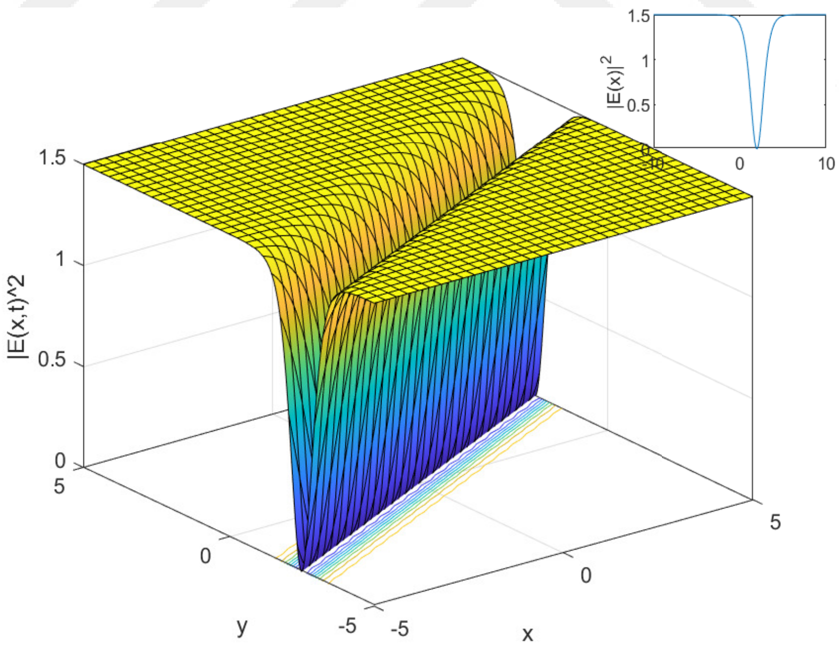

Figure 4.42. 3D surfaces and 2D graphs of $E(x,t)$ in Eq. (4.5.6) using $w = 0.4$ and $k = 2$.

GERFM	MGERFM
Family one, case one, complex exponential function type solution	Family one, case one, tanh type solution
Family one, case two, tanh type solution	Family one, case two, exponential type solution
Family two, case one, tan type solution	Family two, case one, tan type solution
Family two, case two, cot and tan type solution	Family two, case two, cot type solution
Family three, case one, tanh type solution	Family three, case one, cosh and tanh type solution

Table 4.1. Comparison between solutions obtained by GERFM and its newly modified version.

4.6 Result and Discussion

In this part of thesis, the GERF method and the newly MGERF method have been successfully used to investigate SISLWs equations. To better understand the difference between two methods, the same parameters were chosen to solve the proposed system at the same time for both methods, leading in the development of same solutions as well as the different solutions. We found that in family one, Eq. (4.4.3) with Eq. (4.5.2), and Eq.(4.4.4) with Eq. (4.5.3) are different solutions. In family two Eq. (4.4.6) with Eq.

(4.5.4) are similar solutions, and Eq. (4.4.7) with Eq. (4.5.5) are different solutions. In family three Eq. (4.4.9) with Eq. (4.5.6) are different solutions. We conclude that the newly modified method is a powerful method and give different types of solutions comparison with the GERFM.

5. Fractal Differential Equations

In this chapter, some fractal differential equations are proposed for investigation includes electrical circuit involving fractal time, fractal battery discharging model on fractal time sets, and three-term as well as one term fractal differential equations.

5.1 Series RLC Circuit

In this section, we present two examples as applications in which temporal evolution with a fractal structure takes place. In part (i), we take a series RLC circuit, and in part (ii), we take a parallel RLC circuit, which are widely used in the field of physics and engineering [109].

A. Series RLC Circuit

Consider a series RLC circuit such that its dynamics, which include fractal time, is suggested as follows [109]:

$$D_{F^{\kappa},t}^{2\alpha} i\left(t\right) + \frac{R}{L} D_{F^{\kappa},t}^{\alpha} i\left(t\right) + \frac{1}{LC} i\left(t\right) = 0,\ 0 < \alpha \leq 1, \quad t \in F^{\kappa}, \tag{5.1.1}$$

using the initial conditions $i\left(0\right) = A$, and $D_{F^{\kappa},t}^{\alpha} i(t)|_{t=0} = A$. In Eq. (5.1.1), R, L, and C are the resistor, inductor, and the capacitor, respectively.

Applying the fractal Laplace transform to both sides of Eq. (5.1.1), we get

$$\begin{aligned} i_{F^{\kappa}}^{\alpha}\left(w\right) = & \frac{A S_{F^{\kappa}}^{\alpha}\left(w\right)}{S_{F^{\kappa}}^{\alpha}\left(w\right)^{2} + \frac{R}{L} S_{F^{\kappa}}^{\alpha}\left(w\right) + \frac{1}{L*C}} + \frac{A}{S_{F^{\kappa}}^{\alpha}\left(w\right)^{2} + \frac{R}{L} S_{F^{\kappa}}^{\alpha}\left(w\right) + \frac{1}{L*C}} \\ & + \frac{R}{L} \frac{A}{S_{F^{\kappa}}^{\alpha}\left(w\right)^{2} + \frac{R}{L} S_{F^{\kappa}}^{\alpha}\left(w\right) + \frac{1}{L*C}}, \end{aligned} \tag{5.1.2}$$

applying the inverse Laplace to Eq. (5.1.2), then gives

$$i\left(t\right) = \frac{A \mathrm{e}^{-\frac{\left(R + \frac{\sqrt{-4L + CR^{2}}}{\sqrt{C}}\right) S_{F^{\kappa}}^{\alpha}(t)}{2l}}}{2\sqrt{-4L + CR^{2}}} \begin{pmatrix} \sqrt{C}\left(-1 + \mathrm{e}^{\frac{\sqrt{-4L + CR^{2}} S_{F^{\kappa}}^{\alpha}(t)}{\sqrt{C} L}}\right)(2L + R) \\ + \left(1 + \mathrm{e}^{\frac{\sqrt{-4L + CR^{2}} S_{F^{\kappa}}^{\alpha}(t)}{\sqrt{C} L}}\right)\sqrt{-4L + CR^{2}} \end{pmatrix}. \tag{5.1.3}$$

In view of the upper bound of the staircase function ($S_{F^{\kappa}}^{\alpha}(t) \leq t^{\alpha}$) [49,50], we have

$$i\left(t\right) \approx \frac{A \mathrm{e}^{-\frac{\left(R + \frac{\sqrt{-4L + CR^{2}}}{\sqrt{C}}\right) t^{\alpha}}{2l}}}{2\sqrt{-4L + CR^{2}}} \begin{pmatrix} \sqrt{C}\left(-1 + \mathrm{e}^{\frac{\sqrt{-4L + CR^{2}} t^{\alpha}}{\sqrt{C} L}}\right)(2L + R) \\ + \left(1 + \mathrm{e}^{\frac{\sqrt{-4L + CR^{2}} t^{\alpha}}{\sqrt{C} L}}\right)\sqrt{-4L + CR^{2}} \end{pmatrix}. \tag{5.1.4}$$

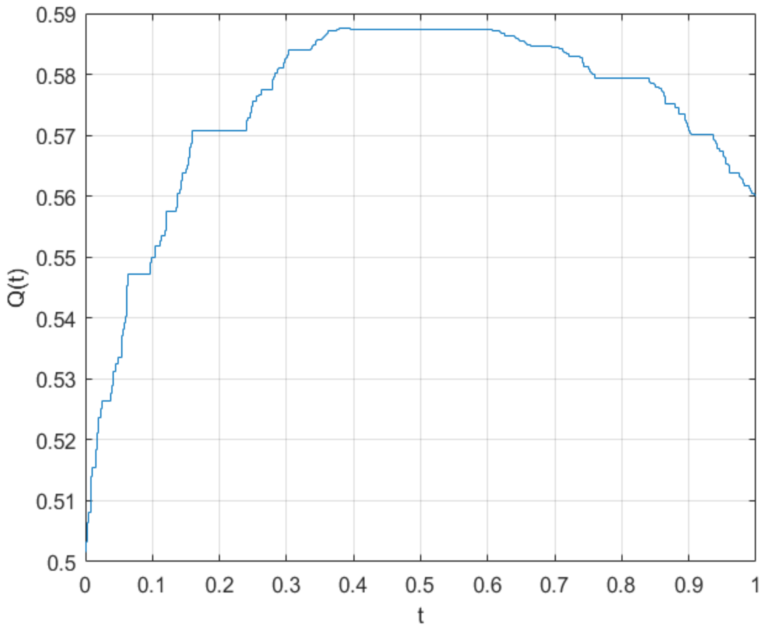

Figure 5.1. The sketch of Eq. (5.1.3) using $A = 0.5$, $R = 3$, $L = 0.8$ and $C = 2$.

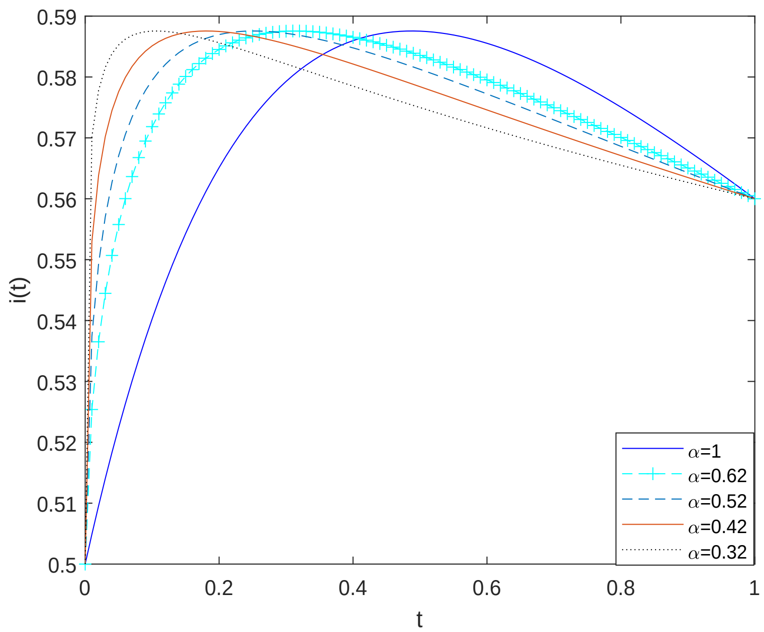

Figure 5.2. The sketch of Eq. (5.1.4) using $A = 0.5$, $R = 3$, $L = 0.8$ and $C = 2$.

Figure 5.1., and Figure 5.2. are corresponding to series RLC circuit.

B. Parallel RLC Circuit

Consider a parallel RLC circuit if its dynamics includes fractal time; therefore, to model it, we can write the following differential equation as [109]

$$D^{2\alpha}_{F^\kappa,t}\upsilon\left(t\right)+\frac{1}{RC}D^{\alpha}_{F^\kappa,t}\upsilon\left(t\right)+\frac{1}{LC}\upsilon\left(t\right)=0,\ 0<\alpha\leq 1,\quad t\in F^\kappa, \tag{5.1.5}$$

using the initial conditions $\upsilon\left(0\right)=A$, and $D^{\alpha}_{F^\kappa,t}\upsilon(t)|_{t=0}=A$, and applying the fractal Laplace transform to both sides of Eq. (5.1.5), then it turns to

$$\begin{aligned}\upsilon^{\alpha}_{F^\kappa}\left(w\right)=A&\frac{S^{\alpha}_{F^\kappa}\left(w\right)}{S^{\alpha}_{F^\kappa}(w)^2+\frac{S^{\alpha}_{F^\kappa}(w)}{RC}+\frac{1}{LC}}+\frac{1}{S^{\alpha}_{F^\kappa}(w)^2+\frac{S^{\alpha}_{F^\kappa}(w)}{RC}+\frac{1}{LC}}\\&+\frac{1}{RC}\frac{1}{S^{\alpha}_{F^\kappa}(w)^2+\frac{S^{\alpha}_{F^\kappa}(w)}{RC}+\frac{1}{LC}}.\end{aligned} \tag{5.1.6}$$

Taking the inverse Laplace of Eq. (5.1.6), we get

$$\begin{aligned}\upsilon\left(t\right)=&\frac{A\mathrm{e}^{-\frac{\left(L+\sqrt{L\left(L-4CR^2\right)}\right)S^{\alpha}_{F^\kappa}(t)}{2CLR}}}{2\sqrt{L\left(L-4CR^2\right)}}\left(-1+\mathrm{e}^{\frac{\sqrt{L\left(L-4CR^2\right)}S^{\alpha}_{F^\kappa}(t)}{CLR}}\right)L\left(1+2CR\right)\\&+\frac{A\mathrm{e}^{-\frac{\left(L+\sqrt{L\left(L-4CR^2\right)}\right)S^{\alpha}_{F^\kappa}(t)}{2CLR}}}{2\sqrt{L\left(L-4CR^2\right)}}\left(1+\mathrm{e}^{\frac{\sqrt{L\left(L-4CR^2\right)}S^{\alpha}_{F^\kappa}(t)}{CLR}}\right)\sqrt{L\left(L-4CR^2\right)}.\end{aligned} \tag{5.1.7}$$

By the upper bound of the staircase function ($S^{\alpha}_{F^\kappa}(t)\leq t^\alpha$), we get

$$\begin{aligned}\upsilon\left(t\right)\approx&\frac{A\mathrm{e}^{-\frac{\left(L+\sqrt{L\left(L-4CR^2\right)}\right)t^\alpha}{2CLR}}}{2\sqrt{L\left(L-4CR^2\right)}}\left(-1+\mathrm{e}^{\frac{\sqrt{L\left(L-4CR^2\right)}t^\alpha}{CLR}}\right)L\left(1+2CR\right)\\&+\frac{A\mathrm{e}^{-\frac{\left(L+\sqrt{L\left(L-4CR^2\right)}\right)t^\alpha}{2CLR}}}{2\sqrt{L\left(L-4CR^2\right)}}\left(1+\mathrm{e}^{\frac{\sqrt{L\left(L-4CR^2\right)}t^\alpha}{CLR}}\right)\sqrt{L\left(L-4CR^2\right)}.\end{aligned} \tag{5.1.8}$$

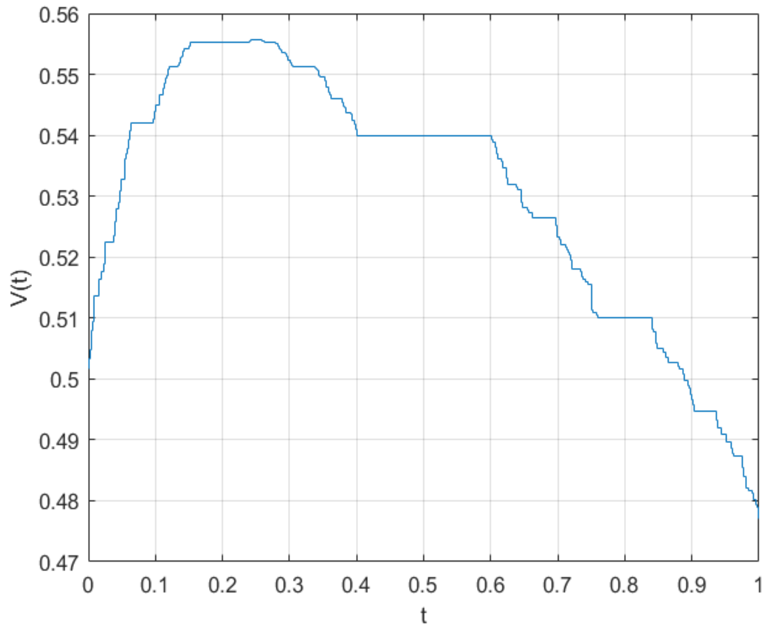

Figure 5.3. The sketch of Eq. (5.1.7) using $A = 0.5$, $R = 2$, $L = 7$ and $C = 0.1$.

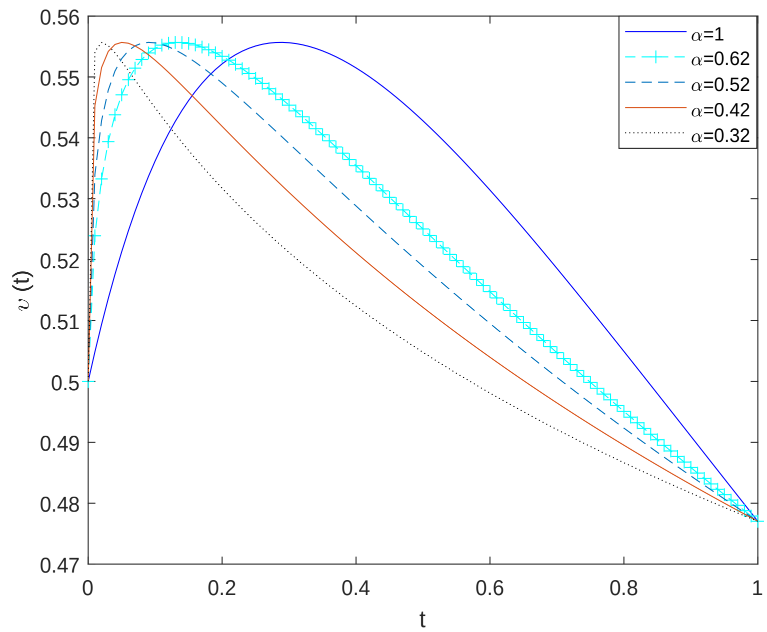

Figure 5.4. The sketch of Eq. (5.1.8) using $A = 0.5$, $R = 2$, $L = 7$ and $C = 0.1$.

Figure 5.3., and Figure 5.4. are corresponding to parallel RLC circuit.

5.2 Battery Discharging Model on Fractal Time Sets

In this section, the mathematical model of battery discharging involving the fractal time [110-112] is proposed for investigation. The discharge of a battery may be defined as an $RC-$circuit with resistance R and capacity C for the charge Q. In the first model, we study the local fractal battery discharging model by virtue of the local fractal Laplace transform. In the second model, we investigate the non-local fractal battery discharging model by mean of the non-local fractal Laplace transform.

First Model.

Consider the local fractal battery discharging model as follows (for the standard version we refer the reader to see [113]):

$$D_{F^\kappa}^{\alpha} Q(t) + \frac{1}{RC} Q(t) = 0, \tag{5.2.1}$$

with the charge amount for the battery at $t = 0$ equal to Q_0 $\quad$ (i.e $Q(0) = Q_0$) . If we apply the local fractal Laplace transform to Eq. (5.2.1), then we have

$$S_{F^\kappa}^{\alpha}(w) L_{F^\kappa}^{\alpha}(Q(t)) - Q_0 + \frac{1}{RC} L_{F^\kappa}^{\alpha}(Q(t)) = 0,$$

or,

$$L_{F^\kappa}^{\alpha}(Q(t)) = \frac{Q_0}{S_{F^\kappa}^{\alpha}(w) + \frac{1}{RC}}. \tag{5.2.2}$$

Taking the inverse Laplace local fractal calculus to both sides of Eq. (5.2.2), we obtain the charge of a battery in the frame of local fractal derivative follows:

$$Q(t) = Q_0 \exp\left(-\frac{1}{RC} S_{F^\kappa}^{\alpha}(t)\right). \tag{5.2.3}$$

Using $(a_1 t^\alpha \leq S_{F^\kappa}^{\alpha}(t) \leq a_2 t^\alpha)$, we can write

$$Q(t) \approx Q_0 \exp\left(-\frac{1}{RC} t^\alpha\right). \tag{5.2.4}$$

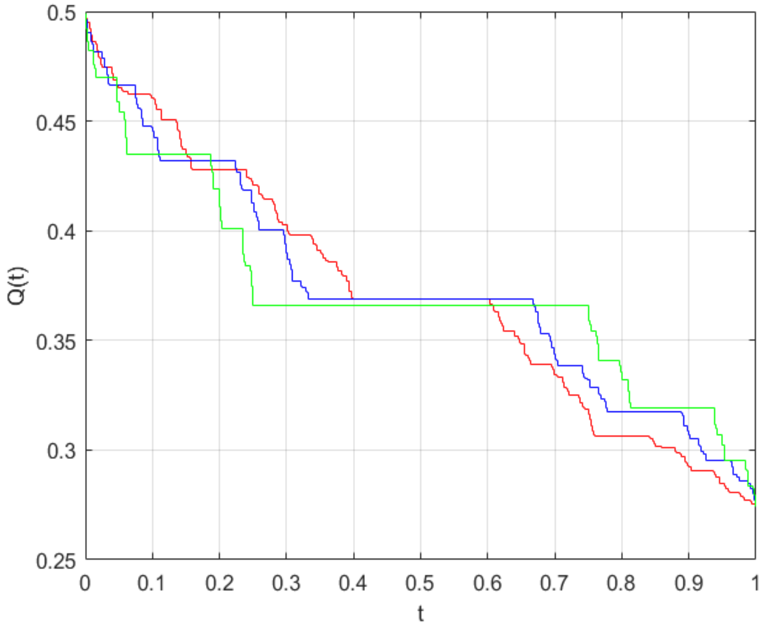

Figure 5.5. We have sketched Eq. (5.2.3) $Q_0 = 0.5$, $R = 5$, $C = 3$. $\kappa = 1/5$ (red color), $\kappa = 1/3$ (blue color) and $\kappa = 1/2$ (green color).

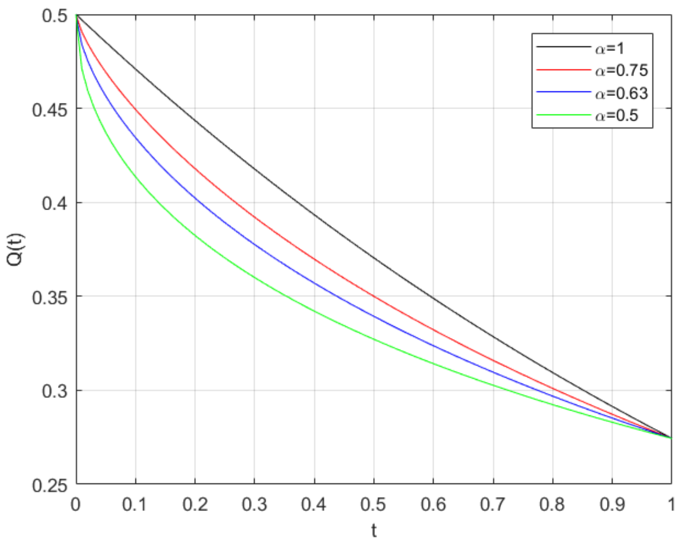

Figure 5.6. We have presented Eq. (5.2.4) using $Q_0 = 0.5$, $R = 5$ and $C = 3$.

In Figure 5.5., and Figure 5.6., we have shown the solution of first model for the discharging batteries.

Remark 1. If we choose $\alpha = 1$, in Eq. (5.2.3), then we arrive the same result in the standard form, where α is the dimension of the fractal set.

Second Model. Consider the non-local fractal battery discharging model as follows:

$$ {}_0^C D_{F^\kappa}^{\beta} Q(t) + \frac{1}{RC} Q(t) = 0, \tag{5.2.5} $$

with using $Q(0) = Q_0$. If we apply the non-local fractal Laplace transform to Eq. (5.2.5), then we obtain

$$ S_{F^\kappa}^{\alpha}(w)^{\beta} L_{F^\kappa}^{\alpha}(Q(t)) - Q_0 S_{F^\kappa}^{\alpha}(w)^{\beta-1} + \frac{1}{RC} L_{F^\kappa}^{\alpha}(Q(t)) = 0, $$

Or,

$$ L_{F^\kappa}^{\alpha}(Q(t)) = Q_0 \frac{S_{F^\kappa}^{\alpha}(w)^{\beta-1}}{S_{F^\kappa}^{\alpha}(w)^{\beta} + \frac{1}{RC}}. \tag{5.2.6} $$

Taking the inverse non-local fractal Laplace transform to both sides of Eq. (5.2.6), we obtain the charge function, which is solution of a battery discharging model in the frame of non-local fractal derivative as follows

$$ Q(t) = Q_0 E_{F^\kappa,\beta}^{\alpha}\left(\frac{-1}{RC} S_{F^\kappa}^{\alpha}(t)^{\beta}\right), \tag{5.2.7} $$

or, equivalently

$$ Q(t) = Q_0 \sum_{n=0}^{\infty} \frac{\left(\frac{-1}{RC} S_{F^\kappa}^{\alpha}(t)^{\beta}\right)^n}{\Gamma(n\beta+1)}. \tag{5.2.8} $$

Utilizing $(a_1 t^\alpha \le S_\kappa^\alpha(t) \le a_2 t^\alpha)$, we get

$$ Q(t) \approx Q_0 \sum_{n=0}^{\infty} \frac{\left(\frac{-1}{RC} t^{\alpha\beta}\right)^n}{\Gamma(n\beta+1)}. \tag{5.2.9} $$

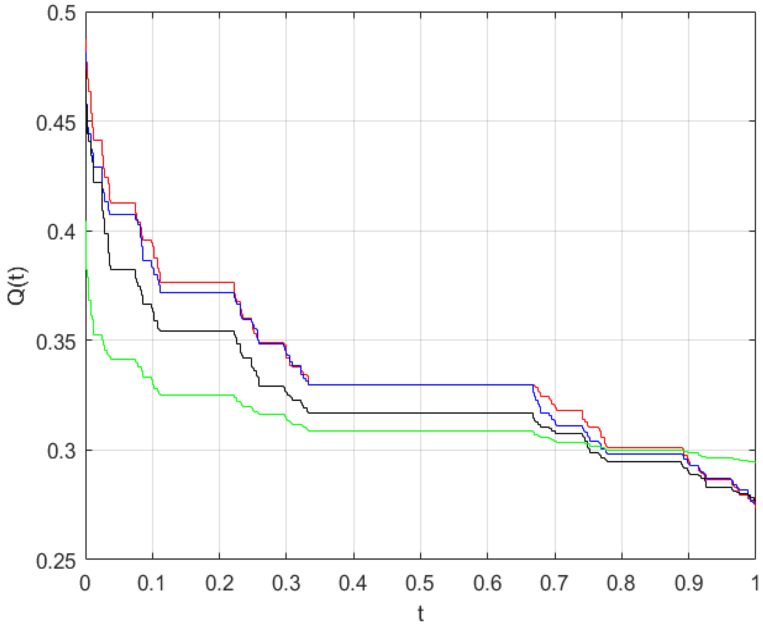

Figure 5.7. We have sketched Eq. (5.2.8) setting $Q_0 = 0.5,\ R = 2,\ C = 2,\ \ \kappa = 1/3(\alpha = 0.63)$, $\beta = 0.9$ (red color), $\beta = 0.8$ (blue color) $\beta = 0.7$ (black color) and $\beta = 0.3$ (green color).

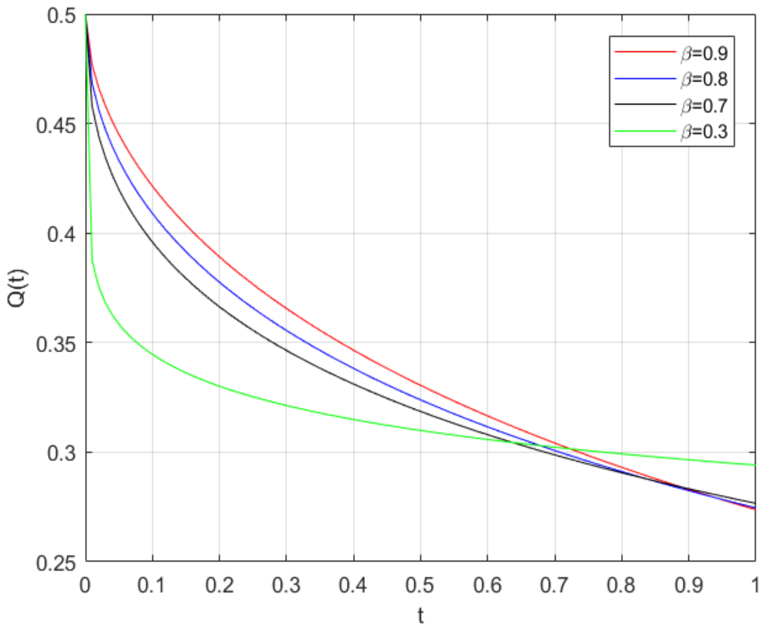

Figure 5.8. We have presented Eq. (5.2.9) using $Q_0 = 0.5,\ R = 2,\ C = 2$ and $\ \alpha = 0.63$.

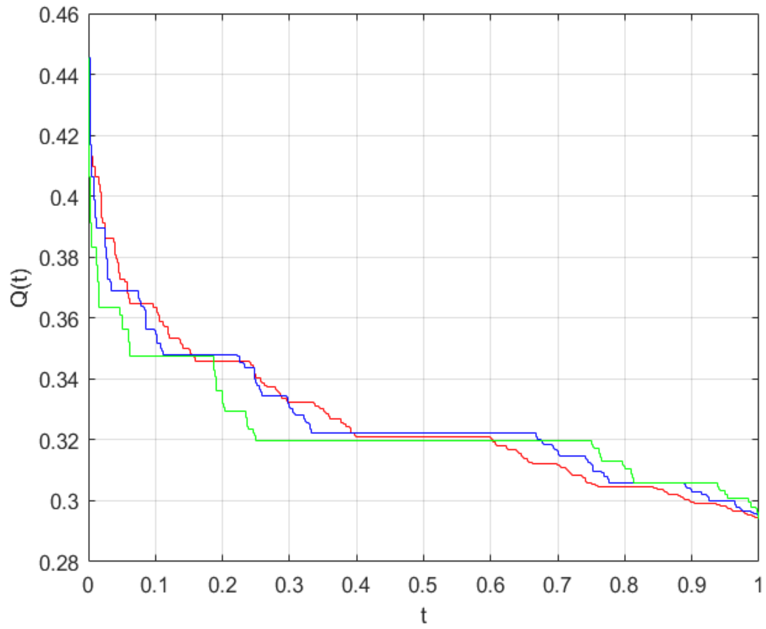

Figure 5.9. We have presented Eq. (5.2.8) using $Q_0 = 0.5$, $R = 2$, $C = 2$, $\beta = 0.3$, $\kappa = 1/5$, (red color), $\kappa = 1/3$ (blue color) $\kappa = 1/2$ (green color)

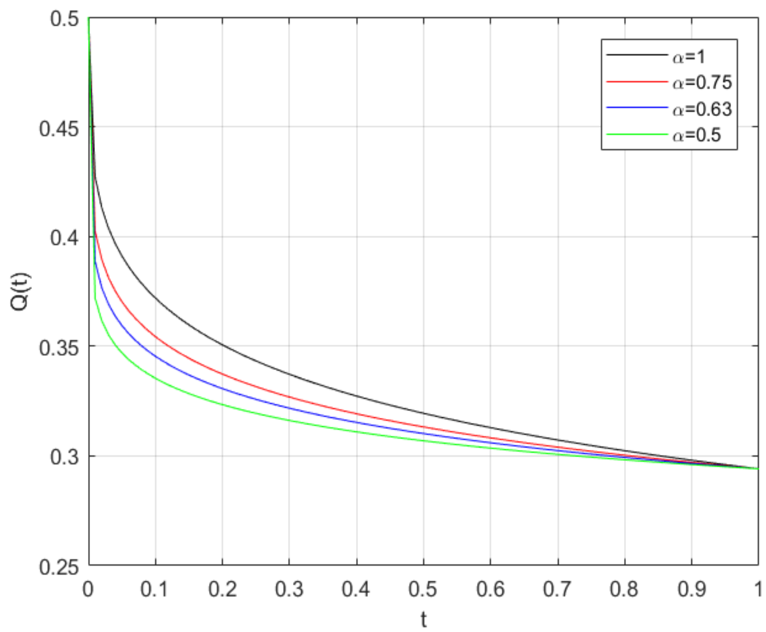

Figure 5.10. We have presented Eq. (5.2.9) using $Q_0 = 0.5$, $R = 2$, $C = 2$ and $\beta = 0.3$.

In Figure 5.7., Figure 5.8., Figure 5.9., and Figure 5.10., we have illustrated the details of the second model.

Remark 2. If we choose $\alpha = 1$ in Eq. (5.2.9), then we get the same result in the standard fractional calculus form. If we choose $\alpha = \beta = 1$ in Eq. (5.2.9), then we get the same result in the standard calculus form, where α is the dimension of the fractal set, and β is the operator of the non-local derivative.

5.3 One-term and Three-term Fractal Differential Equations

In this section, we investigate the fractal version of both one-term and three-term fractal differential equations.

(I) Consider the three-term fractal-order differential equation with constant coefficients, for the standard version see in [114]

$$D^{\alpha}_{F^{\kappa},t} y(t) + \mu \, {}^{C}_{0}\mathbb{D}^{\beta}_{F^{\kappa},t} y(t) + \lambda y(t) = f(t), \qquad \mu > 0,\ 0 < \beta < \alpha \leq 1, \tag{5.3.1}$$

where $y(0) = b$ and $F^{\alpha}_{F^{\kappa}}(w) = \frac{1}{S^{\alpha}_{F^{\kappa}}(w)}$.

Applying the fractal Laplace transform to both sides of Eq. (5.3.1), we have

$$\begin{aligned} Y^{\alpha}_{F^{\kappa}}(w) = {} & b\frac{1}{S^{\alpha}_{F^{\kappa}}(w) + \mu S^{\alpha}_{F^{\kappa}}(w)^{\beta} + \lambda} + b\mu \frac{S^{\alpha}_{F^{\kappa}}(w)^{\beta-1}}{S^{\alpha}_{F^{\kappa}}(w) + \mu S^{\alpha}_{F^{\kappa}}(w)^{\beta} + \lambda} \\ & + \frac{S^{\alpha}_{F^{\kappa}}(w)^{-1}}{S^{\alpha}_{F^{\kappa}}(w) + \mu S^{\alpha}_{F^{\kappa}}(w)^{\beta} + \lambda}. \end{aligned} \tag{5.3.2}$$

Observe that

$$\frac{1}{S^{\alpha}_{F^{\kappa}}(w) + \mu S^{\alpha}_{F^{\kappa}}(w)^{\beta} + \lambda} = \frac{S^{\alpha}_{F^{\kappa}}(w)^{-\beta}}{S^{\alpha}_{F^{\kappa}}(w)^{1-\beta} + \mu} \frac{1}{\left[1 - \left(\frac{-\lambda S^{\alpha}_{F^{\kappa}}(w)^{-\beta}}{S^{\alpha}_{F^{\kappa}}(w)^{1-\beta} + \mu}\right)\right]},$$

where $\left|\frac{-\lambda S^{\alpha}_{F^{\kappa}}(w)^{-\beta}}{S^{\alpha}_{F^{\kappa}}(w)^{1-\beta} + \mu}\right| < 1$.

Recall that

$$(1-t)^{-i} = \sum_{r=0}^{\infty} \binom{i+r-1}{r} t^{r}.$$

This implies

$$
\begin{aligned}
\frac{1}{S^{\alpha}_{F^{\kappa}}(w)+\mu S^{\alpha}_{F^{\kappa}}(w)^{\beta}+\lambda} &= \sum_{i=0}^{\infty}(-\lambda)^{i}\frac{S^{\alpha}_{F^{\kappa}}(w)^{-\beta-i\beta}}{\left(S^{\alpha}_{F^{\kappa}}(w)^{1-\beta}+\mu\right)^{i+1}} \\
&= \sum_{i=0}^{\infty}(-\lambda)^{i}\frac{S^{\alpha}_{F^{\kappa}}(w)^{-\beta-i\beta-(i+1)(1-\beta)}}{\left(1+\mu S^{\alpha}_{F^{\kappa}}(w)^{\beta-1}\right)^{i+1}} \\
&= \sum_{i=0}^{\infty}(-\lambda)^{i}S^{\alpha}_{F^{\kappa}}(w)^{-(i+1)}\left(1+\mu S^{\alpha}_{F^{\kappa}}(w)^{\beta-1}\right)^{-(i+1)} \\
&= \sum_{i=0}^{\infty}(-\lambda)^{i}S^{\alpha}_{F^{\kappa}}(w)^{-(i+1)}\times \\
&\quad \sum_{r=0}^{\infty}\binom{i+r}{r}(-\mu)^{r}S^{\alpha}_{F^{\kappa}}(w)^{r(\beta-1)} \\
&= \sum_{i=0}^{\infty}(-\lambda)^{i}S^{\alpha}_{F^{\kappa}}(w)^{-(i+1)}\times \\
&\quad \sum_{r=0}^{\infty}\frac{(i+r)!}{r!i!}(-\mu)^{r}S^{\alpha}_{F^{\kappa}}(w)^{r(\beta-1)}.
\end{aligned}
\tag{5.3.3}
$$

Inserting Eq. (5.3.3) into Eq. (5.3.2), we have

$$
\begin{aligned}
Y^{\alpha}_{F^{\kappa}}(w) &= b\left(\sum_{i=0}^{\infty}(-\lambda)^{i}\sum_{r=0}^{\infty}\frac{(i+r)!}{r!i!}(-\mu)^{r}S^{\alpha}_{F^{\kappa}}(w)^{(\beta-1)r-(i+1)}\right) \\
&\quad + b\mu\left(\sum_{i=0}^{\infty}(-\lambda)^{i}\sum_{r=0}^{\infty}\frac{(i+r)!}{r!i!}(-\mu)^{r}S^{\alpha}_{F^{\kappa}}(w)^{(\beta-1)r-(i+1)+\beta-1}\right) \\
&\quad + \left(\sum_{i=0}^{\infty}(-\lambda)^{i}\sum_{r=0}^{\infty}\frac{(i+r)!}{r!i!}(-\mu)^{r}S^{\alpha}_{F^{\kappa}}(w)^{(\beta-1)r-(i+1)-1}\right).
\end{aligned}
\tag{5.3.4}
$$

Taking the inverse Laplace of both sides of Eq. (5.3.2), one may get

$$
\begin{aligned}
y(t) &= b\left(\sum_{i=0}^{\infty}(-\lambda)^{i}\sum_{r=0}^{\infty}\frac{(i+r)!}{r!i!}(-\mu)^{r}\frac{S^{\alpha}_{F^{\kappa}}(t)^{(1-\beta)r+i}}{\Gamma^{\alpha}\left((1-\beta)r+i+1\right)}\right) \\
&\quad + b\mu\left(\sum_{i=0}^{\infty}(-\lambda)^{i}\sum_{r=0}^{\infty}\frac{(i+r)!}{r!i!}(-\mu)^{r}\frac{S^{\alpha}_{F^{\kappa}}(t)^{(1-\beta)r+i-\beta+1}}{\Gamma^{\alpha}\left((1-\beta)r+i-\beta+2\right)}\right) \\
&\quad + \left(\sum_{i=0}^{\infty}(-\lambda)^{i}\sum_{r=0}^{\infty}\frac{(i+r)!}{r!i!}(-\mu)^{r}\frac{S^{\alpha}_{F^{\kappa}}(t)^{(1-\beta)r+i+1}}{\Gamma^{\alpha}\left((1-\beta)r+i+2\right)}\right).
\end{aligned}
\tag{5.3.5}
$$

Then

$$y(t)=b\left(\sum_{i=0}^{\infty}(-\lambda)^{i}S_{F^{\kappa}}^{\alpha}(t)^{i}\sum_{r=0}^{\infty}\frac{(i+r)!}{r!i!}(-\mu)^{r}\frac{S_{F^{\kappa}}^{\alpha}(t)^{(1-\beta)r}}{\Gamma^{\alpha}\left((1-\beta)r+i+1\right)}\right)$$
$$+b\mu\left(\sum_{i=0}^{\infty}(-\lambda)^{i}S_{F^{\kappa}}^{\alpha}(t)^{i-\beta+1}\sum_{r=0}^{\infty}\frac{(i+r)!}{r!i!}(-\mu)^{r}\frac{S_{F^{\kappa}}^{\alpha}(t)^{(1-\beta)r}}{\Gamma^{\alpha}\left((1-\beta)r+i-\beta+2\right)}\right)$$
$$+\left(\sum_{i=0}^{\infty}(-\lambda)^{i}S_{F^{\kappa}}^{\alpha}(t)^{i+1}\sum_{r=0}^{\infty}\frac{(i+r)!}{r!i!}(-\mu)^{r}\frac{S_{F^{\kappa}}^{\alpha}(t)^{(1-\beta)r}}{\Gamma^{\alpha}\left((1-\beta)r+i+2\right)}\right). \tag{5.3.6}$$

Hence

$$y(t)=b\left(\sum_{i=0}^{\infty}(-\lambda)^{i}\frac{S_{F^{\kappa}}^{\alpha}(t)^{i}}{i!}{}_{1}\Psi_{1}\left[\begin{array}{c|c}(i+1,1) & \\ (i+1,1-\beta) & (-\mu)\,S_{F^{\kappa}}^{\alpha}(t)^{1-\beta}\end{array}\right]\right)$$
$$+b\mu\left(\sum_{i=0}^{\infty}(-\lambda)^{i}\frac{S_{F^{\kappa}}^{\alpha}(t)^{(i+1-\beta)}}{i!}{}_{1}\Psi_{1}\left[\begin{array}{c|c}(i+1,1) & \\ (i-\beta+2,1-\beta) & (-\mu)\,S_{F^{\kappa}}^{\alpha}(t)^{1-\beta}\end{array}\right]\right)$$
$$+\left(\sum_{i=0}^{\infty}(-\lambda)^{i}\frac{S_{F^{\kappa}}^{\alpha}(t)^{i+1}}{i!}{}_{1}\Psi_{1}\left[\begin{array}{c|c}(i+1,1) & \\ (i+2,1-\beta) & (-\mu)\,S_{F^{\kappa}}^{\alpha}(t)^{1-\beta}\end{array}\right]\right). \tag{5.3.7}$$

By considering Eq. (2.4.20), Eq. (5.3.7) can be rewritten as follows:

$$\begin{aligned}y(t)=b&\left(\sum_{i=0}^{\infty}(-\lambda)^{i}S_{F^{\kappa}}^{\alpha}(t)^{i}E_{1-\beta,i+1}^{\alpha,i+1}\left((-\mu)\,S_{F^{\kappa}}^{\alpha}(t)^{1-\beta}\right)\right)\\&+b\mu\times\left(\sum_{i=0}^{\infty}(-\lambda)^{i}S_{F^{\kappa}}^{\alpha}(t)^{(i+1-\beta)}E_{1-\beta,i-\beta+2}^{\alpha,i+1}\left((-\mu)\,S_{F^{\kappa}}^{\alpha}(t)^{1-\beta}\right)\right)\\&+\left(\sum_{i=0}^{\infty}(-\lambda)^{i}S_{F^{\kappa}}^{\alpha}(t)^{i+1}E_{1-\beta,i+2}^{\alpha,i+1}\left((-\mu)\,S_{F^{\kappa}}^{\alpha}(t)^{1-\beta}\right)\right).\end{aligned} \tag{5.3.8}$$

Furthermore, we have

$$y(t)=b\left(\sum_{n=0}^{\infty}(-\lambda)^{n}S_{F^{\kappa}}^{\alpha}(t)^{n}\sum_{j=0}^{\infty}\frac{(n+1)_{j}}{\Gamma^{\alpha}\left((1-\beta)j+n+1\right)}\frac{\left((-\mu)\,S_{F^{\kappa}}^{\alpha}(t)^{1-\beta}\right)^{j}}{j!}\right)$$
$$+b\mu\times\left(\begin{array}{l}\displaystyle\sum_{n=0}^{\infty}(-\lambda)^{n}S_{F^{\kappa}}^{\alpha}(t)^{(n+1-\beta)}\times\\ \displaystyle\sum_{j=0}^{\infty}\frac{(n+1)_{j}}{\Gamma^{\alpha}\left((1-\beta)j+n-\beta+2\right)}\frac{\left((-\mu)\,S_{F^{\kappa}}^{\alpha}(t)^{1-\beta}\right)^{j}}{j!}\end{array}\right)$$
$$+\left(\sum_{n=0}^{\infty}(-\lambda)^{n}S_{F^{\kappa}}^{\alpha}(t)^{n+1}\sum_{j=0}^{\infty}\frac{(n+1)_{j}}{\Gamma^{\alpha}\left((1-\beta)j+n+2\right)}\frac{\left((-\mu)\,S_{F^{\kappa}}^{\alpha}(t)^{1-\beta}\right)^{j}}{j!}\right).$$

(5.3.9)

(II) Consider a fractal differential equation involving the non-local fractal derivatives as follows:

$$ {}_{0}^{C}\mathbb{D}_{F^{\kappa},t}^{\gamma}y(t)+\mu {}_{0}^{C}\mathbb{D}_{F^{\kappa},t}^{\beta}y(t)+\lambda y(t)=f(t), \qquad \mu>0,\ 0<\beta<\gamma\leq 1, \tag{5.3.10}$$

(by using $y(0)=b$ and $F_{F^{\kappa}}^{\alpha}(w)=\frac{1}{S_{F^{\kappa}}^{\alpha}(w)}$). Applying the fractal Laplace transform to both sides of Eq. (5.3.10), we obtain

$$\begin{aligned} Y_{F^{\kappa}}^{\alpha}(w) &= b\frac{S_{F^{\kappa}}^{\alpha}(w)^{\gamma-1}}{S_{F^{\kappa}}^{\alpha}(w)^{\gamma}+\mu S_{F^{\kappa}}^{\alpha}(w)^{\beta}+\lambda}+b\mu\frac{S_{F^{\kappa}}^{\alpha}(w)^{\beta-1}}{S_{F^{\kappa}}^{\alpha}(w)^{\gamma}+\mu S_{F^{\kappa}}^{\alpha}(w)^{\beta}+\lambda} \\ &+\frac{F_{F^{\kappa}}^{\alpha}(w)}{S_{F^{\kappa}}^{\alpha}(w)^{\gamma}+\mu S_{F^{\kappa}}^{\alpha}(w)^{\beta}+\lambda}. \end{aligned} \tag{5.3.11}$$

Observe that

$$\frac{1}{S_{F^{\kappa}}^{\alpha}(w)^{\gamma}+\mu S_{F^{\kappa}}^{\alpha}(w)^{\beta}+\lambda}=\frac{S_{F^{\kappa}}^{\alpha}(w)^{-\beta}}{S_{F^{\kappa}}^{\alpha}(w)^{\gamma-\beta}+\mu}\frac{1}{\left[1-\left(\frac{-\lambda S_{F^{\kappa}}^{\alpha}(w)^{-\beta}}{S_{F^{\kappa}}^{\alpha}(w)^{\gamma-\beta}+\mu}\right)\right]},$$

where $\left|\frac{-\lambda S_{F^{\kappa}}^{\alpha}(w)^{-\beta}}{S_{F^{\kappa}}^{\alpha}(w)^{\gamma-\beta}+\mu}\right|<1$.

Recall that

$$(1-t)^{-i}=\sum_{r=0}^{\infty}\binom{i+r-1}{r}t^{r}.$$

This implies

$$\begin{aligned} \frac{1}{S_{F^{\kappa}}^{\alpha}(w)^{\gamma}+\mu S_{F^{\kappa}}^{\alpha}(w)^{\beta}+\lambda} &= \sum_{i=0}^{\infty}(-\lambda)^{i}\frac{S_{F^{\kappa}}^{\alpha}(w)^{-\beta-i\beta}}{\left(S_{F^{\kappa}}^{\alpha}(w)^{\gamma-\beta}+\mu\right)^{i+1}} \\ &= \sum_{i=0}^{\infty}(-\lambda)^{i}\frac{S_{F^{\kappa}}^{\alpha}(w)^{-\beta-i\beta-(i+1)(\gamma-\beta)}}{\left(1+\mu S_{F^{\kappa}}^{\alpha}(w)^{\beta-\gamma}\right)^{i+1}} \\ &= \sum_{i=0}^{\infty}(-\lambda)^{i}S_{F^{\kappa}}^{\alpha}(w)^{-(i+1)\gamma}\left(1+\mu S_{F^{\kappa}}^{\alpha}(w)^{\beta-\gamma}\right)^{-(i+1)} \\ &= \sum_{i=0}^{\infty}(-\lambda)^{i}S_{F^{\kappa}}^{\alpha}(w)^{-(i+1)\gamma}\sum_{r=0}^{\infty}\binom{i+r}{r}(-\mu)^{r}\times \\ &\quad S_{F^{\kappa}}^{\alpha}(w)^{r(\beta-\gamma)} \\ &= \sum_{i=0}^{\infty}(-\lambda)^{i}\sum_{r=0}^{\infty}\frac{(i+r)!}{r!i!}(-\mu)^{r}S_{F^{\kappa}}^{\alpha}(w)^{-(i+1)\gamma+r(\beta-\gamma)}. \end{aligned} \tag{5.3.12}$$

Inserting Eq. (5.3.13) into Eq. (5.3.12), we get

$$\begin{aligned} Y_{F^{\kappa}}^{\alpha}(w) &= b\left(\sum_{i=0}^{\infty}(-\lambda)^{i}\sum_{r=0}^{\infty}\frac{(i+r)!}{r!i!}(-\mu)^{r}S_{F^{\kappa}}^{\alpha}(w)^{(\beta-\gamma)r-i\gamma-1}\right) \\ &\quad + b\mu\left(\sum_{i=0}^{\infty}(-\lambda)^{i}\sum_{r=0}^{\infty}\frac{(i+r)!}{r!i!}(-\mu)^{r}S_{F^{\kappa}}^{\alpha}(w)^{(\beta-\gamma)r-(i+1)\gamma+\beta-1}\right) \\ &\quad + \left(\sum_{i=0}^{\infty}(-\lambda)^{i}\sum_{r=0}^{\infty}\frac{(i+r)!}{r!i!}(-\mu)^{r}S_{F^{\kappa}}^{\alpha}(w)^{(\beta-\gamma)r-(i+1)\gamma-1}\right). \end{aligned} \tag{5.3.13}$$

Taking the Laplace inverse to both sides of Eq. (5.3.13), we have

$$\begin{aligned} y(t) &= b\left(\sum_{i=0}^{\infty}(-\lambda)^{i}\sum_{r=0}^{\infty}\frac{(i+r)!}{r!n!}(-\mu)^{r}\frac{S_{F^{\kappa}}^{\alpha}(t)^{(\gamma-\beta)r+i\gamma}}{\Gamma^{\alpha}((\gamma-\beta)r+i\gamma+1)}\right) \\ &\quad + b\mu\left(\sum_{i=0}^{\infty}(-\lambda)^{i}\sum_{r=0}^{\infty}\frac{(i+r)!}{r!i!}(-\mu)^{r}\frac{S_{F^{\kappa}}^{\alpha}(t)^{(\gamma-\beta)r+(i+1)\gamma-\beta}}{\Gamma^{\alpha}((\gamma-\beta)r+(i+1)\gamma-\beta+1)}\right) \\ &\quad + \left(\sum_{i=0}^{\infty}(-\lambda)^{i}\sum_{r=0}^{\infty}\frac{(i+r)!}{r!i!}(-\mu)^{r}\frac{S_{F^{\kappa}}^{\alpha}(t)^{(\gamma-\beta)r+(i+1)\gamma}}{\Gamma^{\alpha}((\gamma-\beta)r+(i+1)\gamma+1)}\right). \end{aligned} \tag{5.3.14}$$

Therefore, we obtain the following:

$$\begin{aligned} y(t) &= b\left(\sum_{n=0}^{\infty}(-\lambda)^{n}\frac{S_{F^{\kappa}}^{\alpha}(t)^{\gamma n}}{n!}\,{}_{1}\Psi_{1}\left[\begin{array}{c|c}(n+1,1) & \\ (\gamma n+1,\gamma-\beta) & (-\mu)\,S_{F^{\kappa}}^{\alpha}(t)^{\gamma-\beta}\end{array}\right]\right) \\ &\quad + b\mu\left(\begin{array}{l}\displaystyle\sum_{n=0}^{\infty}(-\lambda)^{n}\frac{S_{F^{\kappa}}^{\alpha}(t)^{(n+1)\gamma-\beta}}{n!}\times \\ {}_{1}\Psi_{1}\left[\begin{array}{c|c}(n+1,1) & \\ ((n+1)\gamma-\beta+1,\gamma-\beta) & (-\mu)\,S_{F^{\kappa}}^{\alpha}(t)^{\gamma-\beta}\end{array}\right]\end{array}\right) \\ &\quad + \left(\sum_{n=0}^{\infty}(-\lambda)^{n}\frac{S_{F^{\kappa}}^{\alpha}(t)^{(n+1)\gamma}}{n!}\,{}_{1}\Psi_{1}\left[\begin{array}{c|c}(n+1,1) & \\ ((n+1)\gamma,\gamma-\beta) & (-\mu)\,S_{F^{\kappa}}^{\alpha}(t)^{\gamma-\beta}\end{array}\right]\right), \end{aligned} \tag{5.3.15}$$

By taking into account Eq. (2.4.20), Eq. (5.3.15) can be rewritten in the following form:

$$\begin{aligned} y(t) &= b\left(\sum_{i=0}^{\infty}(-\lambda)^{i}S_{F^{\kappa}}^{\alpha}(t)^{i\gamma}E_{\gamma-\beta,i\gamma+1}^{\alpha,i+1}\left((-\mu)\,S_{F^{\kappa}}^{\alpha}(t)^{\gamma-\beta}\right)\right) \\ &\quad + b\mu\times\left(\sum_{i=0}^{\infty}(-\lambda)^{i}S_{F^{\kappa}}^{\alpha}(t)^{(i+1)\gamma-\beta}E_{\gamma-\beta,(i+1)\gamma-\beta+1}^{\alpha,i+1}\left((-\mu)\,S_{F^{\kappa}}^{\alpha}(t)^{\gamma-\beta}\right)\right) \\ &\quad + \left(\sum_{i=0}^{\infty}(-\lambda)^{i}S_{F^{\kappa}}^{\alpha}(t)^{(i+1)\gamma}E_{\gamma-\beta,(i+1)\gamma+1}^{\alpha,i+1}\left((-\mu)\,S_{F^{\kappa}}^{\alpha}(t)^{\gamma-\beta}\right)\right). \end{aligned} \tag{5.3.16}$$

Furthermore, we have

$$y(t) = b\left(\sum_{n=0}^{\infty} (-\lambda)^n S_{F^\kappa}^{\alpha}(t)^{n\gamma} \sum_{j=0}^{\infty} \frac{(n+1)_j}{\Gamma^\alpha((\gamma-\beta)j+n\gamma+1)} \frac{\left((-\mu) S_{F^\kappa}^{\alpha}(t)^{\gamma-\beta}\right)^j}{j!} \right)$$
$$+ b\mu \times \left(\begin{array}{l} \sum_{n=0}^{\infty} (-\lambda)^n S_{F^\kappa}^{\alpha}(t)^{(n+1)\gamma-\beta} \times \\ \sum_{k=0}^{\infty} \frac{(n+1)_j}{\Gamma^\alpha((\gamma-\beta)j+(n+1)\gamma-\beta+1)} \frac{\left((-\mu) S_{F^\kappa}^{\alpha}(t)^{\gamma-\beta}\right)^j}{j!} \end{array} \right)$$
$$+ \left(\begin{array}{l} \sum_{n=0}^{\infty} (-\lambda)^n S_{F^\kappa}^{\alpha}(t)^{(n+1)\gamma} \times \\ \sum_{k=0}^{\infty} \frac{(n+1)_j}{\Gamma^\alpha((\gamma-\beta)j+(n+1)\gamma+1)} \frac{\left((-\mu) S_{F^\kappa}^{\alpha}(t)^{\gamma-\beta}\right)^j}{j!} \end{array} \right). \tag{5.3.17}$$

(III) Consider the following one-term fractal differential equation with constant coefficient and local fractal derivatives:

$$bD_{F^\kappa}^{\alpha} y(t) = f(t), \quad b \in \mathbf{R}. \tag{5.3.18}$$

By taking the Laplace transform to both sides of Eq. (5.3.18), we have

$$L_{F^\kappa}^{\alpha}(y(t)) = \frac{1}{bS_{F^\kappa}^{\alpha}(w)} F\left(S_{F^\kappa}^{\alpha}(w)\right). \tag{5.3.19}$$

Let us now take the Laplace inverse to both sides of Eq. (5.3.19), and using Eq. (2.4.24), we get

$$y(t) = \frac{1}{b} \int_0^t f(\tau)\, d_{F^\kappa}^{\alpha} \tau. \tag{5.3.20}$$

Remark 5.3.1. When we put $\alpha = 1$, we get the standard ordinary calculus results [121].
(IV) Consider a fractal differential equation involving the non-local fractal derivatives as follows:

$$b\, {}_0^C\mathbb{D}_t^{\sigma} y(t) = f(t), \tag{5.3.21}$$

where $0 < \sigma < 1,\ b \in \mathbf{R}$.
By taking the Laplace transform to both sides of Eq. (5.3.21), we have

$$L_{F^\kappa}^{\alpha}(y(t)) = \frac{1}{b\ S_{F^\kappa}^{\alpha}(w)^{\sigma}} F\left(S_{F^\kappa}^{\alpha}(w)\right). \tag{5.3.22}$$

Taking the Laplace inverse to both sides of Eq. (5.3.22), and using Eq. (2.4.24), we get

$$y(t) = \frac{1}{b\,\Gamma(\sigma)} \int_0^t \frac{1}{(t-\tau)^{1-\sigma}} f(\tau)\, d^{\alpha}_{F^{\kappa}}\tau. \tag{5.3.23}$$

Remark 5.3.2. When we put $\alpha = 1$, get the standard fractional calculus results [121].

5.4 Numerical Examples

In this section, the simulation of all obtained solutions are analyzed.

1. Assume that $b = 0$ i.e $y(0) = 0$ in Eq. (5.3.9), we get

$$y(t) = \left(\sum_{i=0}^{\infty} (-\lambda)^i S^{\alpha}_{F^{\kappa}}(t)^{i+1} \sum_{j=0}^{\infty} \frac{(i+1)_j}{\Gamma^{\alpha}((1-\beta)j+i+2)} \frac{\left((-\mu) S^{\alpha}_{F^{\kappa}}(t)^{1-\beta}\right)^j}{j!} \right), \tag{5.4.1}$$

$$\approx \left(\sum_{i=0}^{\infty} (-\lambda)^i t^{\alpha(i+1)} \sum_{j=0}^{\infty} \frac{(i+1)_j}{\Gamma((1-\beta)j+i+2)} \frac{\left(-\mu(t)^{\alpha*1-\alpha\beta}\right)^j}{j!} \right). \tag{5.4.2}$$

In Figure 5.11., we have plotted exact solution of Eq. (5.4.1).

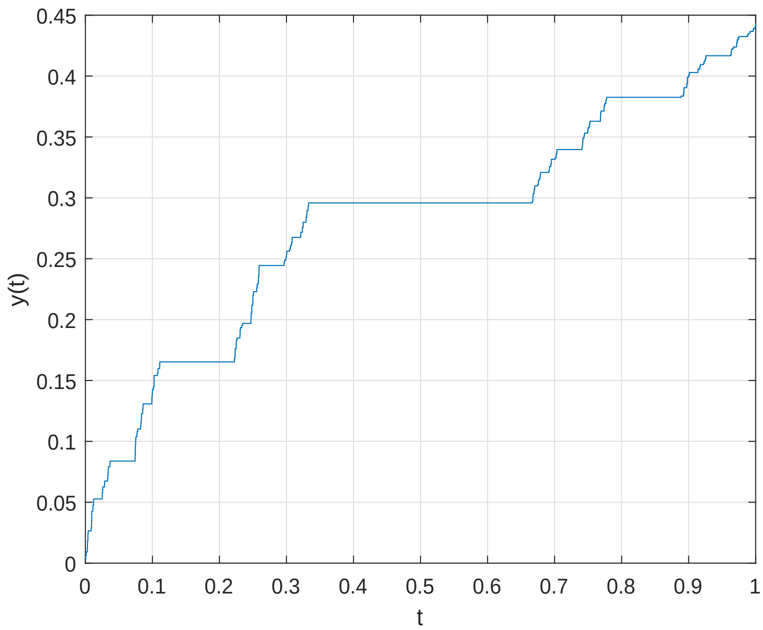

Figure 5.11. The sketch of Eq. (5.4.1) using $\alpha = 0.62$, $\beta = 0.5$ $\mu = 0.9$ and $\lambda = 0.8$.

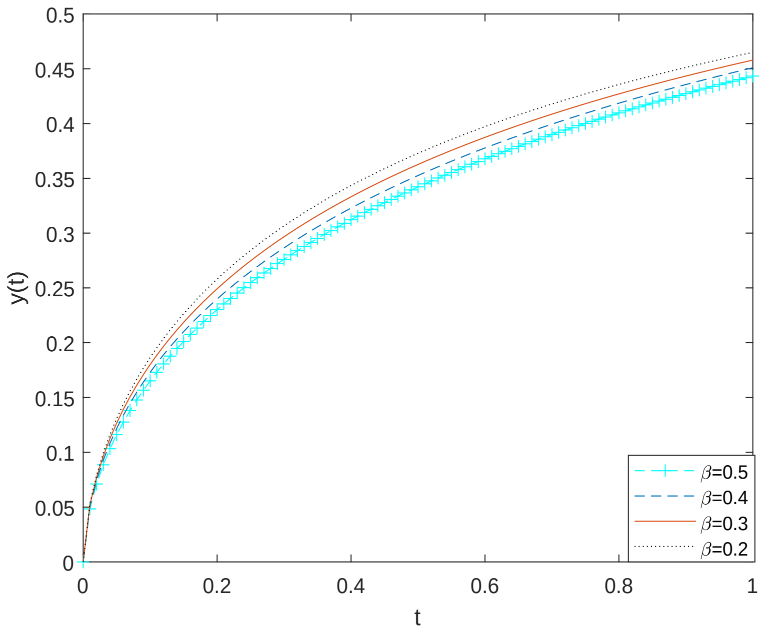

Figure 5.12. The sketch of Eq. (5.4.2) using $\alpha = 0.62$ $\mu = 0.9$ and $\lambda = 0.8$.

In Figure 5.12., we have plotted exact solution of Eq. (5.4.2) under the effect of fractional parameter β.

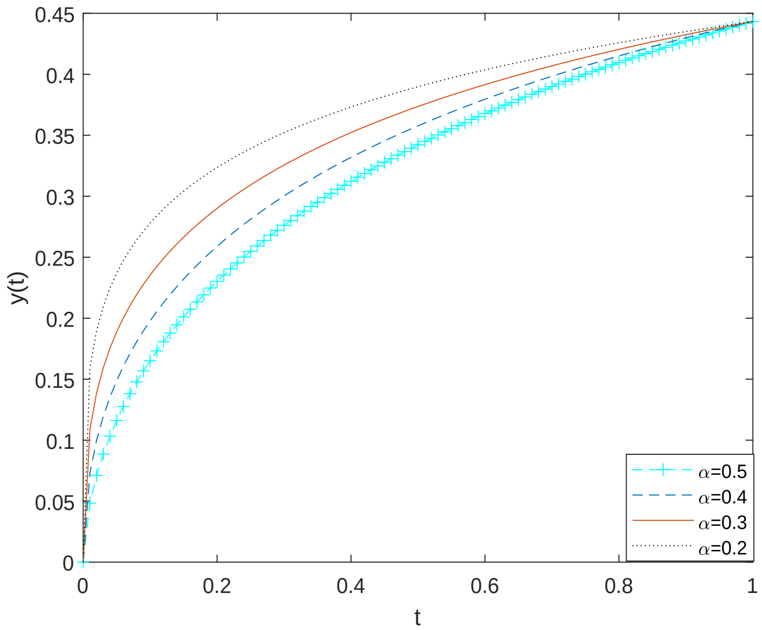

Figure 5.13. The sketch of Eq. (5.4.2) using $\beta = 0.5$, $\mu = 0.9$ and $\lambda = 0.8$.

In Figure 5.13., we have plotted exact solution of Eq. (5.4.2) under the effect of fractal parameter α.

2. Assume that $b = 0$ i.e $y(0) = 0$ in Eq. (5.3.17), we get

$$y(t) = \sum_{i=0}^{\infty} (-\lambda)^i S^{\alpha}_{F^\kappa}(t)^{(i+1)\gamma} \times \sum_{j=0}^{\infty} \frac{(i+1)_j}{\Gamma^\alpha\left((\gamma-\beta)j + (i+1)\gamma + 1\right)} \frac{\left((-\mu) S^{\alpha}_{F^\kappa}(t)^{\gamma-\beta}\right)^j}{j!}, \tag{5.4.3}$$

$$\approx \left(\sum_{i=0}^{\infty} (-\lambda)^i t^{\alpha\gamma(i+1)} \sum_{j=0}^{\infty} \frac{(i+1)_j}{\Gamma\left((1-\beta)j + i + 2\right)} \frac{\left(-\mu(t)^{\alpha\gamma-\alpha\beta}\right)^j}{j!} \right). \tag{5.4.4}$$

In the approximation of Eqs. (5.4.2) and (5.4.3) we used upper bound as $S^{\alpha}_{C^\kappa}(t) \le t^\alpha$.

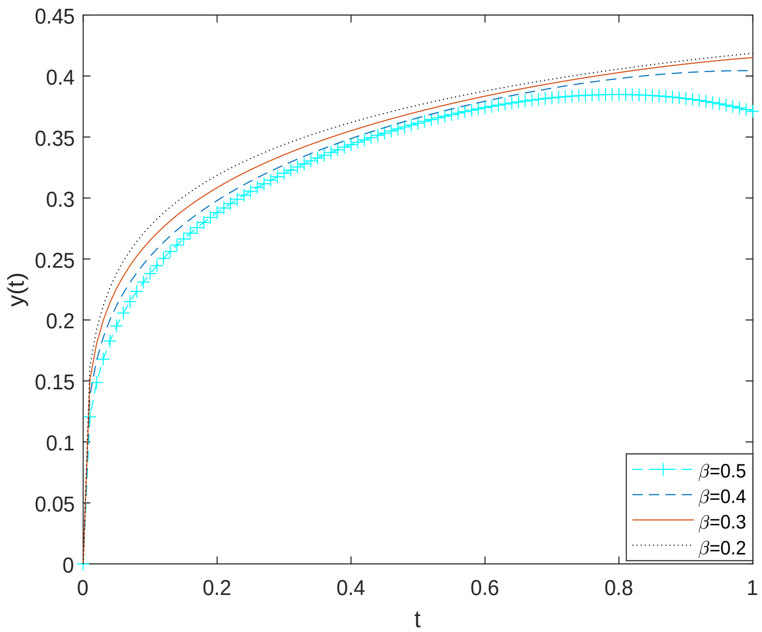

Figure 5.14. The sketch of Eq. (5.4.3) using $\alpha = 0.62$, $\mu = 0.9$, $\lambda = 0.8$ and $\gamma = 0.55$.

In Figure 5.14., we have plotted exact solution of Eq. (5.4.3) under the effect of fractional parameter β.

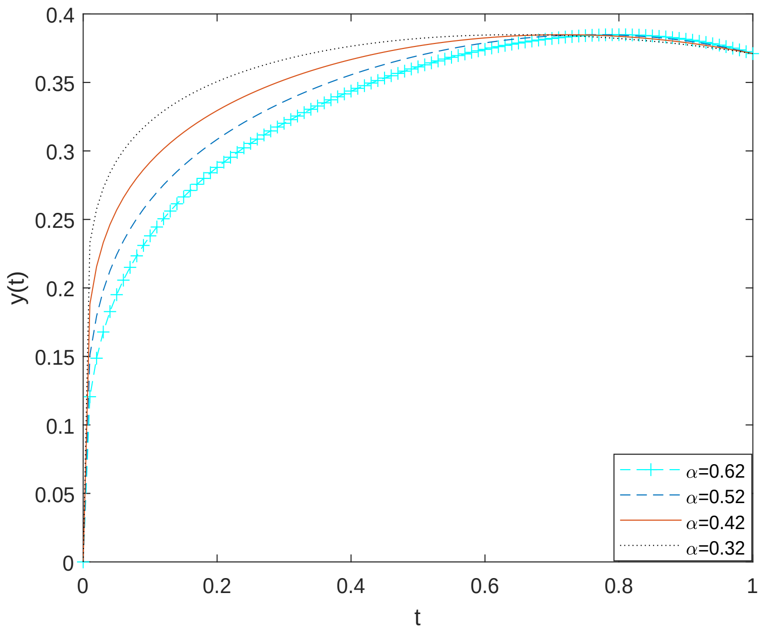

Figure 5.15. The sketch of Eq. (5.4.3) using $\beta = 0.55$, $\mu = 0.9$, $\lambda = 0.8$ and $\gamma = 0.55$.

In Figure 5.15., we have plotted exact solution of Eq. (5.4.3) under the effect of fractal parameter α.

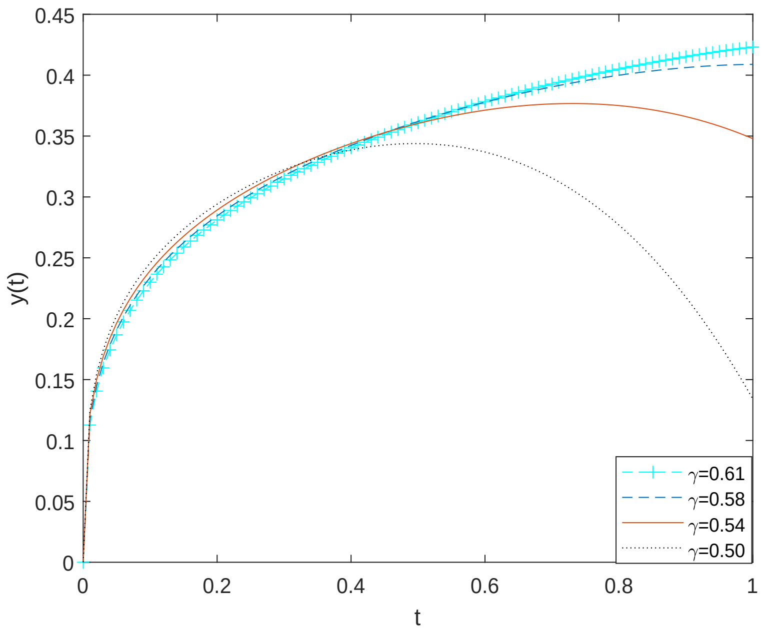

Figure 5.16. The sketch of Eq. (5.4.3) using $\beta = 0.5$, $\mu = 0.9$, $\lambda = 0.8$ and $\alpha = 0.62$.

In Figure 5.16., we have plotted exact solution of Eq. (5.4.3) under the effect of fractal

Mittag-Leffler parameter γ.

CONCLUSION

This thesis provided a comprehensive study on the theory and applications to some nonlinear partial differential equations, local, and non local fractal differential equations. The technique of generalized exponential rational function and its newly modified version are used to construct exact solutions fro some NPDEs. The GERFM and its modify are the most powerful methods because constructing solutions via these two methods are depend on the include constants r_j, s_j $(1 \leq j \leq 4)$, in other words, when we change the values of r_j, s_j $(1 \leq j \leq 4)$ the solutions are change, so, by continuous the processes, we can get abundant families of different solutions. In order to convert the proposed non linear partial differential equations into a NODEs, a traveling wave transformation has been implemented. Singular solutions, compound singular solutions, complex solutions, and topological and non-topological solutions are reported for the Gilson-Pickering equation that arise in plasma physics by using the GERFM. Non-topological solutions, periodic singular solutions, topological solutions, singular solutions, and periodic like lump solutions are constructed for the micro-strain wave in micro-structured solids using the mentioned method. The GERFM method and the novel MGERFM method have been successfully used to investigate the system based on the ion sound and Langmuir waves equations which arise in various area such as plasma physics, engineering sciences. To better understand the difference between the two methods, the same variables were chosen to solve the model at the same time for both schemes, leading in the development of the same solutions as well as the different solutions, we gave more details about difference of two methods in the subsection result and discussion in chapter 4. All produced solutions satisfy the studied governing equations. Furthermore, the dynamic behavior of all reported solutions are addressed in 2D, 3D, and contour surfaces by selecting suitable values for free involved parameters.

The local fractal Laplace transform and non-local Fractal Laplace transform in the sense of Caputo derivative have applied to investigate some fractal differential equations such electrical circuits involving fractal in both of serious and parallel RLC circuit, battery discharging model on fractal time sets as well as one-, and three-term fractal differential equations. In addition to, some new concepts of fractal calculus have been defined.

Time and space with a fractal structure in physical models give us new and more general results [115,116]. In [117], a general technique has developed to retrieve the fractal dimension of self-similar soils through microwave (radar) scattering. Researchers have usually studied the laws of physics in spaces with higher dimensions. However, studying the laws of physics in the spaces of non-integer dimensions, which are seen in nature and laboratories, has its own place [118,119]. A polariton gas that is confined in a quasiperiodic one-dimensional cavity gives a fractal energy spectrum and log-periodic oscillations of the integrated density of states [120]. The fractal structure in a space random walker leads to a broad distribution and non-equilibrium phenomena or anomalous diffusion on fractally disordered media such as the backbone of a percolating cluster (see Ref. [121] and the references therein).

The fractal calculus includes fractional order derivatives that have the following benefits. First, it has a local property that plays an important role in application because measurements are also local in physics. Second, it has a geometric meaning; that is, the order of the fractal derivatives is equal to the dimension of the domain of the functions. Third, it has a physical meaning; that is, Einstein's law states the relationship between the random walk dimension D_w, electric resistance exponent resistance ζ , and the spectral dimension ds, which reads as $D_w = 2\zeta/2 - d_s$ (see Refs. 122 and 123). Also, according to the relation of Alexander–Orbach, $D_w = 2D/d_s$ where D is the fractal (e.g., Hausdorff, box counting, or Ψ-dimension) dimension such that $\zeta = D_w - D$ (see Ref. [53]).

We have generalized the fractal calculus and investigated the series and parallel RLC circuits by considering their corresponding fractal differential equations that give their dynamics with fractal time. The local fractal Laplace transform has been used to obtain some new analytical solutions for the equations under consideration. Some examples using the local fractal Laplace transform have been provided. Furthermore, we carry out the comparison analysis by solving the governing equations in the standard version and in the fractal calculus; also, we demonstrate that when $\alpha = 1$, we get the same results in the standard version. In order to study the effect of fractal derivatives, we have changed the value of α in given models. A simulation analysis has been carried out in order to explain the effect of the dimension of the fractal time on these systems so that it can provide a new mathematical model for experimental data.

The battery discharging model on a thin Cantor set from the viewpoint of the fractal calculus. The local and non-local fractal Laplace transforms have been used to obtain some new analytical solutions for the equations under consideration. It is worth pointing out that in all the obtained solutions, for model one, the case of $\alpha = 1$, we get the same result in the standard calculus, for model two, the case of $\alpha = 1$, we get the same result in the standard fractional calculus, and also if we choose $\alpha = \beta = 1$, we get the same result in the standard calculus; this shows us the power of the used method. In addition, simulation analysis has been carried out in order to shed more light on the physical characteristics of the given equations. To study the effect of fractal and fractional parameters, we have changed the values of κ in Figures 5.5, 5.9, and the values of α in Figures 5.6, 5.10, also the values of β in Figure 5.8. The parameter α is a dimension of the fractal set, the parameter κ is a length of removed open interval from the Cantor set, and β is a parameter of the non-local derivative.

The one-term and three-term fractional differential equations from the viewpoints of local and non-local fractal derivatives have been explored. The well-known Laplace transform has been used to form some new analytical solutions for the mentioned models. Furthermore, we carry out a comparative analysis by solving the governing equation in the contexts of the standard version and fractal calculus for two cases in which one can also demonstrate that when $\alpha = \gamma = \beta = 1$, the same results are obtained in the standard version (see [114,121]). To study the effect of a fractional order derivative, we have fixed one index while changing the other one. A simulation analysis has been carried out to explain the effect of the orders of derivatives for both local and non-local cases on bound solutions that might be helpful in providing a mathematical model for experimental data in physical phenomena. All in all, exact solutions are non-differentiable in the sense of standard derivatives.

References

[1] Carapella, G., & Costabile, G. (2000). Coupled Structures of Long Josephson Junctions. In Nonlinear Science at the Dawn of the 21st Century (pp. 103-119). Springer, Berlin, Heidelberg.

[2] Kivshar, Y. S., & Agrawal, G. (2003). Optical solitons: from fibers to photonic crystals. Academic press.

[3] Ablowitz, M. J., Ablowitz, M. A., Clarkson, P. A., & Clarkson, P. A. (1991). Solitons, nonlinear evolution equations and inverse scattering (Vol. 149). Cambridge university press.

[4] Ali, K. K., Yilmazer, R., Yokus, A., & Bulut, H. (2020). Analytical solutions for the (3+ 1)-dimensional nonlinear extended quantum Zakharov–Kuznetsov equation in plasma physics. Physica A: Statistical Mechanics and its Applications, 548, 124327.

[5] Ismael, H., & Bulut, H. (2020). On the wave solutions of (2+ 1)-dimensional time-fractional Zoomeron equation. Konuralp Journal of Mathematics (KJM), 8(2), 410-418.

[6] Ali, K. K., Yilmazer, R., Baskonus, H. M., & Bulut, H. (2021). New wave behaviors and stability analysis of the Gilson–Pickering equation in plasma physics. Indian Journal of Physics, 95(5), 1003-1008.

[7] Zhao, Z., & Han, B. (2017). Lie symmetry analysis of the Heisenberg equation. Communications in Nonlinear Science and Numerical Simulation, 45, 220-234.

[8] Vakhnenko, V. O., Parkes, E. J., & Morrison, A. J. (2003). A Bäcklund transformation and the inverse scattering transform method for the generalised Vakhnenko equation. Chaos, Solitons & Fractals, 17(4), 683-692.

[9] Ali, K. K., Yilmazer, R., Baskonus, H. M., & Bulut, H. (2020). Modulation instability analysis and analytical solutions to the system of equations for the ion sound and Langmuir waves. Physica Scripta, 95(6), 065602.

[10] Akram, G., & Gillani, S. R. (2021). Sub pico-second Soliton with Triki–Biswas equation by the extended (G'/G) −expansion method and the modified auxiliary equation method. Optik, 229, 166227.

[11] Steinfeld, B., Scott, J., Vilander, G., Marx, L., Quirk, M., Lindberg, J., & Koerner, K. (2015). The role of lean process improvement in implementation of evidence-based practices in behavioral health care. The Journal of Behavioral Health Services & Research, 42(4), 504-518.

[12] Ismael, H. F., Baskonus, H. M., & Bulut, H. (2021). Abundant novel solutions of the conformable Lakshmanan-Porsezian-Daniel model. Discrete & Continuous Dynamical Systems-S, 14(7), 2311.

[13] Tarla, S., Ali, K. K., Sun, T. C., Yilmazer, R., & Osman, M. S. (2022). Nonlinear pulse propagation for novel optical solitons modeled by Fokas system in monomode optical fibers. Results in Physics, 105381.

[14] Tarla, S., Ali, K. K., Yilmazer, R., & Osman, M. S. (2022). New optical solitons based on the perturbed Chen-Lee-Liu model through Jacobi elliptic function method. Optical and Quantum Electronics, 54(2), 1-12.

[15] Dutta, H., Günerhan, H., Ali, K. K., & Yilmazer, R. (2020). Exact soliton solutions to the cubic-quartic non-linear Schrödinger equation with conformable derivative. Frontiers in Physics, 8, 62.

[16] Ismael, H. F., & Bulut, H. (2021). Multi soliton solutions, M-lump waves and mixed soliton-lump solutions to the awada-Kotera equation in (2+ 1)-dimensions. Chinese Journal of Physics, 71, 54-61.

[17] Ismael, H. F., Seadawy, A., & Bulut, H. (2021). Multiple soliton, fusion, breather, lump, mixed kink-lump and periodic solutions to the extended shallow water wave model in (2+1)-dimensions. Modern Physics Letters B, 35(08), 2150138.

[18] Ismael, H. F., Seadawy, A., & Bulut, H. (2021). Construction of breather solutions and N-soliton for the higher order dimensional Caudrey–Dodd–Gibbon–Sawada–Kotera equation arising from wave patterns. International Journal of Nonlinear Sciences and Numerical Simulation.

[19] Ali, K. K., Yilmazer, R., & Osman, M. S. (2022). Dynamic behavior of the (3+ 1)-dimensional KdV–Calogero–Bogoyavlenskii–Schiff equation. Optical and Quantum Electronics, 54(3), 1-15.

[20] Ali, K. K., Yilmazer, R., & Osman, M. S. (2021). Extended Calogero-Bogoyavlenskii-Schiff equation and its dynamical behaviors. Physica Scripta, 96(12), 125249.

[21] Gilson, C., & Pickering, A. (1995). Factorization and Painlevé analysis of a class of nonlinear third-order partial differential equations. Journal of Physics A: Mathematical and General, 28(10), 2871.

[22] Ali, K. K., Dutta, H., Yilmazer, R., & Noeiaghdam, S. (2020). On the new wave behaviors of the Gilson-Pickering equation. Frontiers in Physics, 8, 54.

[23] Porubov, A. V., & Pastrone, F. (2004). Non-linear bell-shaped and kink-shaped strain waves in microstructured solids. International Journal of Non-Linear Mechanics, 39(8), 1289-1299.

[24] Zabusky, N. J., & Kruskal, M. D. (1965). Interaction of" solitons" in a collisionless plasma and the recurrence of initial states. Physical review letters, 15(6), 240.

[25] Alam, M. N., Akbar, M. A., & Mohyud-Din, S. T. (2014). General traveling wave solutions of the strain wave equation in microstructured solids via the new approach of generalized (G'/G) −expansion method. Alexandria Engineering Journal, 53(1), 233-241.

[26] Hafez, M. G., & Akbar, M. A. (2015). An exponential expansion method and its application to the strain wave equation in microstructured solids. Ain Shams Engineering Journal, 6(2), 683-690.

[27] Ayati, Z., Hosseini, K., & Mirzazadeh, M. (2017). Application of Kudryashov and functional variable methods to the strain wave equation in microstructured solids. Nonlinear Engineering, 6(1), 25-29.

[28] Esen, A., Sulaiman, T. A., Bulut, H., & Baskonus, H. M. (2018). Optical solitons to the space-time fractional (1+1)-dimensional coupled nonlinear Schrödinger equation. Optik, 167, 150-156.

[29] Ali, K. K., Yilmazer, R., Bulut, H., Aktürk, T., & Osman, M. S. (2021). Abundant exact solutions to the strain wave equation in micro-structured solids. Modern Physics Letters B, 35(26), 2150439.

[30] Baskonus, H. M., & Bulut, H. (2016). New wave behaviors of the system of equations for the ion sound and Langmuir waves. Waves in Random and Complex Media, 26(4), 613-625.

[31] Manafian, J. (2017). Application of the ITEM for the system of equations for the ion sound and Langmuir waves. Optical and Quantum Electronics, 49(1), 1-26.

[32] Alexeff, I., & Neidigh, R. V. (1963). Observations of ionic sound waves in plasmas: Their properties and applications. Physical Review, 129(2), 516.

[33] Thejappa, G., MacDowall, R. J., & Bergamo, M. (2013). Observational evidence for the collapsing Langmuir wave packet in a solar type III radio burst. Journal of Geophysical Research: Space Physics, 118(7), 4039-4052.

[34] Mandelbrot, B. B., & Mandelbrot, B. B. (1982). The fractal geometry of nature (Vol. 1). New York: WH freeman.

[35] Pietronero, L., & Tosatti, E. (Eds.). (2012). Fractals in physics. Elsevier.

[36] Edgar, G. A. (1998). Fractal measures. In Integral, Probability, and Fractal Measures (pp. 1-67). Springer, New York, NY.

[37] Miyazima, S., & Stanley, H. E. (1987). Intersection of two fractal objects: Useful method of estimating the fractal dimension. Physical Review B, 35(16), 8898.

[38] Bunde, A., & Havlin, S. (Eds.). (2013). Fractals in science. Springer.

[39] Barnsley, M. F. (2014). Fractals everywhere. Academic press.

[40] Dewey, T. G. (1998). Fractals in molecular biophysics. Oxford University Press.

[41] Wójcik, D., Białynicki-Birula, I., & Życzkowski, K. (2000). Time evolution of quantum fractals. Physical Review Letters, 85(24), 5022.

[42] Iliasov, A. A., Katsnelson, M. I., & Yuan, S. (2020). Hall conductivity of a Sierpiński carpet. Physical Review B, 101(4), 045413.

[43] Czachor, M. (2017). Waves along fractal coastlines: From fractal arithmetic to wave equations. arXiv preprint arXiv:1707.06225.

[44] Freiberg, U., & Zähle, M. (2002). Harmonic calculus on fractals-a measure geometric approach I. Potential analysis, 16(3), 265-277.

[45] Kigami, J. (2001). Analysis on fractals (No. 143). Cambridge University Press.

[46] Nottale, L. (2011). Scale relativity and fractal space-time: a new approach to unifying relativity and quantum mechanics. World Scientific.

[47] Stillinger, F. H. (1977). Axiomatic basis for spaces with noninteger dimension. Journal of Mathematical Physics, 18(6), 1224-1234.

[48] Zubair, M., Mughal, M. J., & Naqvi, Q. A. (2012). Electromagnetic fields and waves in fractional dimensional space. Springer Science & Business Media.

[49] Parvate, A., & Gangal, A. D. (2009). Calculus on fractal subsets of real line—I: Formulation. Fractals, 17(01), 53-81.

[50] Parvate, A., & Gangal, A. D. (2011). Calculus on fractal subsets of real line—II: conjugacy with ordinary calculus. Fractals, 19(03), 271-290.

[51] Parvate, A., Satin, S., & Gangal, A. D. (2011). Calculus on fractal curves in Rn. Fractals, 19(01), 15-27.

[52] Golmankhaneh, A. K., & Fernandez, A. (2018). Fractal calculus of functions on Cantor tartan spaces. Fractal and Fractional, 2(4), 30.

[53] Golmankhaneh, A. K., & Balankin, A. S. (2018). Sub-and super-diffusion on Cantor sets: Beyond the paradox. Physics Letters A, 382(14), 960-967.

[54] Golmankhaneh, A. K. (2019). A review on application of the local fractal calculus. Num. Com. Meth. Sci. Eng, 1, 57-66.

[55] Khalili Golmankhaneh, A., Fernandez, A., Khalili Golmankhaneh, A., & Baleanu, D. (2018). Diffusion on middle-ξ Cantor sets. Entropy, 20(7), 504.

[56] Golmankhaneh, A. K., & Baleanu, D. (2016). Diffraction from fractal grating Cantor sets. Journal of Modern Optics, 63(14), 1364-1369.

[57] Khalili Golmankhaneh, A., & Cattani, C. (2019). Fractal logistic equation. Fractal and Fractional, 3(3), 41.

[58] Golmankhaneh, A. K., & Tunç, C. (2020). Stochastic differential equations on fractal sets. Stochastics, 92(8), 1244-1260.

[59] Golmankhaneh, A. K., & Tunç, C. (2019). Sumudu transform in fractal calculus. Applied Mathematics and Computation, 350, 386-401.

[60] Golmankhaneh, A. K., & Baleanu, D. (2016). Non-local integrals and derivatives on fractal sets with applications. Open Physics, 14(1), 542-548.

[61] Golmankhaneh, A. K., Tunç, C., Nia, S. M., & Golmankhaneh, A. K. (2019). A review on local and non-local fractal calculus. Num. Com. Meth. Sci. Eng, 1, 19-31.

[62] Khalili Golmankhaneh, A., & Kamal Ali, K. (2021). Fractal Kronig-Penney model involving fractal comb potential. Journal of Mathematical Modeling, 9(3), 331-345.

[63] Khalili Golmankhaneh, A., K Ali, K., Yilmazer, R., & KA Kaabar, M. (2021). Economic models involving time fractal. Journal of Mathematics and Modeling in Finance, 1(1), 159-178.

[64] Khalili Golmankhaneh, A., Ali, K. K., Yilmazer, R., & Kaabar, M. K. A. (2021). Local fractal fourier transform and applications. Computational Methods for Differential Equations.

[65] Myint-U, T., & Debnath, L. (2007). Linear partial differential equations for scientists and engineers. Springer Science & Business Media, Birkhäuser Boston.

[66] Khalili Golmankhaneh, A., Tunç, C., & Şevli, H. (2021). Hyers–Ulam stability on local fractal calculus and radioactive decay. The European Physical Journal Special Topics, 230(21), 3889-3894.

[67] Khalili Golmankhaneh, A., & Nia, S. M. (2021). Laplace equations on the fractal cubes and Casimir effect. The European Physical Journal Special Topics, 230(21), 3895-3900.

[68] Cetinkaya, F. A., & Golmankhaneh, A. K. (2021). General characteristics of a fractal Sturm-Liouville problem. Turkish Journal of Mathematics, 45(4).

[69] El-Nabulsi, R. A., & Khalili Golmankhaneh, A. (2021). Dynamics of particles in cold electrons plasma: fractional actionlike variational approach versus fractal spaces approach. Waves in Random and Complex Media, 1-22.

[70] Golmankhaneh, A. K., & Sibatov, R. T. (2021). Fractal stochastic processes on thin cantor-like sets. Mathematics, 9(6), 613.

[71] Khalili Golmankhaneh, A., Kamal Ali, K., Yilmazer, R., & Welch, K. (2021). Electrical circuits involving fractal time. Chaos: An Interdisciplinary Journal of Nonlinear Science, 31(3), 033132.

[72] Ali, K. K., Golmankhaneh, A. K., & Yilmazer, R. (2021). Battery discharging model on fractal time sets. International Journal of Nonlinear Sciences and Numerical Simulation.

[73] Ali, K. K., Golmankhaneh, A. K., Yilmazer, R., & Abdullah, M. A. (2022). Solving fractal differential equations via fractal Laplace transforms. Journal of Applied Analysis.

[74] Ghanbari, B., Gómez-Aguilar, J. F., & Bekir, A. (2021). Soliton solutions in the conformable (2+ 1)-dimensional chiral nonlinear Schrödinger equation. Journal of Optics, 1-28.

[75] Ghanbari, B., & Kuo, C. K. (2021). Abundant wave solutions to two novel KP-like equations using an effective integration method. Physica Scripta, 96(4), 045203.

[76] Ghanbari, B. (2020). Exact and approximate solutions for a generalized form of the Schrödinger nonlinear equation. Journal of New Researches in Mathematics, 6(27), 79-92.

[77] Ghanbari, B., & Liu, J. G. (2020). Exact solitary wave solutions to the (2+ 1)-dimensional generalised Camassa–Holm–Kadomtsev–Petviashvili equation. Pramana, 94(1), 1-11.

[78] Osman, M. S., & Ghanbari, B. (2018). New optical solitary wave solutions of Fokas-Lenells equation in presence of perturbation terms by a novel approach. Optik, 175, 328-333.

[79] Ghanbari, B. (2019). Abundant soliton solutions for the Hirota–Maccari equation via the generalized exponential rational function method. Modern Physics Letters B, 33(09), 1950106.

[80] Camassa, R., & Holm, D. D. (1993). An integrable shallow water equation with peaked solitons. Physical review letters, 71(11), 1661.

[81] Fokas, A. S., & Fuchssteiner, B. (1981). The hierarchy of the Benjamin-Ono equation. Physics letters A, 86(6-7), 341-345.

[82] Rosenau, P., & Hyman, J. M. (1993). Compactons: solitons with finite wavelength. Physical Review Letters, 70(5), 564.

[83] Fornberg, B., & Whitham, G. B. (1978). A numerical and theoretical study of certain nonlinear wave phenomena. Philosophical Transactions of the Royal Society of London. Series A, Mathematical and Physical Sciences, 289(1361), 373-404.

[84] Whitham, G. B. (1967). Variational methods and applications to water waves. Proceedings of the Royal Society of London. Series A. Mathematical and Physical Sciences, 299(1456), 6-25.

[85] Whitham, G. B. (2011). Linear and nonlinear waves. John Wiley & Sons.

[86] Fan, X., Yang, S., & Zhao, D. (2009). Travelling wave solutions for the Gilson-Pickering equation by using the simplified G/G-expansion method. Int. J. Nonlinear Sci, 8, 368-373.

[87] Baskonus, H. M. (2019). Complex soliton solutions to the Gilson–Pickering model. Axioms, 8(1), 18.

[88] Aslan, İ. (2011). Exact and explicit solutions to nonlinear evolution equations using the division theorem. Applied mathematics and computation, 217(20), 8134-8139.

[89] Raza, N., Seadawy, A. R., Jhangeer, A., Butt, A. R., & Arshed, S. (2020). Dynamical behavior of micro-structured solids with conformable time fractional strain wave equation. Physics Letters A, 384(27), 126683.

[90] Baskonus, H. M., Sulaiman, T. A., & Bulut, H. (2018). Novel complex and hyperbolic forms to the strain wave equation in microstructured solids. Optical and Quantum Electronics, 50(1), 1-9.

[91] Seadawy, A. R., Arshad, M., & Lu, D. (2020). Dispersive optical solitary wave solutions of strain wave equation in micro-structured solids and its applications. Physica A: Statistical Mechanics and its Applications, 540, 123122.

[92] Arshad, M., Seadawy, A. R., & Lu, D. (2019). Study of bright–dark solitons of strain wave equation in micro-structured solids and its applications. Modern Physics Letters B, 33(33), 1950417.

[93] Seadawy, A. R., Kumar, D., Hosseini, K., & Samadani, F. (2018). The system of equations for the ion sound and Langmuir waves and its new exact solutions. Results in Physics, 9, 1631-1634.

[94] Seadawy, A. R., Lu, D., & Iqbal, M. (2019). Application of mathematical methods on the system of dynamical equations for the ion sound and Langmuir waves. Pramana, 93(1), 1-12.

[95] Bogolubsky, I. L. (1977). Some examples of inelastic soliton interaction. Computer Physics Communications, 13(3), 149-155.

[96] Degtiarev, L. M., Nakhankov, V. G., & Rudakov, L. I. (1975). Dynamics of the formation and interaction of Langmuir solitons and strong turbulence. Soviet Physics-JETP, 40(2), 264-268.

[97] Degtyarev, L. M., Zakharov, V. E., Sagdeev, R. Z., Solov'ev, G. I., Shapiro, V. D., & Shevchenko, V. I. (1983). Langmuir collapse under pumping and wave energy dissipation. Zh. Eksp. Teor. Fiz, 85, 1221-1231.

[98] Anisimov, S. I., Berezovskiĭ, M. A., Ivanov, M. F., Petrov, I. V., Rubenchick, A. M., & Zakharov, V. E. (1982). Computer simulation of the Langmuir collapse. Physics Letters A, 92(1), 32-34.

[99] Anisimov, S. I., Berezovskii, M. A., Zakharov, V. E., Petrov, I. V., & Rubenchik, A. M. (1983). Numerical simulation of a Langmuir collapse. Zh. Eksp. Teor. Fiz, 84, 2046-2054.

[100] D'Iachenko, A. I., Zakharov, B. E., Rubenchik, A. M., Sagdeev, R. Z., & Shvets, V. F. (1988). Numerical simulation of two-dimensional Langmuir collapse. Zhurnal Eksperimentalnoi i Teoreticheskoi Fiziki, 94, 144-155.

[101] Rubenchik, A. M., & Zakharov, V. E. (1991). Strong Langmuir turbulence in laser plasma. Handbook of plasma physics, 3, 335-360.

[102] Musher, S. L., Rubenchik, A. M., & Zakharov, V. E. (1995). Weak langmuir turbulence. Physics Reports, 252(4), 177-274.

[103] Yin-Hua, C., Wei, L., & Wen-Hao, W. (2001). The nonlinear langmuir waves in a multi-ion-component plasma. Communications in Theoretical Physics, 35(2), 223.

[104] Soucek, J., Krasnoselskikh, V., Dudok de Wit, T., Pickett, J., & Kletzing, C. (2005). Nonlinear decay of foreshock Langmuir waves in the presence of plasma inhomogeneities: Theory and Cluster observations. Journal of Geophysical Research: Space Physics, 110(A8).

[105] Watanabe, M. (1976). Interaction among Langmuir solitons, coupled solitons and sound waves. Physics Letters A, 57(4), 331-332.

[106] Eliasson, B., & Shukla, P. K. (2004). Trapping of Langmuir waves in ion holes. Physica Scripta, 2004(T107), 192.

[107] Zakharov, V. E. (1972). Collapse of Langmuir waves. Sov. Phys. JETP, 35(5), 908-914.

[108] Zaslavsky, A., Volokitin, A. S., Krasnoselskikh, V. V., Maksimovic, M., & Bale, S. D. (2010). Spatial localization of Langmuir waves generated from an electron beam propagating in an inhomogeneous plasma: Applications to the solar wind. Journal of Geophysical Research: Space Physics, 115(A8).

[109] Nahvi, M., & Edminister, J. A. (2018). Schaum's outline of Electric Circuits. McGraw-Hill Education.

[110] DiMartino, R., & Urbina, W. (2014). On Cantor-like sets and Cantor-Lebesgue singular functions. arXiv preprint arXiv:1403.6554.

[111] Welch, K. (2020). A fractal topology of time: deepening into timelessness, Fox Finding Press, San Francisco.

[112] Golmankhaneh, A. K., & Welch, K. (2021). Equilibrium and non-equilibrium statistical mechanics with generalized fractal derivatives: A review. Modern Physics Letters A, 36(14), 2140002.

[113] Herrmann, R. (2011). Fractional calculus: an introduction for physicists, , World Scientific, Singapore City.

[114] Podlubny, I. (1998). Fractional differential equations: an introduction to fractional derivatives, fractional differential equations, to methods of their solution and some of their applications. Elsevier.

[115] Balankin, A. S., Susarrey, O., & Gonzáles, J. M. (2003). Scaling properties of pinned interfaces in fractal media. Physical review letters, 90(9), 096101.

[116] Xiao, B., Wang, W. E. I., Zhang, X., Long, G., Chen, H., Cai, H., & Deng, L. I. N. (2019). A novel fractal model for relative permeability of gas diffusion layer in proton exchange membrane fuel cell with capillary pressure effect. Fractals, 27(02), 1950012.

[117] Oleschko, K., Korvin, G., Figueroa, B., Vuelvas, M. A., Balankin, A. S., Flores, L., & Carreón, D. (2003). Fractal radar scattering from soil. Physical Review E, 67(4), 041403.

[118] Balankin, A. S., Valdivia, J. C., Marquez, J., Susarrey, O., & Solorio-Avila, M. A. (2016). Anomalous diffusion of fluid momentum and Darcy-like law for laminar flow in media with fractal porosity. Physics Letters A, 380(35), 2767-2773.

[119] Zheng, H., Chen, G., & Rowland, S. M. (2020). The influence of AC and DC voltages on electrical treeing in low density polyethylene. International Journal of Electrical Power & Energy Systems, 114, 105386.

[120] Tanese, D., Gurevich, E., Baboux, F., Jacqmin, T., Lemaître, A., Galopin, E., & Akkermans, E. (2014). Fractal energy spectrum of a polariton gas in a Fibonacci quasiperiodic potential. Physical review letters, 112(14), 146404.

[121] B. Davies, Integral transforms and their applications, vol. 41. Springer Science & Business Media, 2002.

[122] Haynes, C. P., & Roberts, A. P. (2009). Generalization of the fractal Einstein law relating conduction and diffusion on networks. Physical review letters, 103(2), 020601.

[123] Telcs, A. (2006). The art of random walks (No. 1885). Springer Science & Business Media.

CURRICULUM VITAE

Karmina Kamal ALI

[redacted]

[redacted]

[redacted]

[redacted]

[redacted]

[redacted]

[redacted]

[redacted]

[redacted]

[redacted] [redacted]

[redacted]

[redacted]

[redacted]

ACADEMIC ACTIVITIES

Paper :

1. Ali, K. K., Yilmazer, R., & Bulut, H. (2019, April). Analytical solutions to the coupled Boussinesq–Burgers equations via Sine-Gordon expansion method. In International Conference on Computational Mathematics and Engineering Sciences (pp. 233-240). Springer, Cham.

2. Ali, K. K., & Yilmazer, R. (2020). Discrete fractional solutions to the effective mass Schrödinger equation by mean of nabla operator. AIMS Mathematics, 5(2), 894-903.

3. Dutta, H., Günerhan, H., Ali, K. K., & Yilmazer, R. (2020). Exact soliton solutions to the cubic-quartic non-linear Schrödinger equation with conformable derivative. Frontiers in Physics, 8, 62.

4. Ali, K. K., Dutta, H., Yilmazer, R., & Noeiaghdam, S. (2020). On the new wave behaviors of the Gilson-Pickering equation. Frontiers in Physics, 8, 54.

5. Ali, K. K., Yilmazer, R., Baskonus, H. M., & Bulut, H. (2020). Modulation instability analysis and analytical solutions to the system of equations for the ion sound and Langmuir waves. Physica Scripta, 95(6), 065602.

6. Ali, K. K., Yilmazer, R., Yokus, A., & Bulut, H. (2020). Analytical solutions for the (3+ 1)-dimensional nonlinear extended quantum Zakharov–Kuznetsov equation in plasma physics. Physica A: Statistical Mechanics and its Applications, 548, 124327.

7. Ali, K. K., Seadawy, A. R., Yokus, A., Yilmazer, R., & Bulut, H. (2020). Propagation of dispersive wave solutions for (3+ 1)-dimensional nonlinear modified Zakharov–Kuznetsov equation in plasma physics. International Journal of Modern Physics B, 34(25), 2050227.

8. Khalili Golmankhaneh, A., K Ali, K., Yilmazer, R., & KA Kaabar, M. (2021). Economic models involving time fractal. Journal of Mathematics and Modeling in Finance, 1(1), 159-178.

9. Khalili Golmankhaneh, A., Kamal Ali, K., Yilmazer, R., & Welch, K. (2021). Electrical circuits involving fractal time. Chaos: An Interdisciplinary Journal of Nonlinear Science, 31(3), 033132.

10. Ali, K. K., Yilmazer, R., Baskonus, H. M., & Bulut, H. (2021). New wave behaviors and stability analysis of the Gilson–Pickering equation in plasma physics. Indian Journal of Physics, 95(5), 1003-1008.

11. Yilmazer, R., & Ali, K. (2021). Discrete fractional solutions to the k-hypergeometric differential equation. Mathematical Methods in the Applied Sciences, 44(9), 7614-7621.

12. Ali, K. K., Golmankhaneh, A. K., & Yilmazer, R. (2021). Battery discharging model on fractal time sets. International Journal of Nonlinear Sciences and Numerical Simulation.

ACADEMIC ACTIVITIES

Paper :

13. Khalili Golmankhaneh, A., Ali, K. K., Yilmazer, R., & Kaabar, M. K. A. (2021). Local fractal fourier transform and applications. Computational Methods for Differential Equations.

14. Yokus, A., Ali, K. K., Yılmazer, R., & Bulut, H. (2021). On exact solutions of the generalized Pochhammer-Chree equation. Computational Methods for Differential Equations.

15. Ali, K. K., Yilmazer, R., Bulut, H., Aktürk, T., & Osman, M. S. (2021). Abundant exact solutions to the strain wave equation in micro-structured solids. Modern Physics Letters B, 35(26), 2150439.

16. Ali, K. K., Yilmazer, R., & Osman, M. S. (2021). Extended Calogero-Bogoyavlenskii-Schiff equation and its dynamical behaviors. Physica Scripta, 96(12), 125249.

17. Ali, K. K., & Yilmazer, R. (2021). M-lump solutions and interactions phenomena for the (2+ 1)-dimensional KdV equation with constant and time-dependent coefficients. Chinese Journal of Physics.

18. Ali, K. K., Yilmazer, R., Bulut, H., & Yokus, A. (2022). New Wave Behaviours of the Generalized Kadomtsev-Petviashvili Modified Equal Width-Burgers Equation. Appl. Math, 16(2), 249-258.

19. Ali, K. K., Golmankhaneh, A. K., Yilmazer, R., & Abdullah, M. A. (2022). Solving fractal differential equations via fractal Laplace transforms. Journal of Applied Analysis.

20. Tarla, S., Ali, K. K., Yilmazer, R., & Osman, M. S. (2022). New optical solitons based on the perturbed Chen-Lee-Liu model through Jacobi elliptic function method. Optical and Quantum Electronics, 54(2), 1-12.

21. Ali, K. K., Yilmazer, R., & Osman, M. S. (2022). Dynamic behavior of the (3+ 1)-dimensional KdV–Calogero–Bogoyavlenskii–Schiff equation. Optical and Quantum Electronics, 54(3), 1-15.

22. Tarla, S., Ali, K. K., Sun, T. C., Yilmazer, R., & Osman, M. S. (2022). Nonlinear pulse propagation for novel optical solitons modeled by Fokas system in monomode optical fibers. Results in Physics, 105381.

23. Tarla, S., Ali, K., Yilmazer, R., & Osman, M. S. (2022). On dynamical behavior for optical solitons sustained by the perturbed Chen-Lee-Liu model. Communications in Theoretical Physics.